

2019-01-01

Additive Manufactured Ear Pinna For Spatial Cue Preservation In Custom Hearing Devices

Carlos Felipe Acosta Carrasco
University of Texas at El Paso

Follow this and additional works at: https://scholarworks.utep.edu/open_etd



Part of the [Mechanical Engineering Commons](#)

Recommended Citation

Acosta Carrasco, Carlos Felipe, "Additive Manufactured Ear Pinna For Spatial Cue Preservation In Custom Hearing Devices" (2019). *Open Access Theses & Dissertations*. 3067.
https://scholarworks.utep.edu/open_etd/3067

This is brought to you for free and open access by ScholarWorks@UTEP. It has been accepted for inclusion in Open Access Theses & Dissertations by an authorized administrator of ScholarWorks@UTEP. For more information, please contact lweber@utep.edu.

ADDITIVE MANUFACTURED EAR PINNA FOR SPATIAL CUE
PRESERVATION IN CUSTOM HEARING DEVICES

CARLOS FELIPE ACOSTA CARRASCO

Master's Program in Mechanical Engineering

APPROVED:

Ryan B. Wicker, Ph.D., Chair

David Espalin, Ph.D.

Amit Lopes, Ph.D.

Stephen L. Crites, Jr., Ph.D.
Dean of the Graduate School

Copyright ©

by

Carlos Acosta Carrasco

2019

Dedicación

Quisiera dedicar este trabajo principalmente a mi familia y amigos cercanos quienes no solo me han apoyado durante mi maestría, sino durante todos mis años de estudios. Quiero agradecer a mis padres Carlos y Alicia, y a mis hermanos Carolina y Joaquín, quienes han sacrificado de igual o mayor manera yo estar en este momento de mi vida. Quiero agradecer el apoyo de mi abuela Alicia, mi abuelo Carlos, y mi abuela Teresa, quien me impartió los valores necesarios para poder llegar a estas instancias y siempre vivirá en nuestros corazones para guiarnos a tener una vida digna de esfuerzo y dedicación.

ADDITIVE MANUFACTURED EAR PINNA FOR SPATIAL CUE
PRESERVATION IN CUSTOM HEARING DEVICES

by

CARLOS FELIPE ACOSTA CARRASCO, B.S.M.E.

THESIS

Presented to the Faculty of the Graduate School of

The University of Texas at El Paso

in Partial Fulfillment

of the Requirements

for the Degree of

MASTER OF SCIENCE

Department of Mechanical Engineering

THE UNIVERSITY OF TEXAS AT EL PASO

August 2019

Acknowledgements

I would like to start by acknowledging Dr. Ryan Wicker, Director and Founder of The W.M. Keck Center for 3D Innovation, for giving me the opportunity to gain unique experiences by working in his additive manufacturing research lab, through the exposure to a variety of projects throughout my graduate studies. This thesis work would not have been completed without his mentorship and counseling on the G.N. project. I would like to thank my thesis committee, Dr. Amit Lopes, and Dr. David Espalin.

I would also like to acknowledge the collaborators from the G.N. Advanced Science team, Andrew Dittberner and Vidya Krull, whom funded this research, as well as provided me with the opportunity to present the research at the G.N. Advanced Science Conference 2019 at the G.N. headquarters in Denmark. Their expertise on acoustic testing was and will continue to be valuable for this ongoing research project.

I would like to extend my gratitude to those who helped me through the several projects I was involved in during my work at the Keck Center, especially Dr. Espalin and Jose Coronel, who helped advise me during my residency at Autodesk. I want to give a sincere thank you to Jose Coronel for all the support, guidance, and friendship he provided throughout the different projects I was involved in at the Keck Center, including the CAMIEM, Autodesk, and G.N projects. His efforts to aid in my thesis completion have been immense and I will be forever grateful. I would like to acknowledge Luis Ochoa who taught me different design techniques for crucial tasks related to this project. I would like to thank Alex Plasencio and Mahesh Tonde for completing numerous tasks for me to finish this work. I want to extend my gratitude to Dr. Lopes and Dr. Jaime Sanchez for his input on performing the analysis of variance study, as well as Desert Imaging diagnostic imaging and radiology center for their efforts to perform CT scan data which was needed to keep this research moving forward. I would like to the students at the Keck Center which helped me out at different stages of my graduate studies, especially the following people: Alejandra Belmont,

Lluvia Herrera, Leonardo Gutierrez, Kazi Md. Masum Billah, Pablo Castrejon, Jose Motta, Chris Minjares, and Sol Barraza.

Last but not least I want to thank my family and close friends for all their efforts that contributed for this completion of my graduate studies. Their constant support and dedication toward the completion of my studies is acknowledged and will be carried on for the next steps of my professional career.

Abstract

Advancements in additive manufacturing/3D printing technologies has permitted the fabrication of intricate features such as the ones present in the human ear. The outer ear, also known as the pinna, allows for the spectral cues from incoming sound to be captured and identified. The hypothesis of the preservation of auditory localization and externalization relies on the fabrication of an ear pinna via additive manufacturing embedded into a headset for spectral cue preservation and hearing protection. Before exploring these custom circumaural hearing devices, a study on the fabrication process of AM pinnae was performed. The KEMAR system for acoustic research was used as a benchmark for the 3D printed pinnae. The computer models of the KEMAR pinnae were obtained via 3D scanning and CT scanning. Material extrusion, vat photopolymerization and material jetting were the technologies used to carry out the manufacturing process. A selection of industrial and desktop equipment was done to perform an analysis on the printing resolution. Two different designs were used to place the AM pinnae onto the KEMAR. Six different pinnae were printed using three CAD files, and dimensional accuracy measurements were taken on all 3D printed pinnae using three different measurement tools, caliper, image processing software, and measurements from the CAD file derived from the CT scans of each pinna. These measurements were compared to the KEMAR pinna for fabrication evaluation. Results showed consistent measurements from the AM pinnae to KEMAR across the different sections of the pinna. An analysis of variance study was performed to find statistical differences between the baseline pinna and the AM pinnae, as well as AM pinnae among each other. Desktop printers were able to reproduce similar quality parts to the ones produced by the industrial equipment. This is an important determination, since cost will be an important factor when determining if, in the end, custom hearing protection devices can be printed at or near the point of need. Acoustic testing performed on two AM pinnae using the KEMAR system produced a similar frequency response to the one presented by the KEMAR pinnae. The replicas of the KEMAR pinna using additive manufacturing were successful. Even though the incorporation of

an embedded pinna into a headset was designed but not tested, preliminary results on the acoustic analysis of the AM pinna motivates the development of AM custom hearing devices.

Table of Contents

Acknowledgements.....	v
Abstract.....	vii
Table of Contents.....	ix
List of Tables	xi
List of Figures.....	xii
Chapter 1: Introduction.....	1
1.1 Background.....	1
1.2 Motivation.....	2
1.3 Objectives	3
Chapter 2: Literature review	4
2.1 3D printing.....	4
2.2 3D scanning & CT scanning.....	10
2.3 3D printed ear pinnae.....	11
2.4 Acoustics.....	14
2.5 Embedded electronics	16
Chapter 3: Experimental setup and procedures	18
3.1 Ear pinna 3D modeling.....	18
3.2 Pinna 3D printing fabrication.....	24
3.3 AM pinna on KEMAR setup	30
3.4 AM pinna embedded in headset.....	31
Chapter 4: Results	35
4.1 Dimensional accuracy for 3D printed pinna	35
4.2 AM pinna analysis of variance for desktop vs industrial equipment comparison	46
4.3 KEMAR pinna vs 3D printed pinna acoustic measurements.....	56
Chapter 5: Conclusions and Recommendations for Furture Research	62
5.1 Conclusions.....	62
5.2 Recommendations for Future Research	64

References	66
Appendix	72
Vita	93

List of Tables

Table 3.2.1: AM pinna fabrication matrix	24
Table 4.1.1: Average percentage error for measuring tools.....	24
Table 4.2.1: Normal distribution test variables 1-4	24
Table 4.2.2: Normal distribution test variables 5-7	24
Table 4.2.3: GLM variable 1.....	24
Table 4.2.4: GLM variable 2.....	24
Table 4.2.5: GLM variable 3.....	24
Table 4.2.6: GLM variable 4.....	24
Table 4.2.7: GLM variable 5.....	24
Table 4.2.8: GLM variable 6.....	24
Table 4.2.9: GLM variable 7.....	24
Table 4.2.10: Kruskal-Wallis data vs users	24
Table 4.2.11: Kruskal-Wallis variable 1 vs users	24
Table 4.2.12: Kruskal-Wallis variable 3 vs users	24
Table 4.2.13: Kruskal-Wallis variable 5 vs users	24

List of Figures

Figure 3.1.1: Pinna design process	19
Figure 3.1.2: KEMAR manikin system	19
Figure 3.1.3: KEMAR small right pinna vs initial KEMAR CAD (GN)	19
Figure 3.1.4: Back interfaces of KEMAR right small ear	20
Figure 3.1.5: KEMAR interface features modeled and 3D printed	20
Figure 3.1.6: Pinna CAD (GN) surrounding box reconstruction.....	21
Figure 3.1.7: Right and left small KEMAR pinnae	22
Figure 3.1.8: 3D scanning vs CT scan on pinna's inner channels	23
Figure 3.1.9: CT scan file repaired	23
Figure 3.2.1 Material Extrusion AM pinna.....	25
Figure 3.2.2 Vat photopolymerization & material jetting AM pinna	266
Figure 3.2.3: First concept silicone casing for AM pinna.....	277
Figure 3.2.4: Silicone casing for AM pinna final concept fabrication.....	28
Figure 3.2.5 SLA Somos NeXt pinna in silicone casing	29
Figure 3.2.6 AM pinna with o-ring design	Error! Bookmark not defined.
Figure 3.3.1 AM pinnae placement on KEMAR	31
Figure 3.4.1: Headset design process.....	32
Figure 3.4.2: 3D scan of KEMAR head for headset design.....	32
Figure 3.4.3: Initial embedded pinna into headset design	333
Figure 3.4.4: Fabricated initial AM embedded pinna headset design.....	333
Figure 4.1.1: Dimensions methodology model used from Algazi et al. (2001).....	355
Figure 4.1.2: Image setup for NI Vision Assistant	36
Figure 4.1.3: CT scan at Desert Imaging	37
Figure 4.1.4: Material extrusion right pinna (GN) d1-d4	Error! Bookmark not defined.
Figure 4.1.5: Material extrusion right pinna (GN) d5-d7	Error! Bookmark not defined.
Figure 4.1.6: Vat photopolymerization & material jetting right pinna (GN) d1-d4	Error! Bookmark not defined.
Figure 4.1.7: Vat photopolymerization & material jetting right pinna (GN) d5-d7	Error! Bookmark not defined.
Figure 4.1.8: Material extrusion right pinna (UTEP) d1-d4	Error! Bookmark not defined.
Figure 4.1.9: Material extrusion right pinna (UTEP) d5-d7	Error! Bookmark not defined.
Figure 4.1.10: Vat photopolymerization & material jetting right pinna (UTEP) d1-d4	42
Figure 4.1.11: Vat photopolymerization & material jetting right pinna (UTEP) d5-d7	42
Figure 4.1.12: Material extrusion left pinna (UTEP) d1-d4	Error! Bookmark not defined.
Figure 4.1.13: Material extrusion left pinna (UTEP) d5-d7	Error! Bookmark not defined.
Figure 4.1.14: Vat photopolymerization & material jetting left pinna (UTEP) d1-d4	Error! Bookmark not defined.
Figure 4.1.15: Vat photopolymerization & material jetting left pinna (UTEP) d5-d7	Error! Bookmark not defined.
Figure 4.2.1: Pinnae for randomized study	59
Figure 4.2.2: Residuals normality plots variables 1 & 2.....	59
Figure 4.2.3: Residuals normality plots variables 3 & 4.....	59
Figure 4.2.4: Residuals normality plots variables 5 & 6.....	59
Figure 4.2.5: Residuals normality plots variables 7.....	593

Figure 4.2.6: Fisher's LSD KEMAR vs material extrusion.....	59
Figure 4.2.7: Fisher's LSD KEMAR vs vat photopolymerization/material jetting.....	59
Figure 4.2.8: Fisher's LSD material extrusion.....	596
Figure 4.2.9: Fisher's LSD vat photopolymerization	597
Figure 4.2.10: Fisher's LSD industrial systems.....	597
Figure 4.2.11: Fisher's LSD desktop system	598
Figure 4.3.1: AM pinnae tested on KEMAR manikin.....	599
Figure 4.3.2: Frequency response comparative between KEMAR and AM pinnae.....	60

Chapter 1: Introduction

1.1 Background

The research contained in this thesis, documents the fabrication of ear pinnae via additive manufacturing (AM), popularly known as 3D printing. Depending on several factors such as dimensional accuracy, mechanical performance, surface roughness, cost and numerous others, an appropriate AM technology and material can be selected for the desired end product. Having the 3D printed pinna interact with and serve as an extension of the human body would help preserve the spatial cues of incoming sound. Spatial cues refer to the ability to locate sound in space. Retaining sound localization and frequency in custom hearing protection devices will benefit various users and applications. Such devices have broad applications in environments where individuals require sound protection such as the battlefield, airport tarmacs, construction sites, concerts and other high intensity music venues. First responders in emergency situations, along with humans and pets with sensitive hearing, would also benefit from hearing protection. The retention of sound localization was needed for the end product to possess, and influenced the selection of the possible AM technologies to be employed. A common challenge for manufacturing ear models has been to create a product with a material that resembles human tissue. Both the AM technology and printed material were parameters selected during this research, although it should be stated that resembling human tissue was not considered during the material selection process. Industrial and desktop additive manufacturing equipment was selected to assess the dimensional capabilities to print a human pinna.

Current AM technologies are divided among seven process categories, and allow for rapid prototyping of complex features in a variety of fabrication techniques. The combination of 3D scanning equipment and Computer Aided Design (CAD) software also played an important role in producing an AM ear pinna. For computer modeling of custom ear pinnae, a 3D scanner can ensure that intricate features of the human ear are accurately modeled. Reichinger *et al.*, (2016) obtained pinnae 3D scanning accuracy results of 1.36 millimeters, but also mentioned that the complexity of the pinna features, such as undercuts and cavities, can lead to void creations within

the scan. These geometries would require further editing after a scan, in a mesh modeler and/or CAD software. Obtaining the corrected model, a Standard Tessellation Language (STL) file can be generated for processing through a slicer software for the 3D printer. 3D scanning, post-scanning edits, and STL file generation were all executed during this research, in addition to identifying the printing processes and materials to be explored. As previously stated, and as per ASTM International, there are seven process categories for AM technology, each of which interact with specific materials, whether they are polymers, metals, or ceramics, in liquid, powder, or filament form. Each process category is described in detail in the literature review section. This research was performed via collaboration between the W.M. Keck Center for 3D Innovation and G.N. Advanced Science (G.N. Hearing, Glenview, IL, USA).

1.2 Motivation

Additive manufacturing has proven to provide solutions to a wide spectrum of applications, whether it is producing a prototype turbine blade, or custom retainers for teeth alignment. The potential for customization with the AM process, and leveraging its innate flexibility, inspired the focused research of printing a hearing protection device with an embedded pinna for spatial cue preservation capabilities. Placing an individual's 3D printed pinna inside a custom headset would increase the device's functionality by preserving the ability to determine the location of the incoming sound. Understanding the concept behind localized sound can be very intriguing and at the same time very complex. The research presented here aims to replicate the ear pinna geometry, to allow the retention of spatial cues as a human ear would. Replicating the intricate features of a pinna through additive manufacturing may provide unique solutions to developments in the acoustic field and acoustic specific applications. Noteworthy characteristics of 3D printing are the time and material savings, along with the customization that can be achieved. A single change in the design can be easily executed through CAD software and sent to be 3D printed, within a short time frame. These beneficial factors are motivation to contribute towards the possibility of creating custom headsets for people. A personalized device could be implemented by incorporating each

individual's ear into the headset. A 3D scan could create the model from the individual's pinna, and after some CAD manipulation a custom 3D printed device could be created. Embedding a 3D printed pinna onto a headset would simulate an extension of an individual's ear, which is unique to every person. By following the presented hypothesis, retention of localization could be preserved within the custom device.

1.3 Objectives

The following are the objectives that shaped the completion of this thesis:

1. Accurately model a three-dimensional ear pinna geometry using computer aided software
2. Modify the design of the pinna to accommodate for 3D printing and the different tests performed
3. Additively manufacture the ear pinna model in a variety of 3D printing technologies to compare dimensional accuracy
4. Develop and design the headset concept with the embedded 3D printed pinna for the acoustic testing
5. Analyze the dimensional accuracy of the AM fabricated pinnae using different measurement equipment
6. Statistically evaluate the fabricated pinnae for dimensional accuracy by using a formal design of experiments
7. Compare the AM printed approach versus a standard acoustic testing model using an acoustic testing system

Chapter 2: Literature review

2.1 3D printing

Additive manufacturing (AM), also known as 3D printing, is the process of building a part layer-by-layer using a 3D computer model. In the past, this methodology has been referred to as rapid prototyping, solid freeform fabrication, and direct digital manufacturing, among others. According to Guo *et al.*, (2013), 3D printing has been around since the late 1980s, characterized by its ability to reduce the lead time while being cost effective in the creation of single and/or a small set of parts. AM offers the opportunity to create complex features not attainable using conventional/subtractive manufacturing, such as undercuts or inner channels within a part. This facilitates the fabrication of prototypes and functional parts. Depending on the material selection and end-use application, AM-fabricated parts can serve as tools and molds, (Guo *et al.*, 2013). The technology developed for processing a variety of materials within AM has grown exponentially over the last 20 years (Guo *et al.*, 2013). Some AM methods are well established, while others keep evolving, serving as benchmarks for new innovative methods. According to ISO/ASTM 52900-2015(E), the seven process categories of AM are vat photopolymerization, material extrusion, material jetting, binder jetting, powder bed fusion, sheet lamination, and directed energy deposition.

Vat photopolymerization, the first of the seven categories to be described, uses a photosensitive resin in a vat, which is cured selectively by an ultraviolet (UV) laser. Derived from the CAD model, an STL file is sliced into layers, each of which contains information for a single cross-section of the part (Melchels *et al.*, 2010). Those instructions are interpreted in the printer's software, and a single layer is scanned by the UV light source in accordance to the CAD model (Bikas *et al.*, 2015). After scanning, the platform drops the distance of one layer thickness, usually ranging from 25 to 100 micrometers (Melchels *et al.*, 2010). The uncured resin then flows on the surface and the next layer is cured. As the laser cures each layer, the preceding layer forms a bond with the newly cured resin. This process is repeated until all layers are cured, resulting in a part resembling the CAD model. The most commonly known technology from this category, within

the polymers liquid state, is Stereolithography (SL). Wong *et al.*, (2012) stated that SL was the first AM technology available in the market, created by 3D Systems. Some other vendors include EOS, CMET and Formlabs. SL machines can output a resolution around 50 micrometers (Stampfl *et al.*, 2008). Vaezi *et al.*, (2013) explained that SL is divided into two techniques, scanning SL and projection SL. SL scanning consists of a direct laser beam striking a movable platform with a photosensitive polymer (Bartolo, 2011). The SL projection method cures resins by shining a UV lamp through a mask (Bartolo, 2011). Benefits of the scanning SL method are that it achieves a higher quality surface finish and dimensional accuracy, while projection SL proved to have a shorter build time due to the ability to cure an entire layer via exposure through a mask (Vaezi *et al.*, 2013). There is a plethora of material selections for SL including metals, ceramics and polymers. Most of these materials are linked to specific 3D printers available in the market. A photoinduced polymer is required, to interact with the light source and start the polymerization with the focused laser. Depending on the wavelength of the light, accuracy and resolution of the final parts are affected (Bartolo, 2011). Surface finish and dimensional accuracy are important metrics in working with AM. These values determine if a printed model was manufactured to the anticipated dimensions of the computer designed model. Ippolito *et al.* (1995) explained how an SL printed part using 3D Systems' equipment was utilized for surface roughness and dimensional accuracy measurements. The roughness value RA is a detailed measurement of the elevation curve a layer produces for any type of material. In this case for the SL part, the RA was 3.7 micrometers (Ippolito *et al.*, 1995).

Material extrusion is currently the most known and utilized of the AM categories, as evidenced by the commercialization of desktop printers. Filament polymer additive manufacturing was developed in the 1980s (Guo *et al.*, 2013). The main components for material extrusion are the material feed mechanism, the liquefier, gantry, and build platform (Turner *et al.*, 2014). Fused deposition modeling (FDM) is a trademarked name of a 3D printing company, Stratasys, and consists of the placement of molten plastic filament onto a build area (Guo *et al.*, 2013). Although thermoplastic pellets are also under the material extrusion category, filament type material is the

most common feedstock for material extrusion (called fused filament fabrication or FFF in many cases other than the Stratasys FDM process). A set of rollers attached to a stepper motor drive the filament material through a gantry system. A liquefier located before the nozzle, melts the material before it extrudes from the nozzle and contacts the build platform. Once the molten material is deposited on the build platform, it solidifies creating a layer. The material must adhere properly to the build platform to avoid any printing issues. For this reason, the surface of the build plate may change depending on the material being extruded. Melted thermoplastic constantly extrudes through a nozzle mounted on the gantry system. The gantry follows machine instructions generated from the slicing software, to build parts one cross-sectional layer at a time. Consistent with AM, the deposited molten layer will adhere with the preceding layer. This process repeats until all layers are completed and the part is fabricated. Stratasys leads the FDM equipment manufacturing, although there are many rising companies around the globe such as 3D Systems Inc and Delta Micro Factory Corp (Turner *et al.*, 2014). Material extrusion materials are generally tougher and more durable than materials for SL processes because thermoplastics are more stable environmentally (Novakova-Marcincinova *et al.*, 2012). Some of the most common materials used for material extrusion are acrylonitrile butadiene styrene (ABS), which has great mechanical properties and bonds well; polycarbonate (PC) which possesses stronger mechanical properties than ABS; and ULTEM 9085 commonly used for high temperature applications due to its high glass transition temperature of 186°C (367°F) (Novakova-Marcincinova *et al.*, 2012). According to Turner *et al.*, (2014), resolution of a material extrusion part depends on the nozzle size, while dimensional accuracy relies on the CAD and the 3D printer's gantry being aligned properly. Other potential causes to undesirable resolution and dimensional accuracy, relate to the shrinkage and thermal warpage of a part as the temperature gradient between the bottom and top grows. Perez, (2002) published an analysis on the surface roughness of an FDM ABS quarter circle part. Using a profile rugosimeter Perez, (2002) obtained results as high as 7 micrometers.

Material jetting follows the principle of inkjet printing, placing droplets of material in a build platform (Vaezi *et al.*, 2013). One technique from material jetting, utilizing UV curable

polymer, is called Multi-Jet Modeling (MJM) developed by 3D Systems. According to Guo *et al.*, (2013), the print head possesses multiple nozzles which dispense drops of material onto a surface. Each droplet falls into the path generated from the CAD model. A UV lamp then flashes to cure the deposited polymer. This process continues layer-by-layer until the complete fabrication of the part. PolyJet by Stratasys is another material jetting technology, producing the commercially available Objet Connex Series. It uses a print head with several individual nozzles that deposit drops of material to create layers as small as 16 micrometers (Vaezi *et al.*, 2013). These PolyJet printers have the ability of 3D printing two different materials to provide a variety of concentrations and structures, also known as digital materials (Zhou *et al.*, 2011). The material selection of photopolymers ranges from rigid to flexible, including custom shore grade options to print as well (Vaezi *et al.*, 2013). Bickel *et al.*, (2010) used the Objet to fabricate deformable parts of shore 50, using VeroWhite (hard acrylic) and Tango Black Plus (flexible urethane), then using Finite Element Analysis (FEA), compared them to other manufactured deformable parts, such as foams for compression testing. Roughness tests on these materials were tested by Pilipovic *et al.*, (2009). Test results showed that VeroBlack's mean arithmetic deviation on the RA was of 1.64 micrometers, while another material called FullCure, a rigid transparent acrylic, had a mean arithmetic deviation RA of 1 micrometer.

The most commonly used AM process for ceramics is binder jetting, although metals are also used. The inkjet technology-based binder jetting was developed at the Massachusetts Institute of Technology (MIT) (Vaezi *et al.*, 2013). Some of the powders used for this technology are glass and graphite, among the ceramics, as well as Al-based, Cu-based, and Fe-based among the metal/alloy materials (Gokuldoss *et al.*, 2017). Similar to other processes, binder jetting requires a CAD model from which instructions are extracted for fabricating a part (Gaytan *et al.*, 2015). The main difference lies in the jetting of binder, and the use of powder materials. Two materials are used during the 3D printing process; the binder material selected for the part and a sacrificial binder material which is used to bond powder particles selectively to create layers (Gokuldoss *et al.*, 2017). Ceramic/metal in the form of powders are spread over the build plate using a roller, while

the printing beds are mechanically moving in the horizontal direction under the roller. After uniformly laying a powder layer, the build platform returns to its original position and binder liquids are selectively deposited through an inkjet print head. A post process is needed once the part is printed to have a functional part (Gokuldoss *et al.*, 2017). Some examples of these processes are curing, annealing, sintering, etc. In some situations, the post process is more time consuming than the 3D printing itself. Gokuldoss *et al.*, (2017), stated that different combinations with the two-powder ratio selection can give a variety of outputs regarding the mechanical properties of the printed material.

Powder bed fusion AM has developed the ability to build metallic structures in layers. Energy sources employed for AM of metals include electron beam, laser beam, and plasma arc. Powder bed systems, such as the A2 designed by the Swedish company ARCAM, uses electron beam melting (EBM) to join metal powders (Herderick, 2011). There are other powder bed methods, such as direct metal laser sintering (DMLS) and selective laser melting (SLM). Commercially available metal alloys for AM include Ti-6Al-4V, Inconel 718, Stainless Steel 316, among others (Frazier, 2014). Research has been performed on these and other metals to understand the complex process parameters employed depending on the system being used. Murr *et al.* (2012). showed that for EBM and SLM, manipulating parameters such as the print environment, melt scan speed, melt pool dimension, and build speed, affect the overall microstructure of fabricated parts. Any fabricated metal AM process requires post-processing steps performed before end-use application. These post-processing steps may include removing excess powder, removing the component from the build plate, machining of the surface to reduce surface roughness, or even performing thermal treatments to improve mechanical properties (Sames, *et al.* 2016). In comparison to traditional machining, metal AM technology presents an opportunity for mass customization, waste reduction, and quality control (Bak, 2003). However, there are some challenges with producing a part that is ready to use, without some post-processing.

The sheet lamination process consists of placing thin film layers of material on top of each other. One method of sheet lamination uses ultrasonic welding to join the two films together (Tapia

et al., 2014). This method is called Ultrasonic Consolidation (UC) and according to (Vaezi *et al.*, 2013) it is considered a hybrid method due to addition of a subtractive technology to reduce post-processing. The amplitude frequency the ultrasonic exerts creates a solid-state weld, bonding the two layers without reaching the material's melting point (Tapia *et al.*, 2014). After the ultrasonic tool has secured the layer, a milling tool trims down the excess material. This process is repeated until the part is finished. The other method for sheet lamination is Laminated Object Manufacture (LOM) and consists of bonding sheet by sheet of material with glue or adhesive. Once the sheet is placed, a heated roller passes over the material to secure adhesion (Bikas *et al.*, 2016). A laser then cuts the contour and features specified on the CAD's layer. Several metals and ceramics can be used in this technology, including silicon carbide and silicon carbide composites (Vaezi *et al.*, 2013). According to Kruth *et al.*, (1998) some of the challenges regarding sheet lamination are delamination which can cause dimensional inconsistencies throughout the printed part.

Direct energy deposition (DED) is the technology which fuses dispensed material with an energy source (Tapia *et al.*, 2014). Different processes of DED are available depending of the energy source (Ding *et al.*, 2015). The Laser Engineering Net Shape (LENS) technology by Optomec works with a nozzle that extracts powder directly towards a targeted position laser beam, using pressurized gas or simply gravity (Bikas *et al.*, 2016). The interaction between the laser and powder creates a layer of material. Both the nozzle and the laser are one unit and move within the same system (Bikas *et al.*, 2016). Direct metal deposition (DMD) consists of a laser sintering powder material to replicate the CAD model. Similar to LENS, the powder gets deposited by a nozzle creating a pool to raise the material's volume (Peyre *et al.*, 2008). A range of metals such as titanium, stainless steel, and nickel base super alloys are available for these technologies (Vaezi *et al.*, 2013). An advantage of this technology is that full density can be accomplished by changing parameters such as material, laser power, power feed motor, etc. Another DED technology is electron beam freeform fabrication (EBF) and it was developed by NASA Langley Research Center. This process works by using a high power electron beam which strikes a wire fed material (Taminger *et al.*, 2013). EBF works in a vacuum environment. Taminger *et al.*, (2013) documents

initial testing was performed using aluminum and titanium alloys. Wire and arc additive manufacturing, is a technology that uses an electric arc as a heat source and wire as feedstock. It has been known to use commercially available welding equipment, such as metal inert gas (MIG) power sources (Williams *et al.*, 2016). The process consists of having the consumable electrode wire stand coaxial to the welding torch, fusing the material into a platform creating a layer-by-layer part. Materials that have been printed successfully using this technology include titanium alloys, aluminum, and steel among others (Williams *et al.*, 2016).

2.2 3D scanning & CT scanning

3D scanning is commonly known as the method of capturing three-dimensional data from the physical world and converting it into a three-dimensional computer model (Yao *et al.*, 2005). The most common 3D scanning machine is a contact type, in which a probe touches the X, Y, Z points of an object to create profile data. Another method described by Yao *et al.*, (2005), is a non-contact system where a laser or LED photo source interacts with a camera. Laser triangulation, as described in Acosta *et al.*, (2006), is a scanner system that was fabricated using a line laser generator and a Logitech Quick Pro webcam. The camera identified the pixels of an image where the laser was concentrated, taking two images, one with the laser and one without. These two images would then be subtracted to obtain the desired pixels, which would translate to the computer model as cloud points (Acosta *et al.*, 2006). This is one of the fastest methods of 3D scanning that exists (Yao *et al.*, 2005). Once all the points are obtained, a stitching process takes place to create a solid computer model. Four axis equipment such as the eviXmatic HD Quadro Scanner (Evatronix S.A., Bielsko-Biala, Poland) can produce scans with accuracies up to 13 microns (Evatronix S.A., 2019), while an 8-axis FARO ScanArm (FARO Technologies, Lake Mary, FL, USA) has a reported resolution of 75 microns (FARO Technologies, 2018).

Another method to obtain computational models is via helical computed tomography (CT) technologies, which were introduced for clinical usage by Siemens Medical Systems in 1988 (Rydberg *et al.*, 2000). According to Rengler *et al.*, 2010, the evolution of multidetector computed

tomography (MDCT) has improved the radiology diagnostics in terms on image acquisition. A single-section helical CT scanner has one x-ray tube and one row of 500 to 900 detectors with a gantry rotation speed of 1 second per 360 degree, whereas MDCT may have multiple rows of 500 to 900 detectors with a rotation speed nearing 0.5 seconds (Rydberg *et al.*, 2000). The image quality can be determined by the scanner and the scanning parameters, such as tube current, tube voltage and slice thickness among others (Verdun *et al.*, 2015). Resolution can be measured by slice thickness, where Siemens Biograph 64 PET/CT operates with a slice thickness of 0.33 mm (Siemens AG, Munich, Germany) (Siemens, 2009) while Canon Aquilion One has a 0.5 mm resolution (Canon Medical Systems Corporation, Tochigi Prefecture, Japan) (Canon Medical Systems Corporation, 2018). Modern medical imaging obtained from methods such as the CT scanning, requires the images processed to carry as much information as needed for it to be used in its corresponding application (Doi, 2006). Although image noise can be generated by different sources from the CT scanner, such as the detector readout circuits (Verdun *et al.*, 2015), different post processing 3D modeling tools possess segmentation tools to select specific regions or surfaces for 3D rendering (Rydberg *et al.*, 2000). Doyle *et al.*, 2008, explained how using Mimics (Materialise, Leuven, Belgium), the 2D CT scan files were converted to a 3D computational model by using the regions of interest from the CT scan.

2.3 3D printed ear pinnae

Additively manufactured ear prosthetics have been around for several years, employing different technologies to manufacture them. Selection of the specific 3D printing technologies was dictated by the purpose of the prosthesis. Some researchers have integrated multi-functionality into additively manufactured ear pinna. In the case presented by Suaste-Gómez *et al.*, (2016), an ear prosthesis was developed with polyvinylidene fluoride (PVDF). This material possesses piezoelectric, pyroelectric, and ferroelectric properties that were used to characterize pressure and temperature of the pinna. According to Suaste-Gómez *et al.*, (2016), the ear model was designed in accordance to anthropometric parameters, and by using a 3D computer graphics software, a

stereolithography (STL) file was extracted. In this case, the technology employed for prosthesis manufacturing was material extrusion, using a Bits from Bytes (BFB) 3D printer. The layer thickness used was 0.13 mm (0.005”) and the infill material percentage used to print the part was 40%. Suaste-Gómez *et al.*, (2016) stated that the PVDF ear prosthesis was successfully 3D printed and obtained satisfactory results on ferroelectric hysteresis loop measurements, preserving the properties of material after extrusion. Manoor *et al.*, (2013) bionic ears are another example of multi-functional 3D printed pinnae. Manoor *et al.*, (2013) explains the challenges with attempting to mimic native human tissue. A successful replica would not only consist of the aesthetic and visual representation of the prosthesis, but also the functionality a human pinna possesses. The research Manoor *et al.*, (2013) presented was on the combination of 3D printed living cells with a chondrocyte-seeded alginate hydrogel matrix, along with electronic components printed with conductive silver nanoparticles (AgNP). An assembly of the pinna was generated in a CAD software, including distinct sections for each of the materials. The printed cells, hydrogel matrix, and nonconductive silicone were introduced separately into syringes, housed within a syringe extrusion system called Fab@Home 3D printer (The NextFab Store). This allowed for the fabrication to be performed in a single process, resulting in a multi material ear exhibiting acceptable structural integrity after the print. Manoor *et al.*, (2013) concluded that by utilizing the process of additive manufacturing, issues with non-uniformity in seeding alignment were mitigated.

Pinna design and fabrication research has a subsection focused primarily on aesthetics of the prosthesis. Different materials have been used to fabricate an ear prosthesis giving the impression of a real human ear. Xiao *et al.*, (2013) followed the process of 3D scanning to rapid prototyping, to manufacture a pinna with the same color pigmentation as human skin. A 3D photogrammetry system (three pod cameras) was used to capture the computer image of the ear prosthesis. Xiao *et al.*, (2013) used the Z Corp Z510 (3D Systems Inc.), a binder color 3D printing system. Starch powder with a resolution of 0.5 mm (0.02” approximately) was used for printing. Xiao *et al.*, (2013) applied a post process step, to infiltrate the printed object with clear medical

grade silicone (Silkskin 25). The manufactured pinna by Xiao *et al.*, (2013) demonstrated the ability to capture the color needed for reproducing human skin tones. Mohammed *et al.*, (2017) manufactured a similar ear prototype using polyjet multi material technology (Objet 500 Connex). The reasoning behind using this equipment was to obtain a hard-elastic material, and the skin pigmentation required to simulate that of a human ear. The high-resolution (16 to 30 micrometers) provided by the printer contributed to the high-quality surface finish (Mohammed *et al.*, 2017). The material selection for this study was Tango Plus, which has rubber-like properties, and VeroMagenta, a hard shell resin by Stratasys, with colored pigmentation. Mohammed *et al.*, (2017) stated that the combination of these two materials during the print exerted different results depending on the ratio being used. According to Mohammed *et al.*, (2017), a minimum of ten percent of VeroMagenta was needed to provide a visual pigmentation on the ear, while Tango Plus provided the tactile simulation. After experimentation, Mohammed *et al.*, (2017) demonstrated a fabricated ear that when exposed to a compressive force, was capable of reshaping into its original configuration. Mohammed *et al.*, (2017) ear prosthetics were additively manufactured with a high detailed surface finish.

A similar study made by Harder *et al.*, (2016) manufactured the ears as well as the head for a head-ear assembly testing of head related transfer functions (HRTFs). A multi-material polyjet machine was used, the Objet500 Connex (Stratasys). The layer thickness used for this process was 0.03 mm (approximately 0.001"). The ear consisted of a hard-acrylic core printed with VeroWhite, and a softer outer area printed with Tango Plus (Harder *et al.*, 2016). The selection of these materials was made to create a soft material, which could potentially help with the placement of hearing aids. HRTF's studies were performed using human listeners, 3D printed ears, and computational simulations. Results showed similar spectral cues among the human and printed head measurements within the 5 dB range, while the simulation data showed differences of 14 dB (Harder *et al.*, 2016).

Liacouras *et al.*, (2011) presented a medical case in which the patient lost his ear due to a disease. Using additive manufacturing, a new ear pinna was constructed for aesthetic purposes.

The process Liacouras *et al.*, (2011) followed was to obtain the dimensions from the good ear, which were taken using a Computer Tomography (CT) scan. Once the images were obtained, these were transferred to a computer software that converted the point cloud into an STL file. The file was modified to serve as a mold for the pinna. This STL was then exported to a Z Printer (Z corp) to print the mold. A silicone elastomer was injected into the 3D printed mold used to manufacture the final pinna, which served as an implant for the patient.

The additive manufacturing process has played a role in auricular reconstruction. Flores *et al.*, (2017) argued that a total ear reconstruction can become challenging to accomplish due to the anatomy and complexity of the ear pinna. In Flores *et al.*, (2017), a patient with microtia, a congenital ear malformation, had the unaffected ear 3D scanned via high resolution 3D photography. The generated file was uploaded into a 3D graphics software to sculpt and better define the complex areas of the pinna. Once these areas were defined in the computer modeler, the Builder Premium 3D Printer (Builder 3D Printers B.V.), which used material extrusion, was used to print the pinna model, as well as some pinna features (Flores *et al.*, 2017). The material used for this process was white polylactic acid (PLA) with a layer-to-layer resolution of 200 μm . Flores *et al.*, (2017) stated that before the surgical insertion of the 3D printed parts, a sterilization process took place. Flores *et al.*, (2017) reconstruction not only proved to be successful in the fabrication and placement of the product into the patient, but also proved to be cost beneficial.

2.4 Acoustics

The preservation of spatial cues is a research field that has been active for years. Localization of sound can be more intricate than visual localization, where the visual optics allow for the perception of an object's location directly from the eyes, while the combination of the interaction between head/ears and the incoming sound wave interpret sound location from an external source (Middlebrooks & Green 1991). Although the actual capturing of the spatial cues for sound localization and expanding it to sound externalization has been and continues a hard task to accomplish, research has been done performing different testing models. According to Gardner

et al. (1995), the torso, head, and the external ears are the main contributors to the sound localization from the auditory cues. An individual can be exposed to a sound source which can come from any position around the individual's head (Middlebrooks & Green 1991). The dimensions used in two-dimensional sound localization are azimuth and elevation. Azimuth is the horizontal dimensional angle from the sound source with respect to the center of the listener's head on the median plane (Middlebrooks & Green 1991). Elevation is the angle on the horizontal plane that defines the height from the sound source to the center of the head (Middlebrooks & Green 1991). Having the two dimensions at the origin position ($0^\circ, 0^\circ$) places the sound source location in front of the subject at the height centerline from the head (Middlebrooks & Green 1991). The sound localization cues can be captured through the head-related transfer functions (HRTFs). An HRTF is a frequency response which reports the sound pressure from a specific sound source location to the eardrum and/or ear canal (Gardner *et al.* 1995). Perceptual distortions can be encountered on the person to person HRTF variation (Algazi *et al.* 2001), making the HRTF data collection using individuals or manikin systems very complex (Gardner *et al.* 1995).

A system was developed in 1972 that revolutionized the way acoustical testing was performed. During this period, microphones were placed on individuals at different orientations and angles to account for the standard free field hearing aid response testing of a particular subject (Burkhard & Sachs 1975). The KEMAR (Knowles Electronics Manikin for Acoustic Research) was developed to use a real scenario testing device on different hearing aid fittings (Burkhard & Sachs 1975). The KEMAR was designed to be the average anthropometric dimensions of an adult, including the human pinna, and having the ear canal and eardrum be identical to that of humans (Burkhard & Sachs 1975). Another key incorporation to the KEMAR design was to have a system of interchangeable pinnae to allow for exploration of different ear geometries and its effects on acoustic performance (Burkhard & Sachs 1975). This manikin system was designed and fabricated using an average human adult dimensions, giving special consideration to the torso and the head which were noted to be the most critical to reproduce (Burkhard & Sachs 1975). Many tests have

been conducted using the KEMAR system as a baseline to a real person. To facilitate readings from the KEMAR system, tests are usually conducted in an anechoic chamber.

Spatial cues through headphones can be determined through acoustic waveforms, and depending on how these waveforms are perceived, can be divided into two sections; internalization and externalization. Internalized sound is present when sound gets perceived by the inside of the head, while externalized sound comes from a sound source located outside of the head (Kulkarni & Colburn 2001). Preserving the externalization of sound by the use of headphones has been an area of research within acoustic studies. Sound sources can be located on the basis of interaural differences in signal intensity and arrival time of the acoustic waveforms (Hartmann & Wittenberg 1996). Talcott *et al.* 2012 performed an experimental procedure to compare the response of open ear noise to different hearing protection-enhancement devices (HPED), including the Peltor Com-Tac II electronic earmuff (3m, Maplewood, MN). The results showed that significant statistical differences between the Com-Tac II the open ear in several noise conditions such as truck noise and gun shots (Talcott *et al.* 2012).

2.5 Embedded electronics

As AM technologies matured, component design bore a shift, extending beyond common structural applications. Slicing a CAD solid via STL into layers, in addition to print build interrupts, bestowed access to every layer of fabrication to the user (Wong, *et al.* 2012). Intimacy with the process simplified modification, thus triggering the emergence of embedded electronics within printed substrates (Espalin, *et al.* 2014) (Perez, *et al.* 2013). Early work in printed circuitry required the development of conductive traces (Roberson, *et al.* 2011). Having obtained methods for transferring current to power electronics within a printed part, small electronic components such as batteries, sensors, and microcontrollers were designed into printed parts (MacDonald, *et al.* 2014). The concept of interconnecting electronics within a printed substrate was later implemented in the fabrication of printed electronics, primarily within stereolithography and FDM (Joe Lopes, *et al.* 2012). Muse *et al.* (2018) patented the process for fabricating an electronic

gaming die with conductive inks and small electronics embedded in an SL part. Embedded sensors in particular, were a topic of research by several members of the AM community (Shemelya, *et al.* 2013) (Muth, *et al.* 2014) (Ota, *et al.* 2016).

Within the AM technology of material extrusion, research at the W.M. Keck Center for 3D Innovation led to the development of solid conductor embedding (Espalin, *et al.* 2017). Other research was focused on the introduction of embedding metal meshes and copper foils (Shemelya, *et al.* 2015) (MacDonald, *et al.* 2018). Demonstrating an in-depth understanding of wire embedding within substrates, the Keck Center developed the Foundry Multi^{3D} System, capable of transferring a workpiece throughout a layout of both additive and subtractive manufacturing stations (Ambriz, *et al.* 2017), with the use of a six-axis robot arm. While work was performed using robotics for multidirectional AM, the focus of the Foundry System was in employing the robot arm as a material handler (Song, *et al.* 2015). The ability to control build interrupts while transferring the workpiece, led to what was referred to as an “increase in component functionality” (MacDonald, *et al.* 2016) (Coronel, *et al.* 2017). This referred to the ability to embed wires and small electronics within a printed substrate, that would result in a part functional beyond only structure. Along with integrating wiring and electronics, it must be noted that commercially available software did not account for the added complexity of embedded items within the generation of files for AM. Bailey, *et al.* (2018) detailed the development of custom CAD software with the ability to process files for both printing, and embedding wires. As AM continues to grow, the implementation of embedded electronics will be facilitated, leading to rapid fabrication of circuitry driven designs.

Chapter 3: Experimental setup and procedures

3.1 Ear pinna 3D modeling

To begin the design and fabrication process of the custom hearing device, the computer model of an ear pinna was created. A successful replica of an individual pinna would entail that the spatial cues of said individual would be retained. Once an ear pinna was modeled, modifications were made using a CAD software to prepare a part that could be 3D printed. The additively manufactured pinna was then placed in a manikin system where acoustic measurements were made. Figure 3.1.1 shows a flow chart of the overall design process.

The first ear pinna model that was reproduced using computer modeling, was the small right pinna for KEMAR (G.R.A.S Sound & Vibration, Twinsburg, OH, USA), an anthropometric manikin used for acoustic research purposes. The KEMAR system consists of a head and a torso (Figure 3.1.2). Sound capturing electronics such as microphones are placed inside of the head,

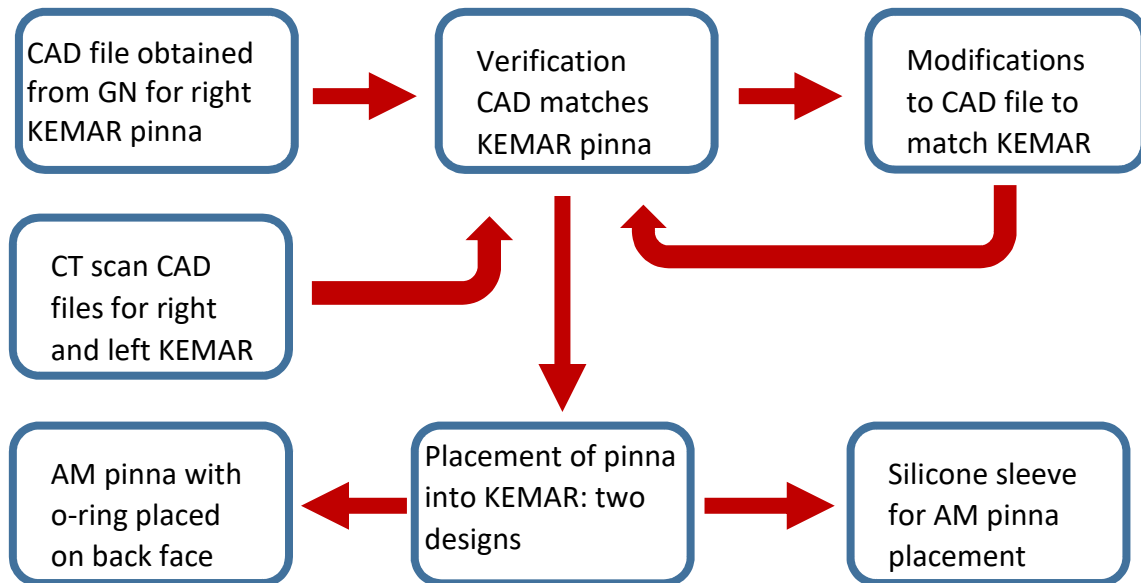


Figure 3.1.1: Pinna design process

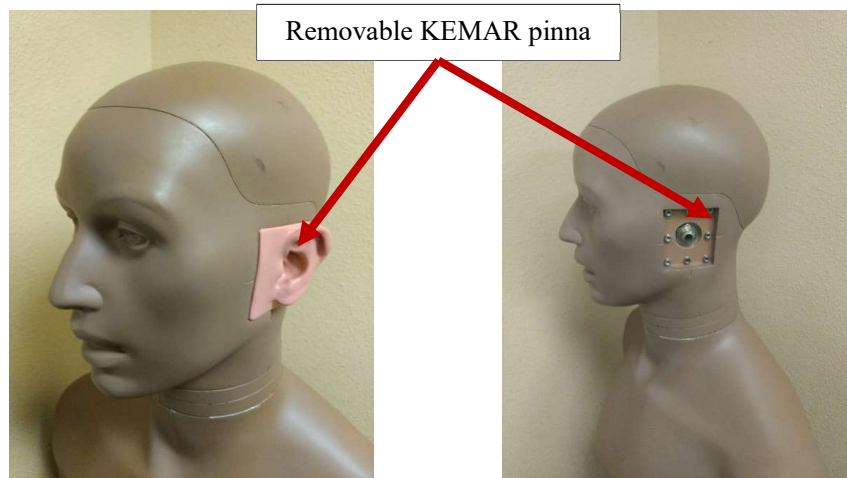


Figure 3.1.2: KEMAR manikin system

while different ear pinnae models can be placed in slots on the outer part of the head. The KEMAR pinna is made of a soft and flexible silicone, shore 55-00, which press fits onto the KEMAR head. This KEMAR right small pinna was 3D scanned by G.N. Advanced Science using a 3Shape HD600 (3Shape, Copenhagen, Denmark). An STL file was then acquired from that 3D scan and shared with UTEP for 3D printing. This CAD was referred to as the GN pinna model, and served as the initial benchmark CAD for modeling and printing (Figure 3.1.3). While the STL file preserved the geometry of the ear, it required modifications to the surrounding box and the interface features which attach to the KEMAR head (Figure 3.1.4). The matching interfaces required reconstruction, since the pinna at its current state would not mate with the KEMAR. The



Figure 3.1.3: KEMAR small right pinna vs initial KEMAR CAD (GN)

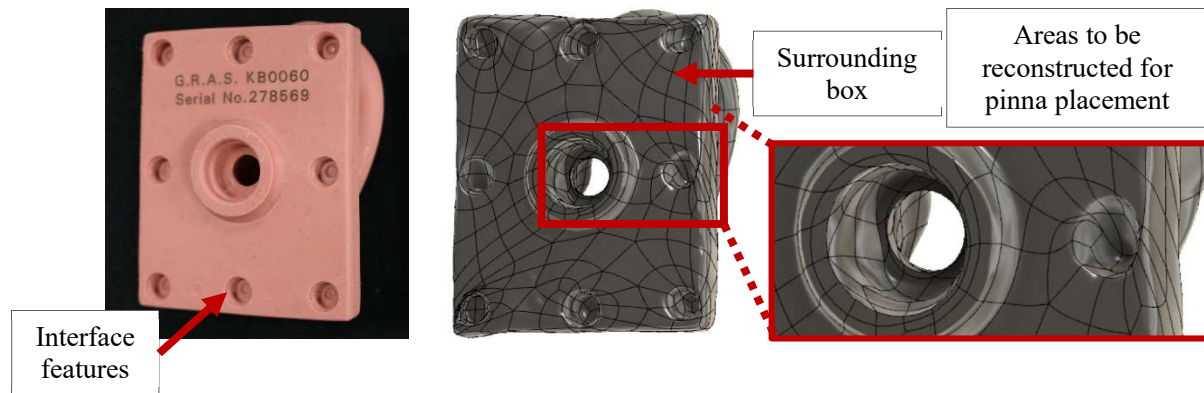


Figure 3.1.4: Back interfaces of KEMAR right small ear

interface features on the KEMAR serve to align the pinna correctly with the ear canal on the manikin head. Measurements were taken of the interface features of the KEMAR head using a caliper. Once measurements were obtained, a fit test sample of the interface features was made using the CAD software Fusion 360 (Autodesk, San Rafael, CA, USA). The model was 3D printed using a Stratasys' Fortus 400mc with polycarbonate (PC) material. The fit test sample was able to corroborate more precise locations of the matching interfaces on the KEMAR head (Figure 3.1.5). The CAD file for the interfaces was then merged to the initial KEMAR pinna CAD file.

An issue was encountered after the newly modified pinna model was 3D printed with the Fortus 400mc. Some regions of the AM pinna surrounding box did not directly match the KEMAR pinna. The original KEMAR pinna box had uneven surfaces, emulating the irregular surfaces of a human head. To attain acceptable acoustic readings from the KEMAR system, the entire pinna

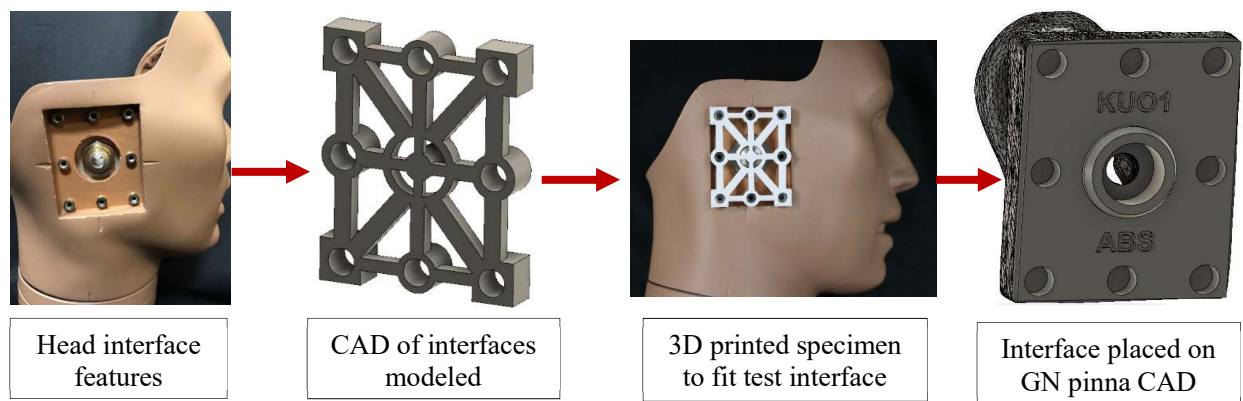


Figure 3.1.5: KEMAR interface features modeled and 3D printed

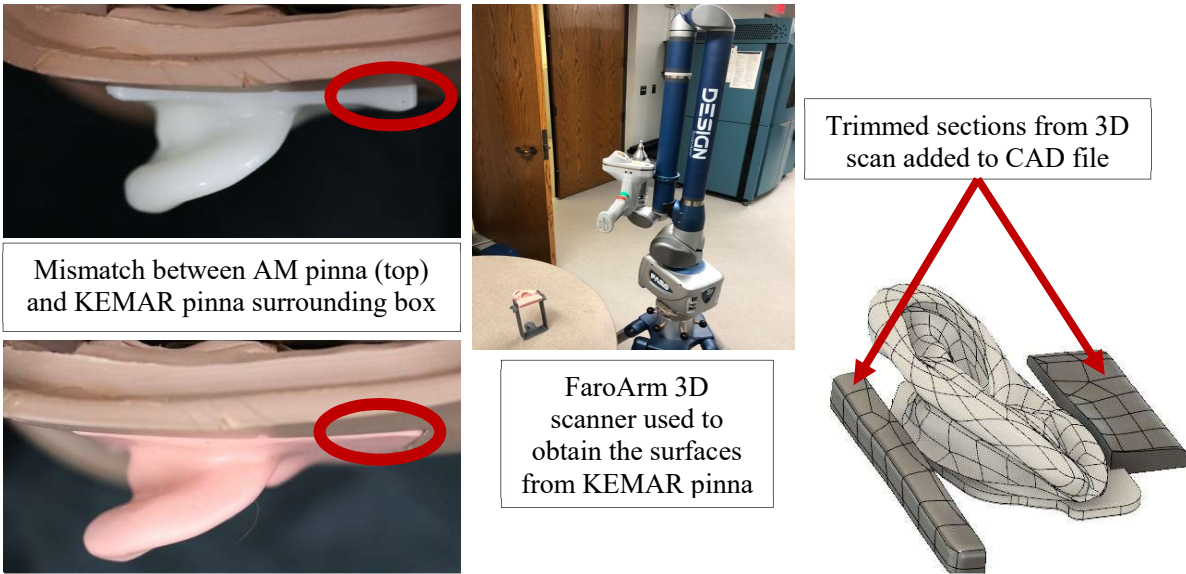


Figure 3.1.6: Pinna CAD (GN) surrounding box reconstruction

including the surrounding box, would have to be reproduced to more precise dimensions (within approximately ± 0.03 mm). The surfaces near the corners of the surrounding box of the right KEMAR pinna were different to the 3D printed pinna. Reconstruction of the erroneous sections was implemented on the model. The first approach was to modify the pinna STL file according to caliper measurements by using Meshmixer (Autodesk, San Rafael, CA, USA), a 3D sculpting CAD software. Caliper measurements were taken using a Mitutoyo 500-196-30 AOS Absolute Caliper (Mitutoyo, Kawasaki, Japan) of the heights for each corner on the surrounding box of the KEMAR pinna. Some regions and faces from the STL, especially the corners of the surrounding box, were smoothed out to match KEMAR's ear. Fusion 360 was used to model the remaining features from the STL file. The contour of the surrounding box was challenging to repair, so a different approach was taken. An 8-axis Faro ScanArm (FARO Technologies, Lake Mary, FL, USA) housed at the Keck Center was used to scan the perimeter of the outer box of the right pinna model. After the scan was completed, the 3D scan point cloud file was then transformed to an STL file with Geomagic Design X (3D systems, Rock Hill, SC, USA). This new pinna STL file was uploaded to the Fusion 360 design space to be modeled. The corner sections of the Keck 3D scan STL were trimmed and merged with the initial GN pinna CAD (Figure 3.1.6). At this point, three

CAD files were stitched together to obtain a final model. These were 1) the GN 3D scan, 2) the Keck 3D scan, and 3) the interface feature CAD. Merging the files allowed for the capture of specific features to obtain the best representation of the small right GN KEMAR pinna within the ± 0.03 mm. Once complete, the final CAD file was ready for fabrication.

To validate the spectral cues within the KEMAR system using the additive manufacturing approach, both pinnae, left and right, needed to be fabricated. The acoustic measurements on KEMAR could be performed by only using one pinna, but having the two pinnae could provide a better understanding on how the pinna was capturing the sound frequency. Each pinna differed in geometry (Figure 3.1.7), while possessing different box shapes as well. The small left KEMAR

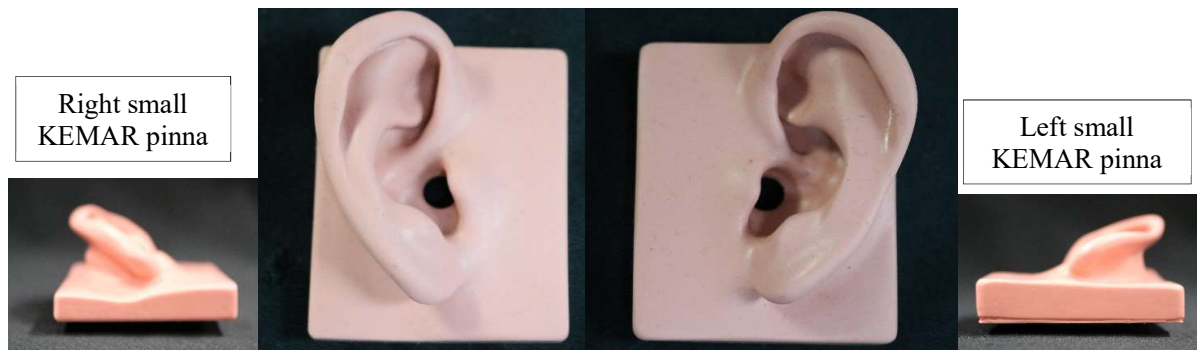


Figure 3.1.7: Right and left small KEMAR pinnae

pinna CAD was not provided by GN Advanced Science, therefore a computer model was obtained internally. 3D scanning using the FARO ScanArm was used as a first attempt for capturing this model. Most of the small left KEMAR pinna was captured, with the exception of sections that were difficult to scan. Some of the undercuts and inner channels of the ear were not fully scanned because of access issues (Figure 3.1.8). A solution to this problem was using a computerized tomography (CT) scan. For further data analysis, both the right and left small KEMAR ears were CT scanned using a 64-Slice GE VCT PET/CT scanner (GE Healthcare, Chicago, IL, USA) at a radiology center in El Paso, TX called Desert Imaging. The CT scan was performed using the parameters for an ear scan, which has the smallest interval per image captured, helical cut thickness

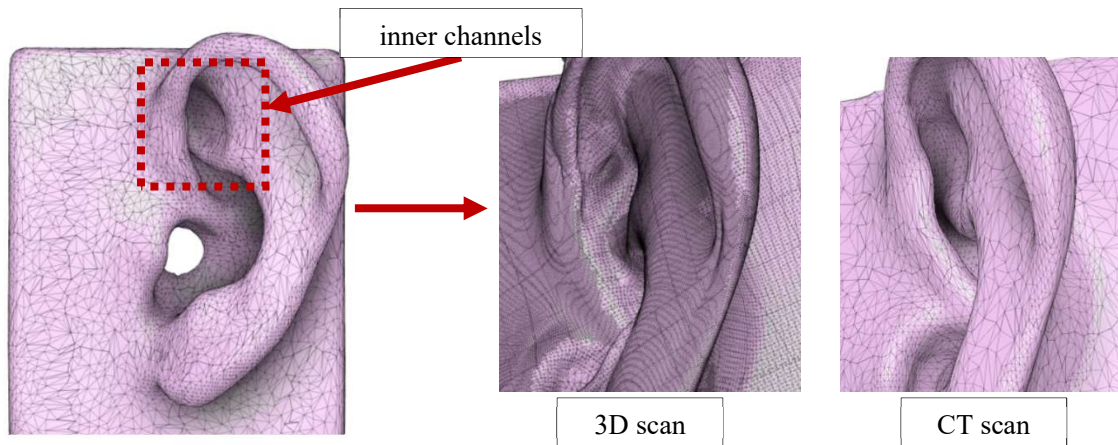


Figure 3.1.8: 3D scanning vs CT scan on pinna's inner channels

of 0.625 mm. Several images from the CT scan were compiled to capture a 3D model. After the scan file was obtained, it was converted to an STL file using the medical imaging process software Mimics (Materialise, Leuven, Belgium), which generates an output STL file processed according to the selected density of the part within the CT scan file. The resulting file from the CT scan was had a finer point cloud resolution than the one obtained from the 3D scan in capturing the inner channels of the pinna (Figure 3.1.8). When the CT scan STL was opened in Fusion 360, discrepancies were noticed on the top and bottom areas of the pinna. It appeared as if the pinnae models had sections trimmed off. This could have been due to two reasons; the density selected in

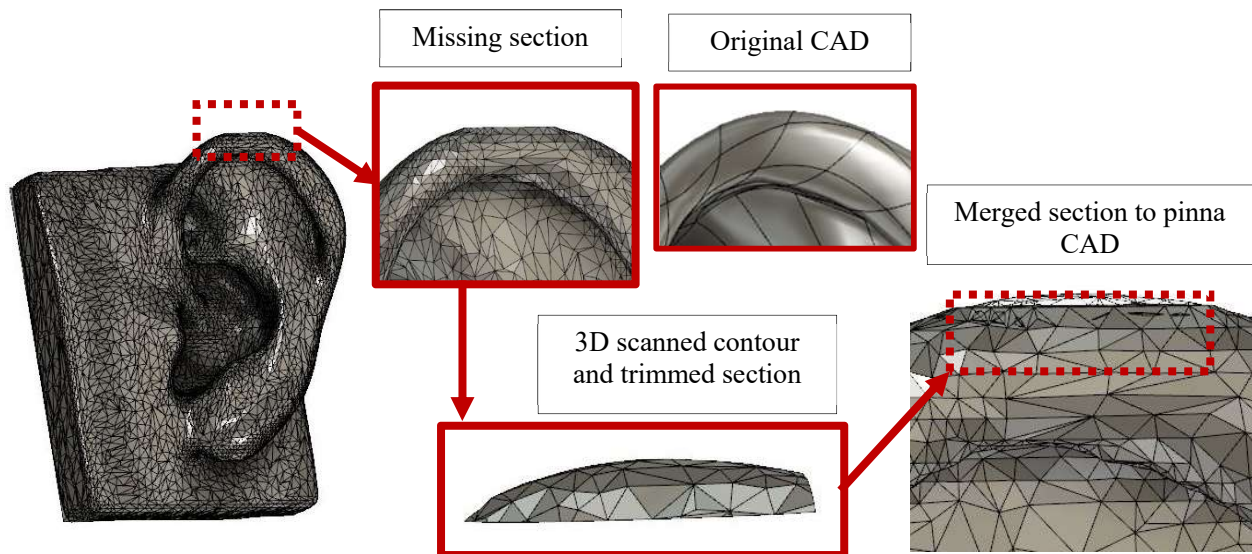


Figure 3.1.9: CT scan file repaired

Mimics at which the STL was processed or the CT scanning process itself. No other irregularities were found on the CT scan file besides these sections. The same process performed with the surrounding box on the previous right GN KEMAR pinna 3D model was used to account for this issue. The FARO ScanArm was used to scan the outer contour of both KEMAR pinnae. The STL files from the FARO 3D scan were then merged to the STL files from the CT scan (Figure 3.1.9). The corrected CT scan files were then amalgamated with the interface feature CAD used for the GN pinna 3D model. These two new models obtained from the CT scan were referred as UTEP right and UTEP left pinna.

3.2 Pinna 3D printing fabrication

The primary goal of this research was to use additive manufacturing technologies to replicate the pinna shape. The Keck Center houses all seven AM processes, allowing the exploration in terms of producing printed pinnae. The technologies had to be selected according to material and manufacturing feasibility. Production time, cost, and accessibility between the different 3D printing technologies and equipment was taken into consideration in terms of fabricating an AM customizable headset device with an embedded pinna. Though industrial AM equipment could produce a higher quality part, it may not be accessible and/or financially viable for a particular dispenser or at the point of need that could require a faster response. Being able to print an AM pinna using a desktop system can potentially aid the manufacturing and distribution model. Making a comparison between different materials and equipment used within AM technologies, along with acoustic measurement testing, determined the best approach for fabricating these custom hearing devices. The three process categories explored were material

Table 3.2.1: AM pinna fabrication matrix

	System (material) for AM pinnae fabrication		
	Material Extrusion	Vat Photopolymerization	Material Jetting
Industrial	FDM Fortus 400 mc (PC)	Viper SLA (Somos NeXt)	J750 (Shore 40 A)
Desktop	uPrint (ABS)	Form 2 (Tough Resin)	
	Lulzbot Taz 6 (ABS)		

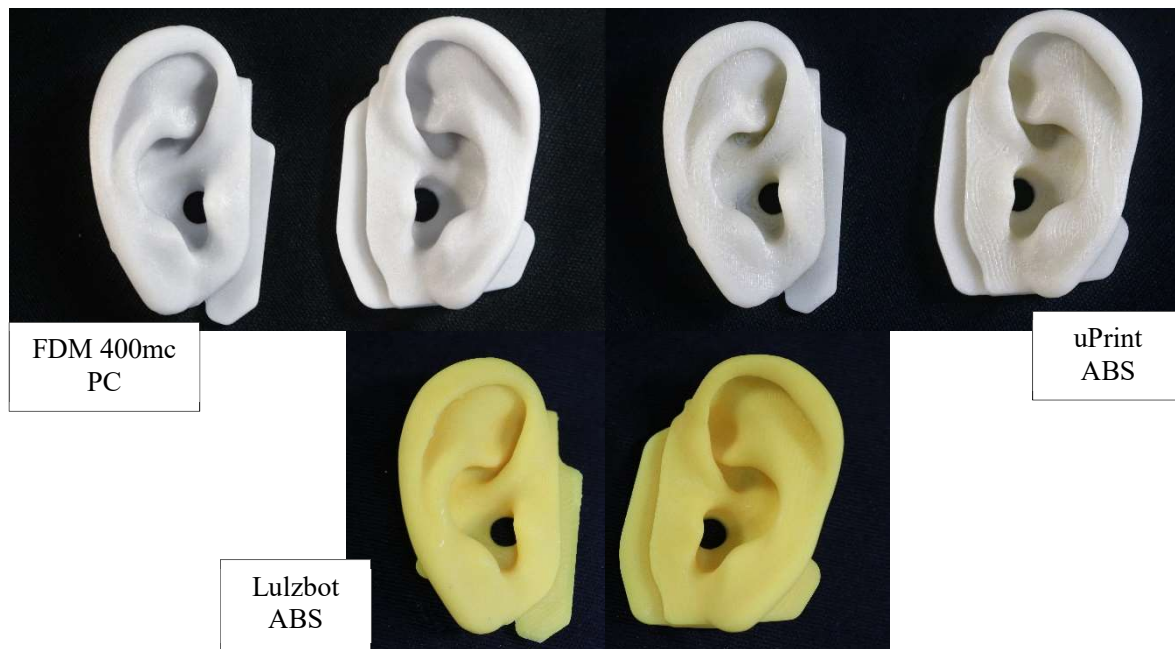


Figure 3.2.1 Material Extrusion AM pinna

extrusion, vat photopolymerization, and material jetting, with equipment ranging from industrial to desktop level (Table 3.2.1). For material extrusion, three different machines were used to fabricate pinnae. These were the Fortus FDM 400mc (Stratasys, Eden Prairie, MN, USA), the uPrint SE Plus (Stratasys, Eden Prairie, MN, USA), and a Lulzbot TAZ 6 (Aleph Objects Inc., Loveland, CO, USA). Resulting prints are shown in Figure 3.2.1. The material selected for the industrial Fortus 400mc was polycarbonate (PC) at a layer thickness of 0.13 mm, amongst the finest resolution for fused deposition modeling. The uPrint's resolution was at 0.25 mm using acrylonitrile butadiene styrene (ABS). The uPrint can be categorized (based on price) somewhere between an industrial and desktop printer. The Lulzbot's desktop system also used ABS at the layer thickness of 0.15 mm. For vat photopolymerization, stereolithography was the technology of choice using the Viper SLA (3D systems, Rock Hill, SC, USA) as the industrial machine, with the Somos NeXt material (DSM, Heerlen, Netherlands), which is a hard acrylic printed at a 0.07 mm layer thickness. The Form 2 (Formlabs, Somerville, MA) desktop stereolithography printer was also utilized, employing their Tough resin at a layer thickness of 0.10 mm. The materials mentioned so far were mechanically rigid, with the intention of capturing the pinna geometry and

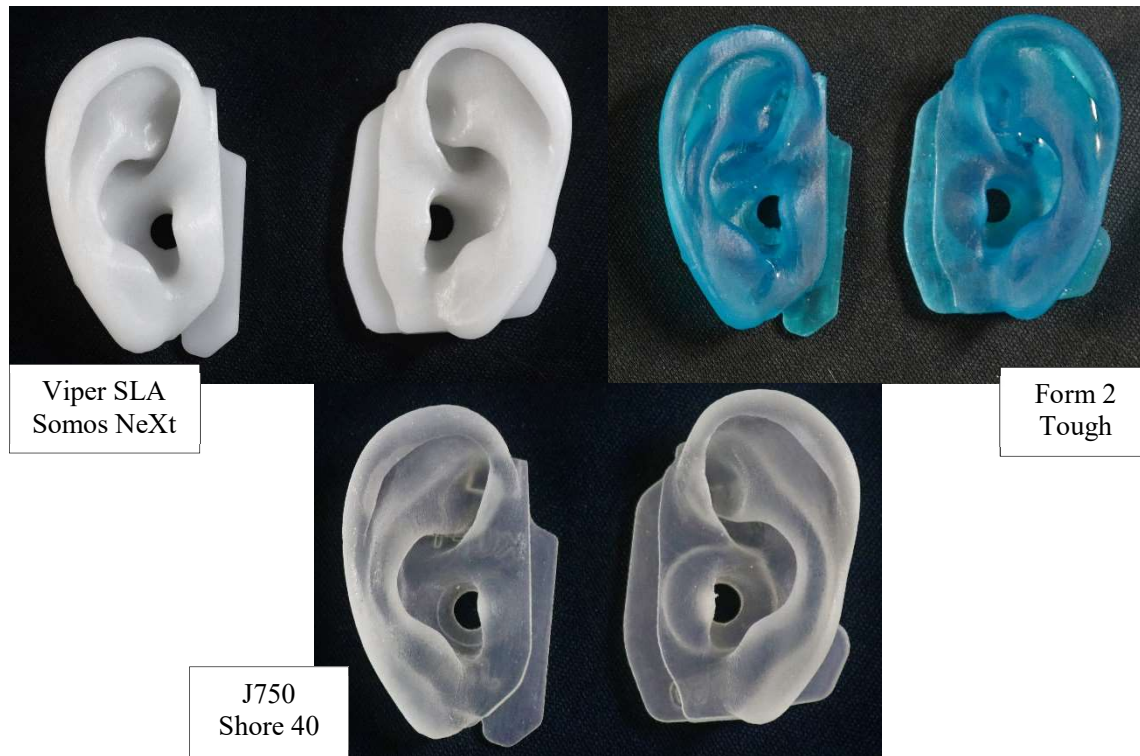


Figure 3.2.2 Vat photopolymerization & material jetting AM pinna

not the pinna's flexibility or softness. With the J750 (Stratasys, Eden Prairie, MN, USA), a material jetting printer, a combination of four photosensitive materials can produce a printed part by the selecting a determined shore on the print's setup. This provided the pinna with a certain flexibility. For this procedure, a shore 40 A pinna sample was fabricated using a combination of the Vero and Tango resins, and a resolution of 0.03 mm layer thickness. The shore 40 A was selected to add flexibility to the pinna while preserving its shape. Both the vat photopolymerization and material jetting pinnae can be observed in Figure 3.2.2.

Two design approaches were implemented for manufacturing the KEMAR pinna to reproduce the features of the receptacle for placement and sealing purposes. The intention of the two designs was to fabricate a pinna model that was to obtain accurate replica of the KEMAR in terms of pinna preservation, as well as matching the surrounding box for fit onto the KEMAR head. Even though dimensional accuracy is the primary aspect to be preserved, the fitting factor the KEMAR pinna provided was essential for the pinnae to remain in place during the acoustic

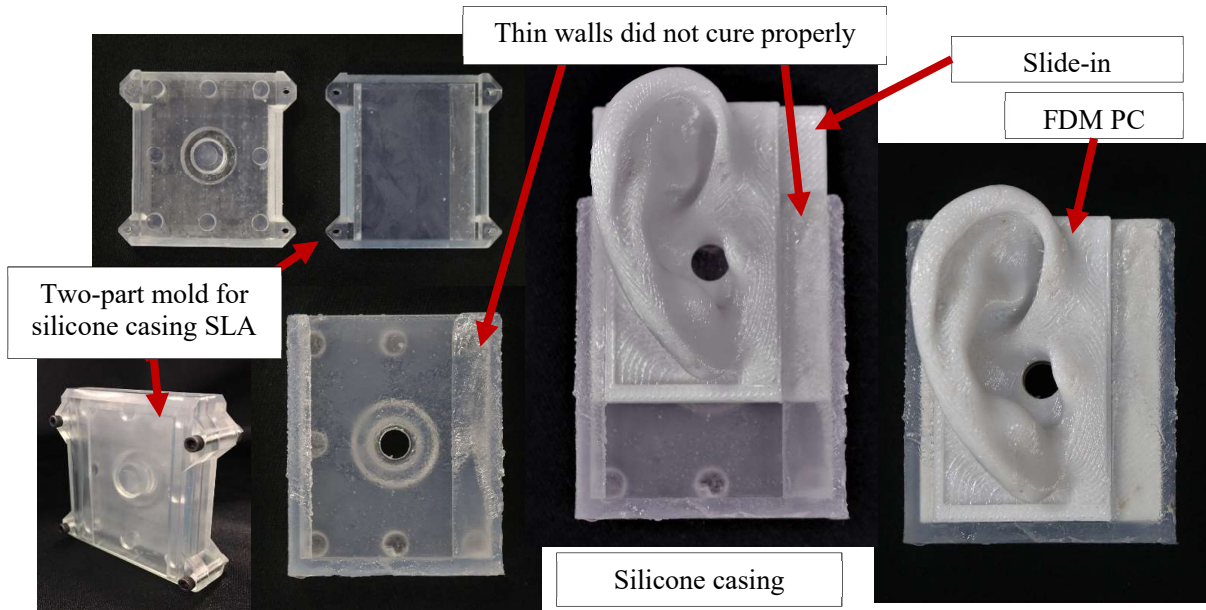


Figure 3.2.3: First concept silicone casing for AM pinna

measurements. The incoming sound that the KEMAR system received was measured via a microphone located in the manikin's ear canal. Just as the KEMAR pinna, the AM pinna was required to cover and seal the area where it interfaced with the head, for the sound to move through the pinna and be captured by the microphone placed in the simulated ear canal. If there were any unsealed gaps within the pinna placement, the acoustic measurements would experience discrepancies due to several incoming sound locations. The KEMAR pinna possessed a 55 Shore 00 which makes it a very soft and flexible material, allowing it to seal and protect the sound inlet by covering the receptacle area. Accounting for these considerations, the two design approaches led to two fabrication processes.

The first design consisted of a sleeve made out of flexible material which would serve as a swappable mechanism for different AM pinnae. The approach to fabricating this soft flexible casing was selecting a material which would withhold the hard-plastic 3D printed material. The first iteration of the pinna casing consisted of having a slit in the casing for the pinna to slide in

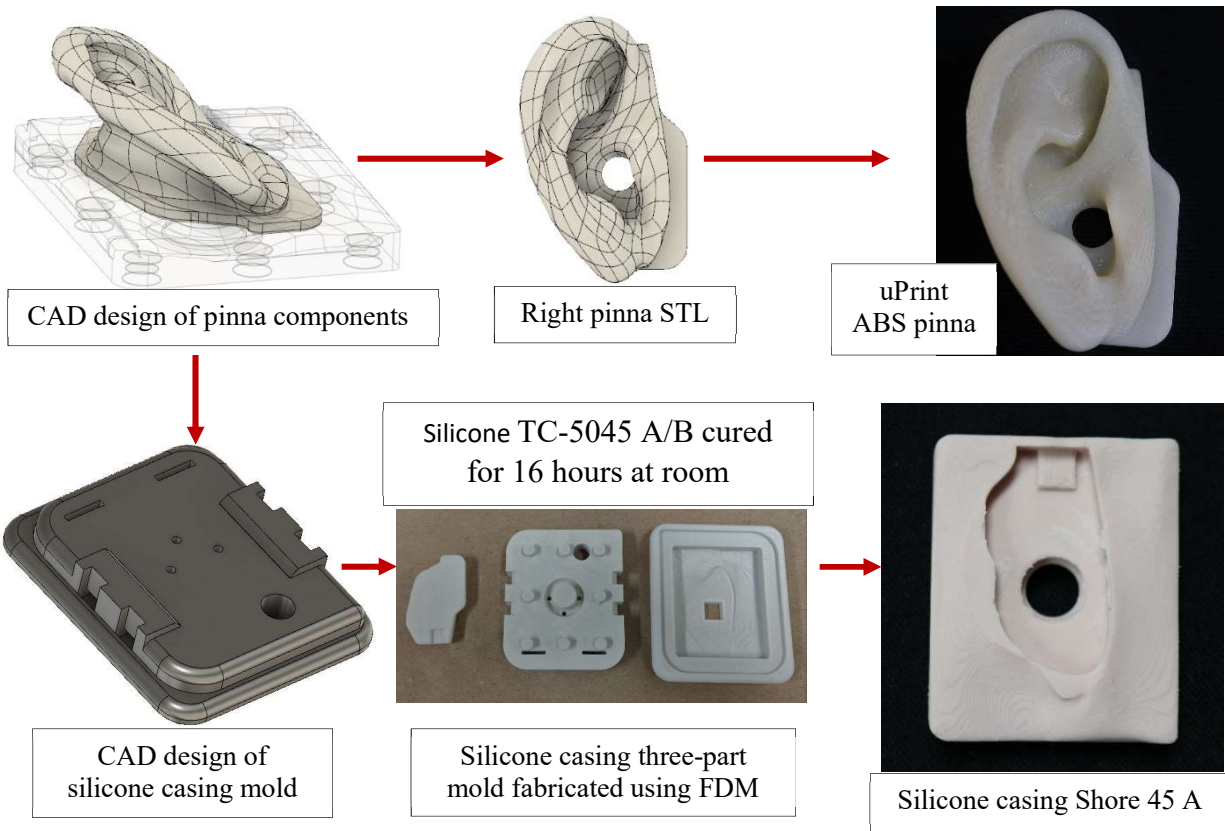


Figure 3.2.4: Silicone casing for AM pinna final concept fabrication

(Figure 3.2.3). The modeling of this approach was made in CAD and a two-piece mold was then designed and fabricated using AM. The materials used for this casing were platinum-based silicone TC-5045 A/B (45 shore A), flexible polyurethanes F-130 REV (Shore 30 ± 5), F-140 REV (Shore 40 ± 5), and WC-540 (Shore 45 ± 5) all from BJB (BJB Enterprises Inc., Tustin, CA, USA). To avoid adhesion from the mold to the silicone/polyurethane, a CRC boron nitride mold release (CRC, Horsham, Pennsylvania, Texas) was applied to the mold. Issues were encountered with this model in terms of fitting, where the hard material of the pinna started protruding from the casing, making it hard for the placement of the pinna with casing to the KEMAR. Another issue that arose was that the polyurethanes and the silicone were not curing properly in some of the thinner areas of casing (Figure 3.2.3). This was noticeable more on the silicone case than on the polyurethane casing. The last issue was that the polyurethanes were more prone to tearing than the silicone cases. Taking all of these issues into consideration, the modeling of the casing changed, and the material

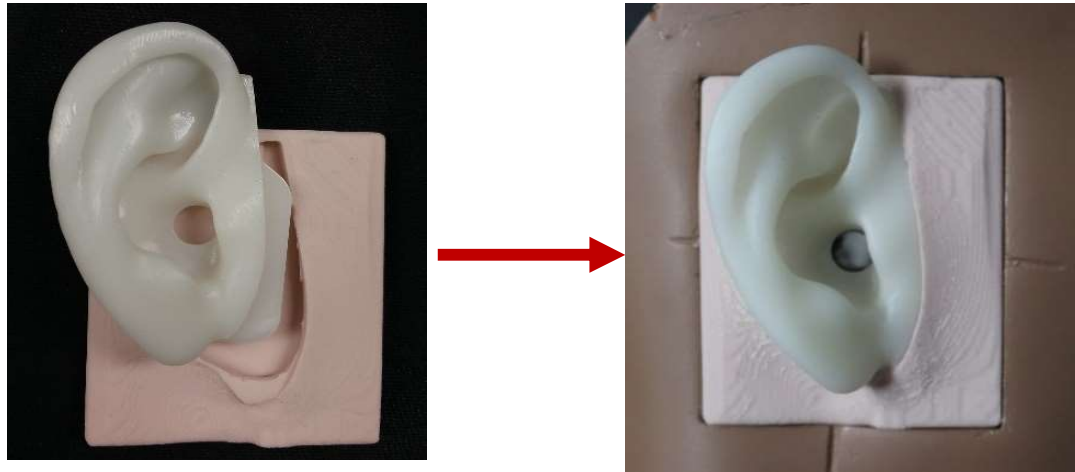


Figure 3.2.5 SLA Somos NeXt pinna in silicone casing

selected was the TC-5045 A/B silicone. A three-part mold was designed and 3D printed out of PC on the Fortus 400mc. The same mold release was used to avoid adhesion between the part and the mold. The platinum-based silicone TC-5045 A/B was deposited and cured in the mold for 16 hours (Figure 3.2.4). Once the casing was cured and removed from the mold, the 3D printed pinna was fitted to the casing and placed onto KEMAR for overall fit check (Figure 3.2.5).

The second approach to fabricating the pinna consisted of 3D printing the whole pinna and attaching an o-ring on the back interface for sealing purposes. For this model to fit the KEMAR head, some modifications to the CAD were performed on the back interfaces. the circular interface

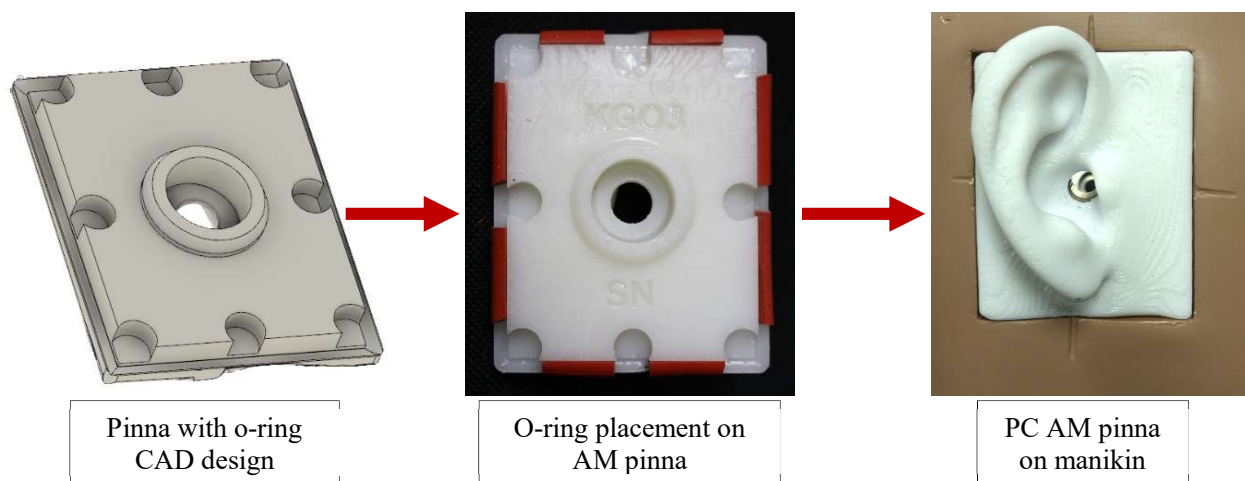


Figure 3.2.6 AM pinna with o-ring design

spacing on the back of the pinna design model was given a tolerance of +0.254 mm to make sure no interference between the receptacle and KEMAR would occur. Also, the channels for the o-ring to be placed were modeled in the CAD file. A silicone o-ring with Shore 70 A (AZ-S70.103/10, Small Parts, USA) of 2 millimeters in diameter was cut in half longways, and sectioned to allow it to interface with the back side of the 3D printed pinna. The o-ring segments were glued to the AM pinna using a polyurethane adhesive (Gorilla Super Glue Clear, Gorilla Glue Company, Sharonville, Ohio, USA). With the use of the o-ring, the installation of the pinna to the manikin was similar to a press fit (Figure 3.2.6). As previously mentioned, the purpose of the two design approaches was to create a seal so that the sound waves would travel through the modeled ear canal.

3.3 AM pinna on KEMAR setup

The pinna fabrication process eventually led to fit testing the specimens for acoustic testing. This was performed in the Keck Center, along with all the fabrication processes, while all of the acoustic measurements were taken in G.N. Advanced Facilities in Chicago, IL. In comparison to the silicone case pinna, the o-ring had a stiffer placement to the manikin. The soft casing of the silicone material made the pinna placement easier due to the small deformation that the casing can experience, a scenario that cannot be achieved using the hard casing from the 3D printed pinna with the o-ring. Several pinnae were fit placed on the KEMAR head (Figure 3.3.1). Once the pinnae were fabricated, some samples were shipped to G.N. to carry out the acoustic testing. The acoustic measurement setup consisted of the KEMAR being placed in the middle of a room surrounded by four speakers. The speakers were positioned one meter away from the KEMAR at 0, 90, 180, and 270 degrees. Signals were sent to the KEMAR system for the frequency

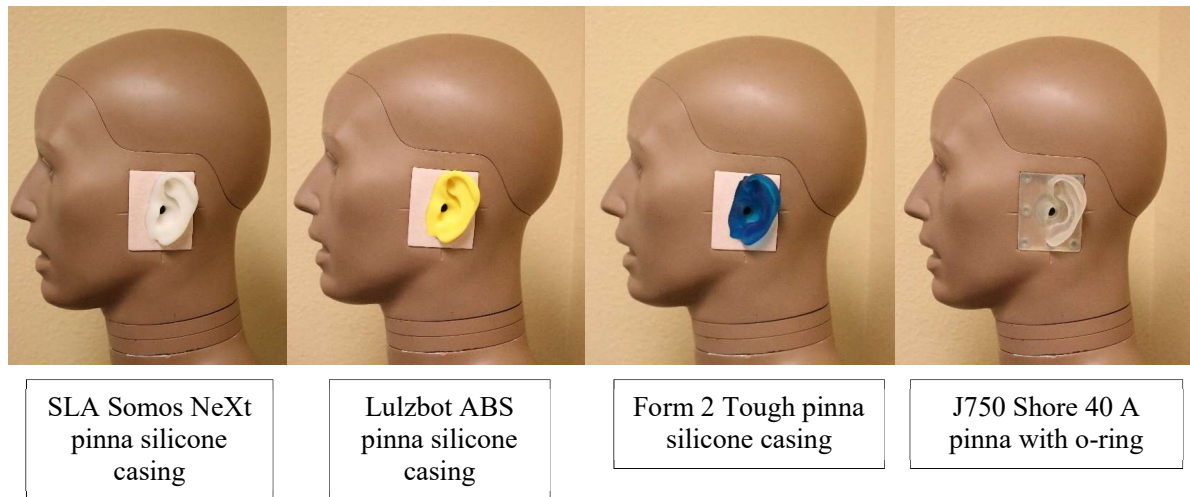


Figure 3.3.1 AM pinnae placement on KEMAR

readings to be captured. The pinnae that were placed onto KEMAR for capturing acoustic data were the PC o-ring model as well as the Somos NeXt silicone casing model.

3.4 AM pinna embedded in headset

The modeling and fabrication of the 3D printed pinna led to the design of a headset with an embedded pinna. The purpose of this designing this device was to follow the hypothesis that spatial cues could be preserved by printing a hearing device with embedded pinnae. A set of steps

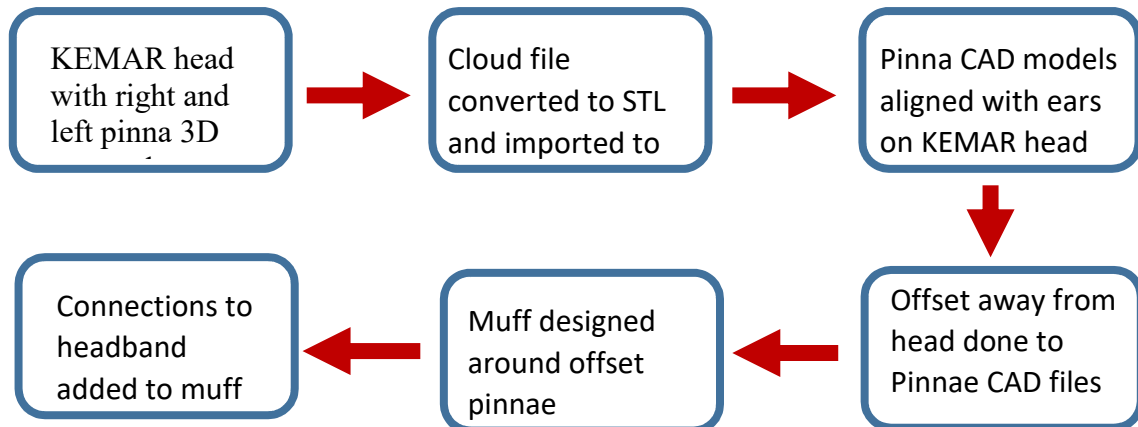


Figure 3.4.1: Headset design process

were taken to carry out this first design for preliminary acoustic data. Figure 3.4.1 presents a flowchart of the design process for the headset. The first consideration on designing this headset was to have an offset between the pinna on the KEMAR head and the pinna on the headset. For this, the KEMAR head along with the KEMAR small pinnae were 3D scanned using the Faro ScanArm (Figure 3.4.2). The purpose of this was to use this model as a reference when offsetting the pinna. The KEMAR head with the KEMAR pinnae was scanned and the point cloud was processed in Design X. Once the KEMAR head was on the Fusion 360, the CAD models from the o-ring 3D printed pinnae were uploaded onto the design. These ear models were aligned with the ears on the KEMAR manikin. After being aligned to the position and angle of the ears placed on the KEMAR head, the offset pinnae models were given a 38.1 mm (1.5 inch) offset from the head on the horizontal axis (Figure 3.4.3). The headset was then modeled surrounding this pinna offset.

An over the ear muff model was implemented to prevent the KEMAR pinna from being squished or deformed inside of the headset. For the headset design, the 3D printed pinna would be

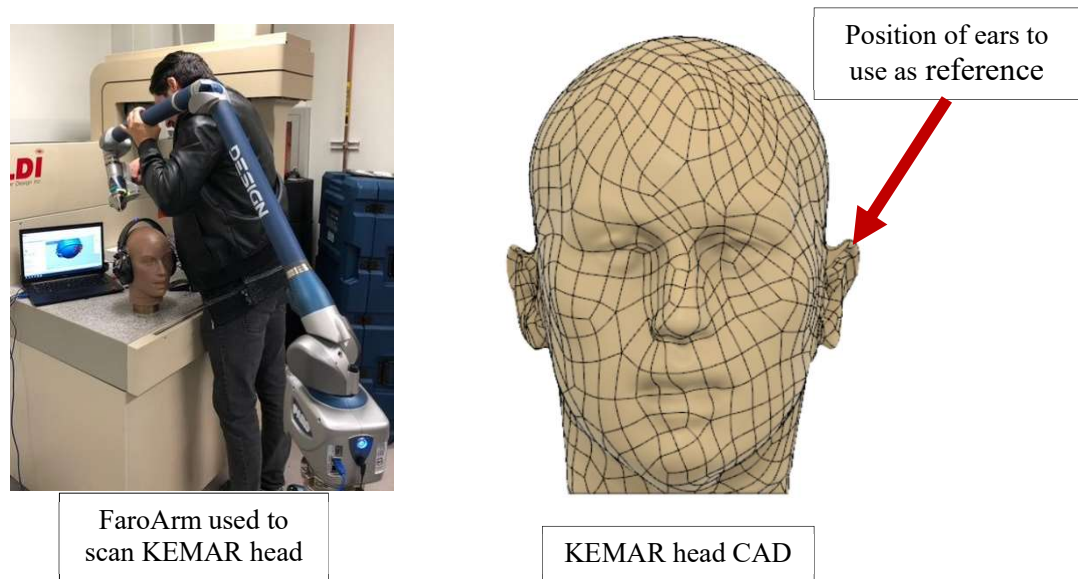


Figure 3.4.2: 3D scan of KEMAR head for headset design

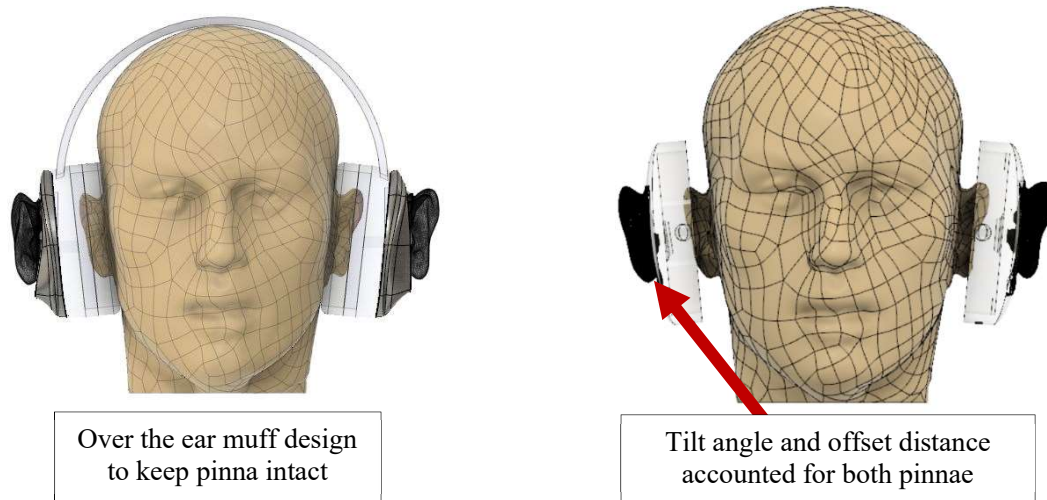


Figure 3.4.3: Initial embedded pinna into headset design

embedded and placed on the external face of the muff. The box shape of the pinnae was preserved on the muff to compare the response to the KEMAR readings. Two muffs were designed, one for each pinna, left and right. For the 3D printed muff to be placed on the KEMAR head, commercially available headset accessories were used. A headband from a 3M™ PELTOR™ Tactical Sport™ Communications Headset (MT16H210F-SV, 3M, Maplewood, MN, USA) was used to connect



Figure 3.4.4: Fabricated initial AM embedded pinna headset design

both AM muffs. The muff design had pins incorporated for connecting to this particular headband. Padding from a hearing protection headset (En352-1, Western Safety, Seattle, WA) was also added to the muff by modeling screw holes on the muff design in Fusion 360. The model was additively manufactured using the Viper SLA with the Somos NeXt material (Figure 3.4.4). The hypothesis behind this headset was that the single opening on the ear receptacle of the 3D printed specimen would carry the sound to the inner ear, in this case, the KEMAR pinnae placed on the manikin.

Chapter 4: Results

4.1 Dimensional accuracy for 3D printed pinna

To validate the 3D printed replica of the KEMAR pinna, dimensional measurements were taken using different approaches. The ear pinna possesses a set of unique features that can be quantified dimensionally. Algazi *et al.* (2001) specified a set of geometric dimensions of the pinna that were used as reference for this research (Figure 4.1.1). A subset of seven distances were chosen from Algazi *et al.* (2001) to measure the KEMAR pinnae as well as the bevy of 3D printed pinnae. A total of 18 additively manufactured pinnae were measured: 3 different CAD files (GN right, UTEP right, and UTEP left) printed in 6 different versions, across the three different technologies (3 material extrusion pinnae, 2 vat photopolymerization, and 1 material jetting). Three measurements were taken per variable. First, the measurements were taken using a caliper instrument. For the manual readings, three individuals took the measurements for each of the seven distances. The reasoning behind having three individuals take caliper measurements, was to account for the human error that could have influenced the measurements. The data for the caliper readings were recorded as the pinnae were fabricated. A Mitutoyo 500-196-30 AOS Absolute

Name	Variable
Cavum concha height	d1
Cymba concha height	d2
Cavum concha width	d3
Fossa height	d4
Pinna height	d5
Pinna width	d6
Intertragal incisure width	d7

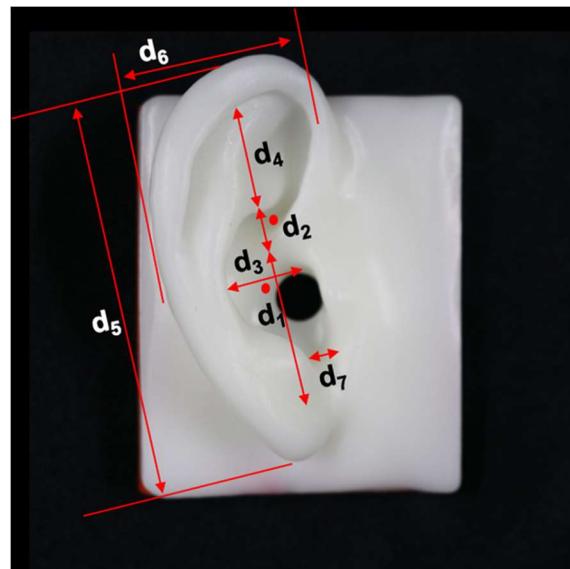


Figure 4.1.1: Dimensions taken from Algazi et al. (2001)

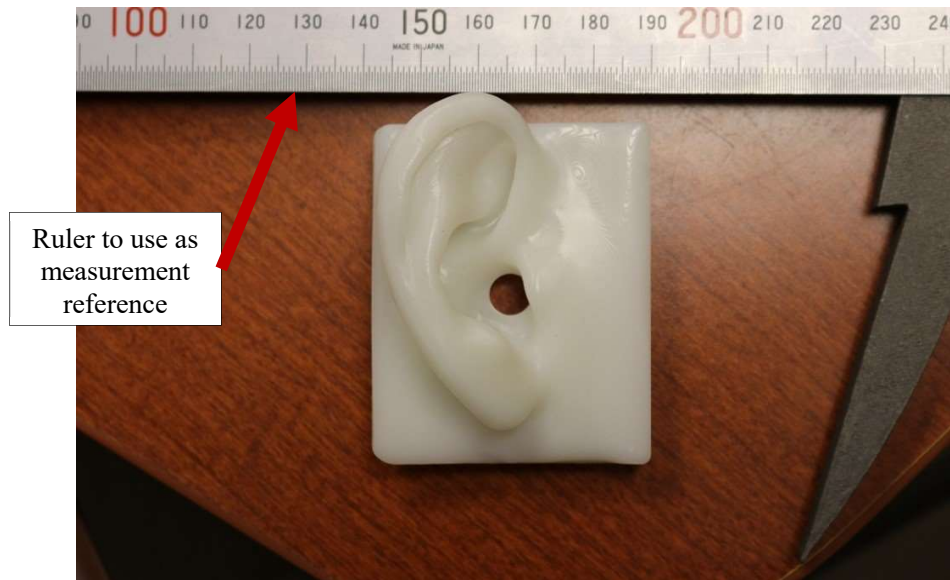


Figure 4.1.2: Image setup for NI Vision Assistant

caliper (Mitutoyo, Kawasaki, Japan) was used to conduct this procedure. To correlate to these caliper measurements, an image processing software, National Instruments (NI) Vision Assistant (National Instruments, Austin, Texas, USA), was utilized. Images were taken of the KEMAR and AM pinnae alongside a ruler, which the software used as a baseline to scale and correlate distances on the pinnae (Figure 4.1.2). Individual pinnae images were captured as the different AM technology prints were fabricated. The images were taken perpendicular to the pinna positioned at the center of the focal point, and the ruler was positioned above the pinna at the same height of the pinna box. The camera was set up using a tripod with a leveling tool. The camera position was found using the camera's alignment setting to capture images completely perpendicular to the pinnae. This was done to obtain the most accurate measurements accounting for the perception of depth of the camera lens. Once the images were taken, a calibration job was performed within the NI Vision Assistant software to attain the desired measurements. A baseline distance was obtained within the VA software, by selecting two points on the captured image, from which pixel distance was identified. A correlation can be made between the pixel distance to a real-world distance, in this case millimeters. Lines drawn with the two-point selection were then used to capture the pinnae measurements. Just as with the caliper readings, three measurements per variable were



Discovery CT/PET scanner at
Desert Imaging



Pinnae setup for CT scan

Figure 4.1.3: CT scan at Desert Imaging

taken. Once the measurements were taken from the caliper and the image processing software, a computational model dimensional analysis was performed. The software GOM Inspect (GOM GmbH, Braunschweig, Germany) was used to perform CAD measurements of the GN and UTEP CAD files, as well as the 3D printed parts. For this last procedure, a second CT scan was performed on the all additively manufactured pinnae using the system protocol parameters designated for the ear, just as the first CT scan made (Figure 4.1.3). All of the pinnae were CT scanned and the output file from the scan was processed using Mimics. Each individual model was obtained and converted to an STL to be brought into GOM Inspect. Once imported into GOM, each individual STL from the CT scanned pinnae was aligned and measured by constructing a two-point line per variable. This line was made to fall within the same plane in which the pinna was aligned. The right GN pinna, right UTEP pinna, and left UTEP pinna CAD models were also measured following this procedure. Three measurements were taken for each variable and the mean values obtained were compared to the mean measurement from caliper and NI Vision Assistant readings.

The results for the mean measurements of the KEMAR pinnae were obtained first to use as a baseline for comparison against the other 3D printed pinnae. Figures 4.1.4 and 4.1.5 show the dimensions obtained from the small right pinna GN model on the material extrusion AM technology. Readings from d1 showed correlation from KEMAR to the AM pinnae where slight variation within 0.08 mm was found across the three measuring tools (Figure 4.1.4). These tool measurements remained consistent throughout the different variables with the exception of the measurements obtained from the NI Vision Assistant Software. While the caliper and the GOM measurements were similar to KEMAR within 1 mm, discrepancies were found on d5 of the NI Vision Assistant measurements (Figure 4.1.5). These measurements had a variation of 3 mm with respect to the ones obtained from the caliper and GOM Inspect, and were projected through all the AM pinnae including KEMAR using the NI Vision Assistant software. This could signify that the orientation at which the image of the pinnae was taken contributed to this mismatch between the rest of the data set. Variable d5 relates to the pinna height which is the largest distance measured, entailing that the readings of the projection of an image can relate to the depth perception. Nevertheless, by focusing only on the measurements of d5 using Vision Assistant, the measurements remained constant across the AM pinnae to KEMAR which showed a average percentage error of 2.2% for FDM, 0.6% for uPrint, and 0.2% for Lulzbot. The set of charts presented next, shows the dimensional comparison between the vat photopolymerization and material jetting pinna for the KEMAR, (Figures 4.1.6 and 4.1.7) for the same right GN pinna model. Measurements were similarly represented just as the material extrusion pinnae. For instance, d1 and d2 measured close to the KEMAR model in all the models, being the J750 caliper and Somos NeXt which possessed the largest difference of 2.1 mm (Figure 4.1.6). Slight variation occurred on d4, where there was consistency from the caliper measurements to the other two measurement tools showing 5% error and below (Figure 4.1.6). In Figure 4.1.7, that data exemplified peaks on the d5 (pinna height) found using the Vision Assistant software. Just as the material extrusion GN right pinna results, the peak only was observed on the Vision Assistant software and the measurements remained consistent. Figures 4.1.8, 4.1.9 (material extrusion) and

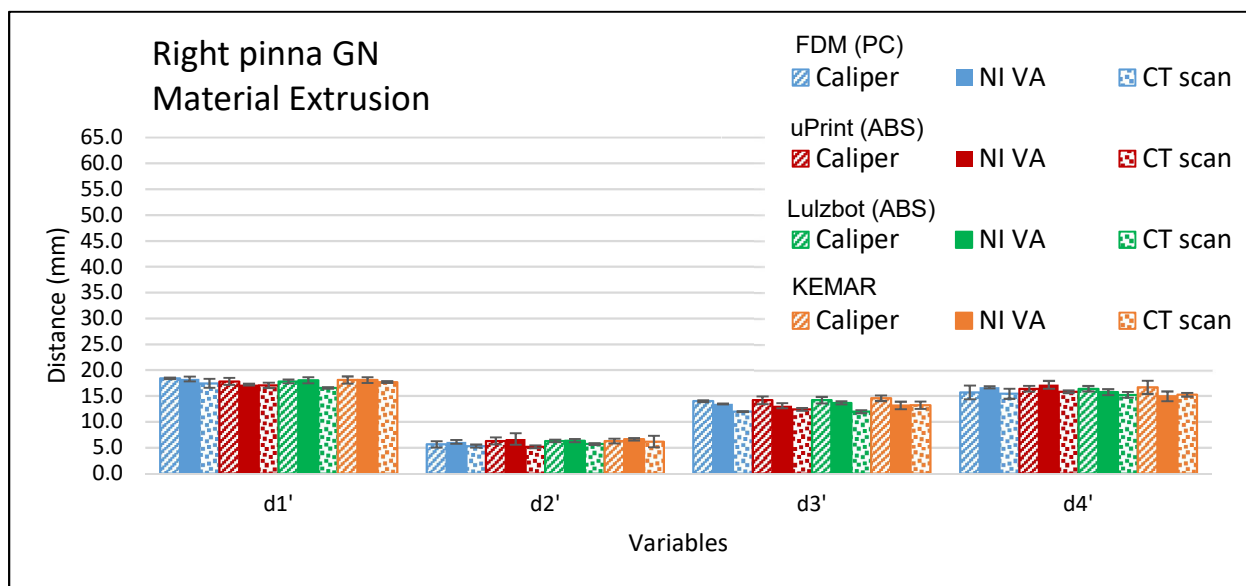


Figure 4.1.4: Material extrusion right pinna (GN) d1-d4

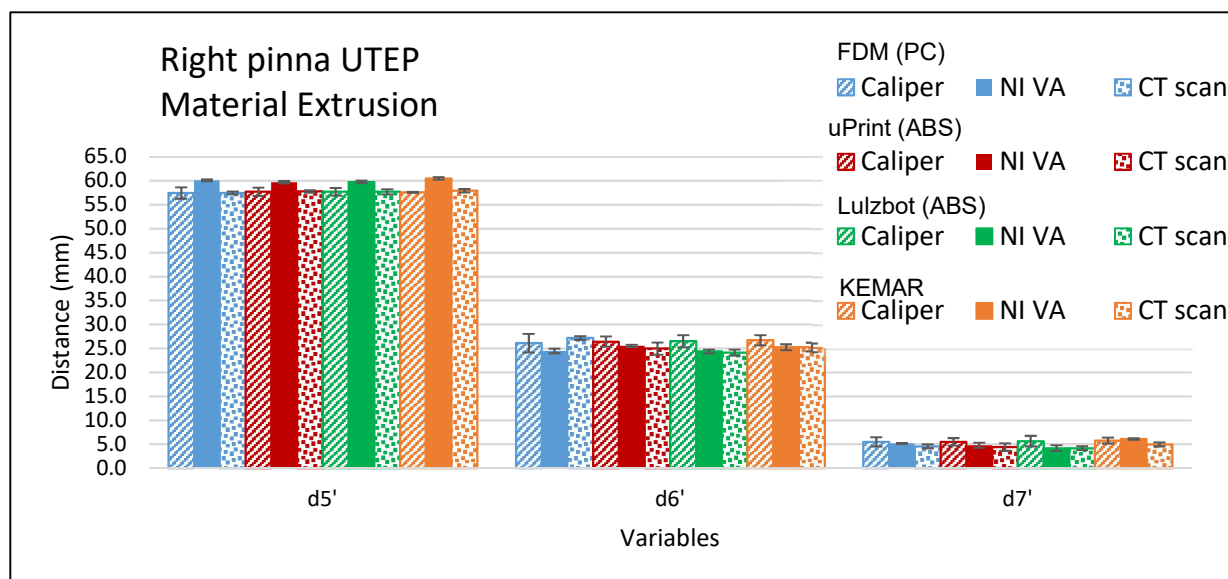


Figure 4.1.5: Material extrusion right pinna (GN) d5-d7

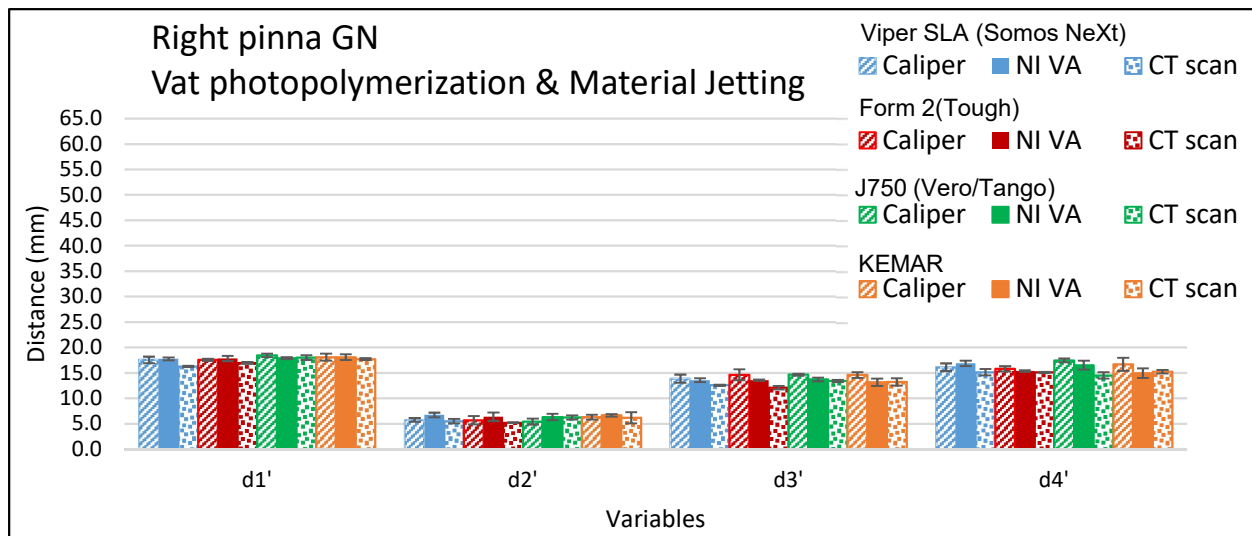


Figure 4.1.6: Vat photopolymerization & material jetting right pinna (GN) d1-d4

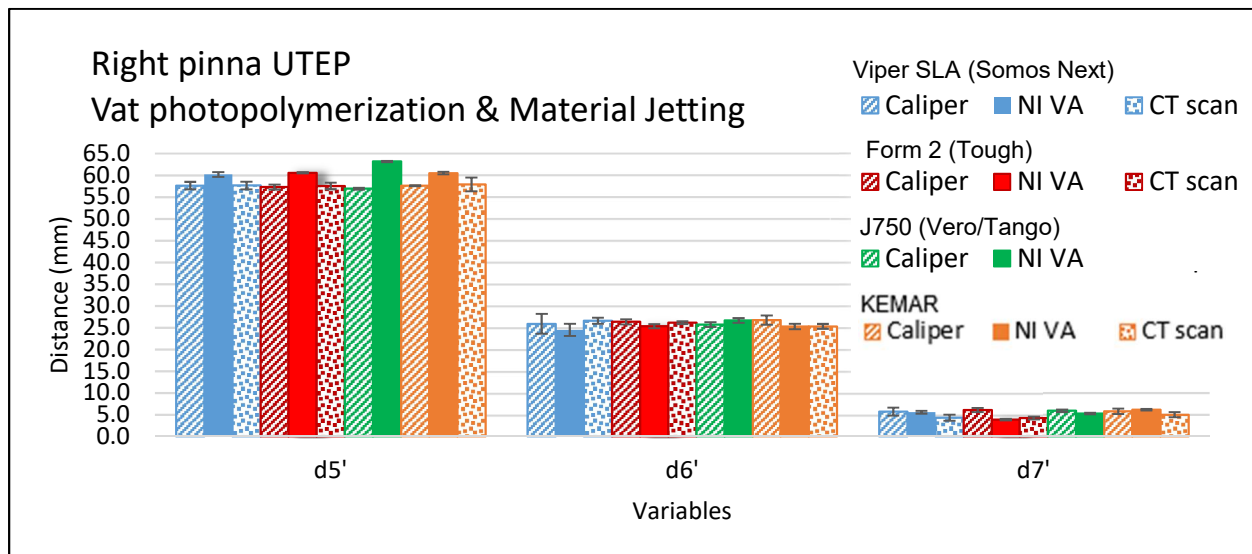


Figure 4.1.7: Vat photopolymerization & material jetting right pinna (GN) d5-d7

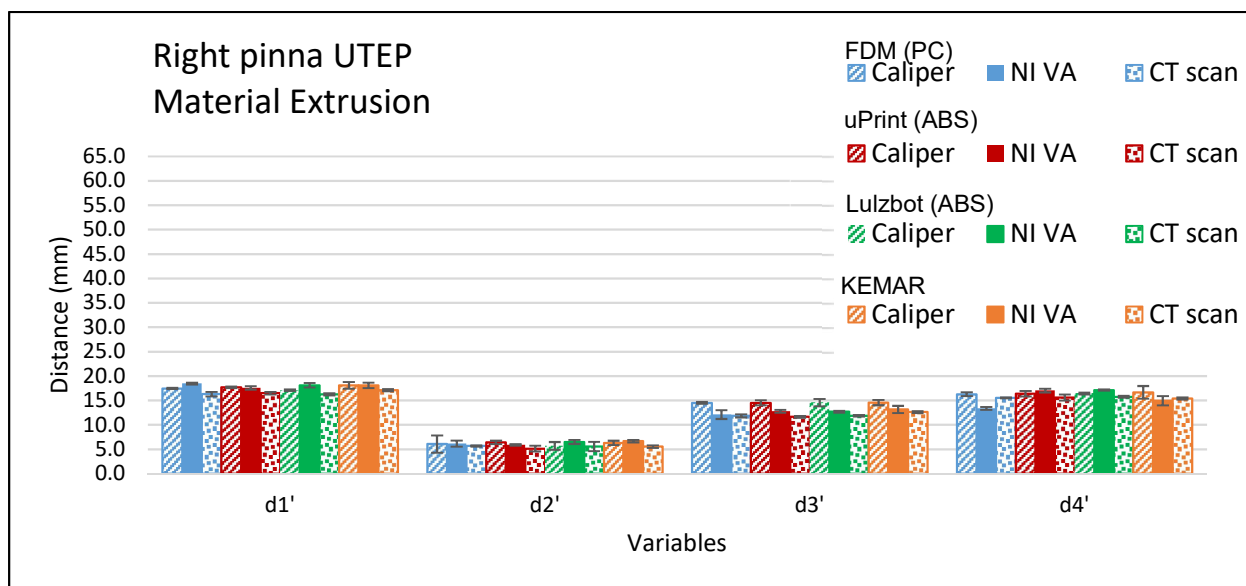


Figure 4.1.8: Material extrusion right pinna (UTEP) d1-d4

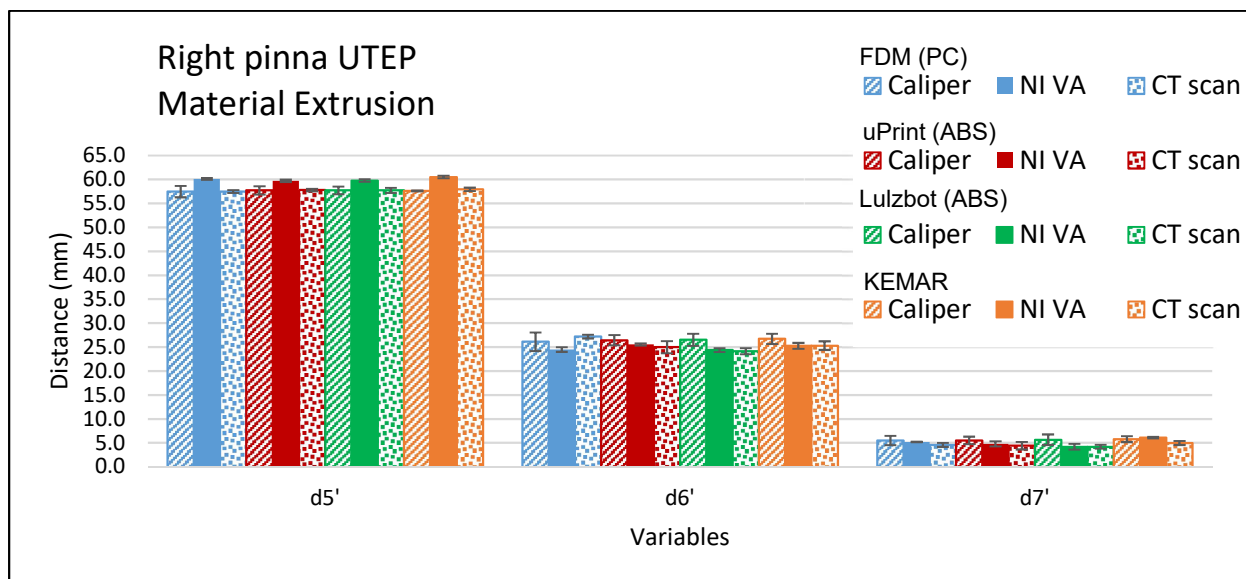


Figure 4.1.9: Material extrusion right pinna (UTEP) d5-d7

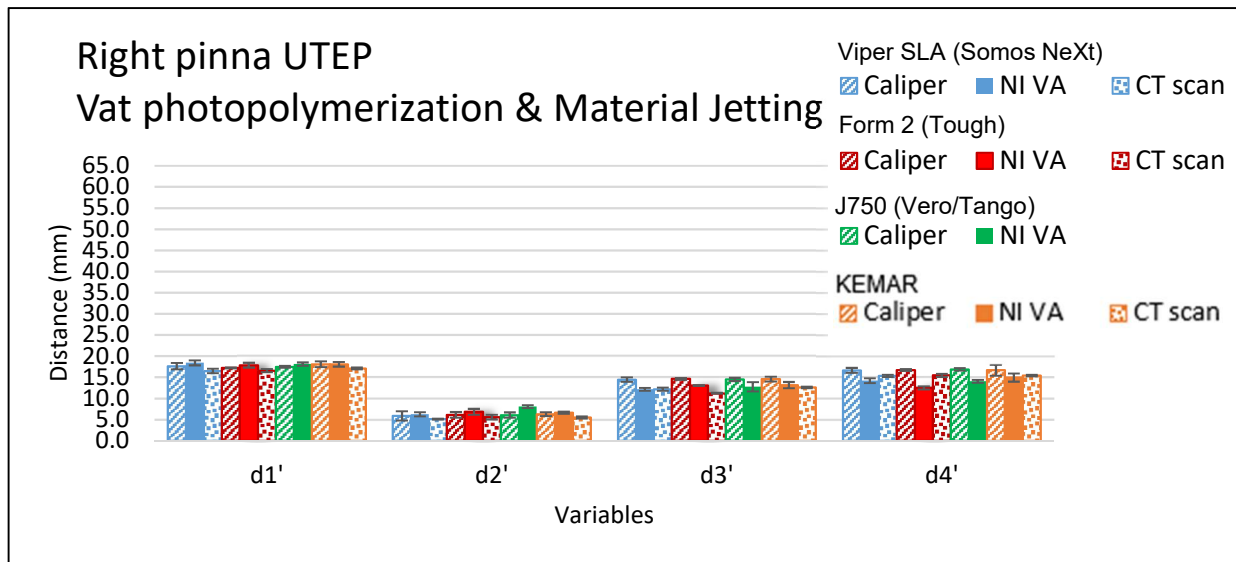


Figure 4.1.10: Vat photopolymerization & material jetting right pinna (UTEP) d1-d4

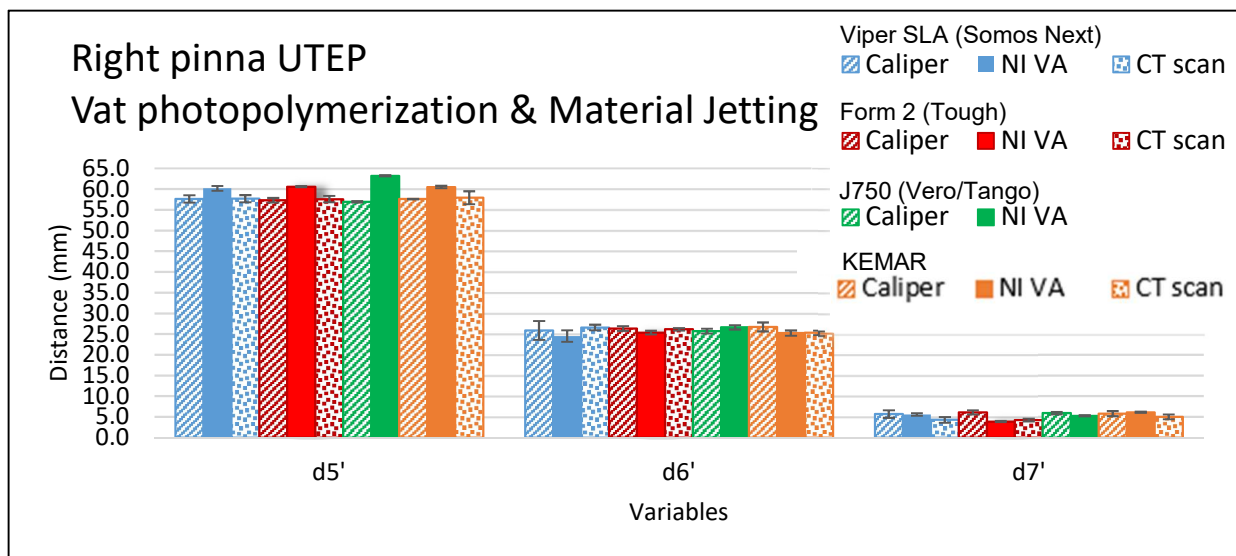


Figure 4.1.11: Vat photopolymerization & material jetting right pinna (UTEP) d5-d7

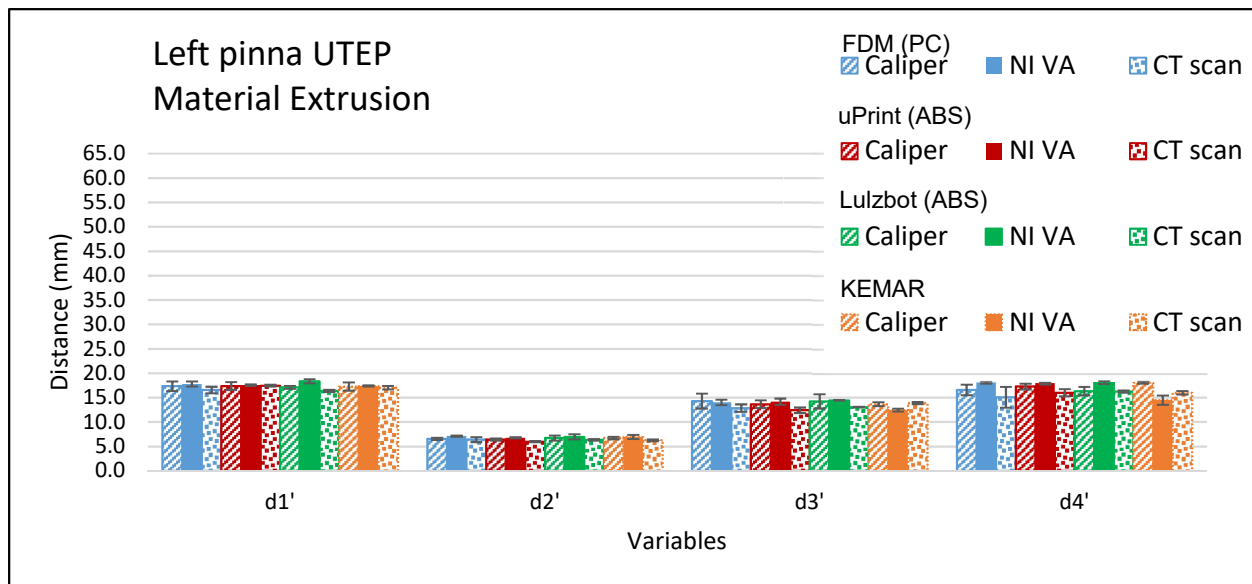


Figure 4.1.12: Material extrusion left pinna (UTEP) d1-d4

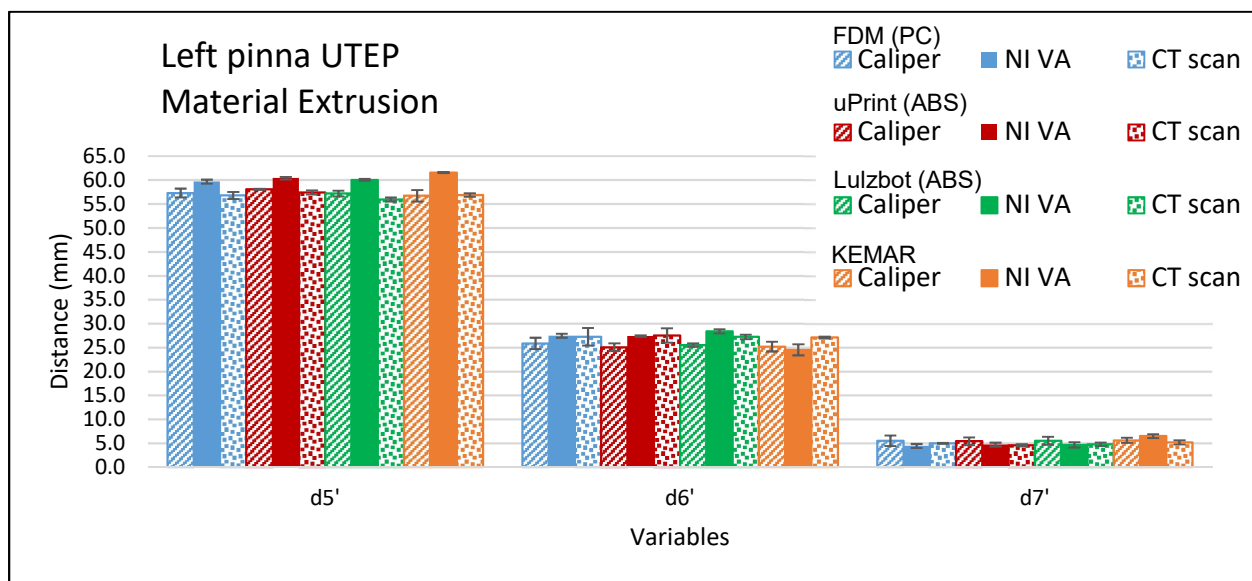


Figure 4.1.13: Material extrusion left pinna (UTEP) d5-d7

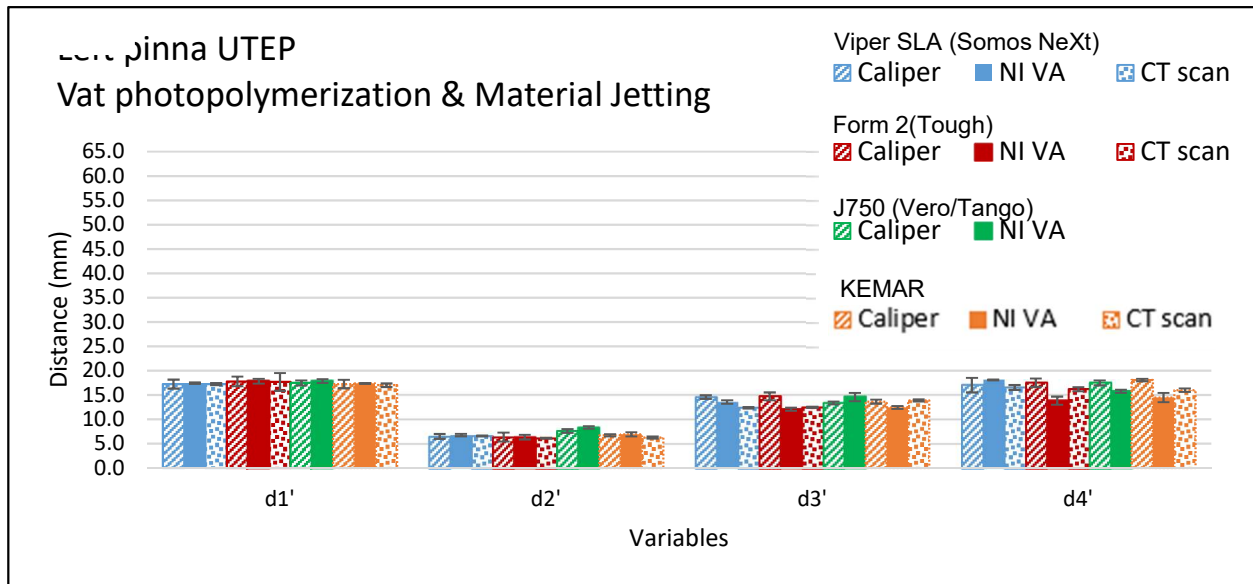


Figure 4.1.14: Vat photopolymerization & material jetting left pinna (UTEP) d1-d4

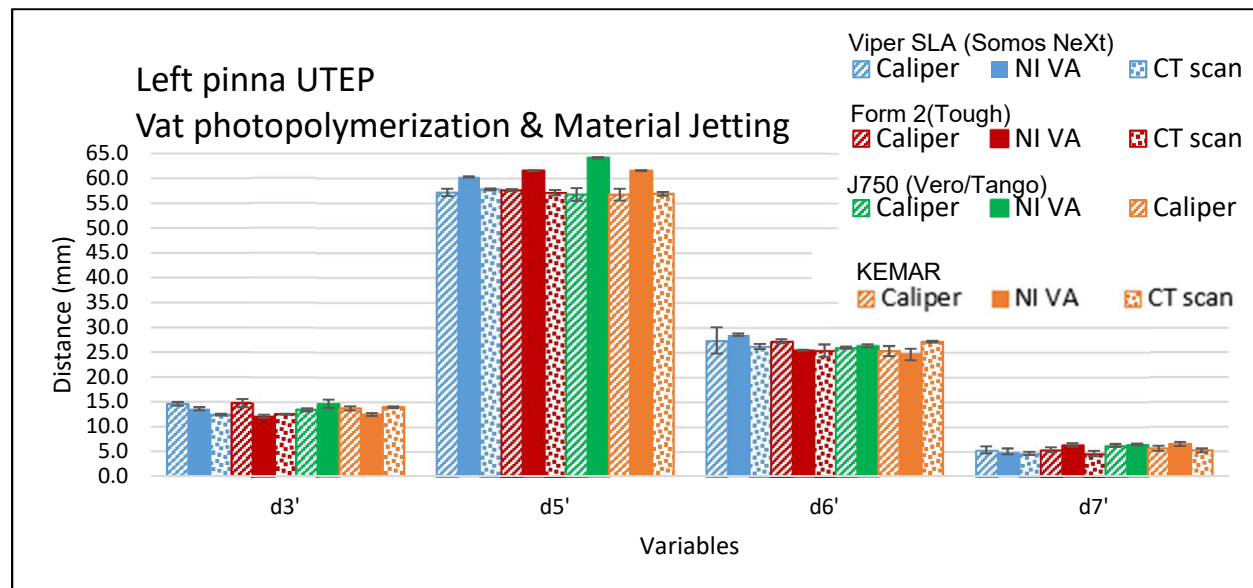


Figure 4.1.15: Vat photopolymerization & material jetting left pinna (UTEP) d5-d7

4.1.10, 4.1.11 (vat photopolymerization and material jetting) showed results for the right pinna UTEP. Caliper readings in variable d3 resulted larger for all three material extrusion pinnae than the Vision Assistant and the GOM Inspect measurements within a 2 mm range (Figure 4.1.8). In the same graph, the Vision Assistant measurement for the FDM PC pinna was off the marker, with a difference of about 2 mm to the CT scan and Vision Assistant readings measurements (Figure 4.1.8). Divergences of 3 mm can be found in d5 on the Vision Assistant software for all the measurements. Referring to the previous data from the right GN pinna, measurements on the right UTEP pinna were correlated for most of the variables to the measurements obtained to KEMAR. The same caliper and Vision Assistant measurements were used as comparison for both the right GN model and the right UTEP model. The file used for the CAD dimensional analysis in GOM inspect was different for both, each having its respective CAD file, small right GN pinna and small right UTEP pinna. The vat photopolymerization and the material jetting right UTEP pinnae also showed mismatch on the image processing software (Figures 4.1.10 and 4.1.11). It has to be noted that due to machine unavailability, the J750 models were not fabricated at the time of the CT scan. Measurements for caliper and Vision Assistant were obtained but GOM inspect measurements for the J750 was omitted for the UTEP right and left models. Variables d4 and d5 had the most difference (3.6mm) with respect to the caliper and the GOM measurements. The J750 pinna had error of 4.5 % on the Vision Assistant for the pinna height variable (d5). Besides those readings, the measurements obtained from the different technologies corresponded to the data obtained for KEMAR. Finally, Figures 4.1.12, 4.1.13 (material extrusion) and 4.1.14, 4.1.15 (vat photopolymerization and material jetting) show results for the left pinna UTEP. As previously mentioned, there was no starting left pinna model, so only comparisons within the left UTEP pinna model were obtained. The data obtained for the material extrusion pinnae shows consistency within all the variables, with the exceptions of d4 through d6 (Figures 4.1.12 and 4.1.13). Caliper measurements showed a percentage error of 8.4% for d4 while NI Vision assistant of 24.8%. Measurements on vat photopolymerization were consistent while the material jetting pinna showed slight peaks at d2 (Figure 4.1.12). Measurements across d3 and d4 show small peaks on caliper

readings for the all technologies. Table 4.1.1 shows the average percentage error calculated from AM pinna model to KEMAR with respect to measuring tool. From all three measuring tools, caliper proved to provide a lower average percentage error for the three pinna models available. The data presented shows correlation between the KEMAR dimensions and the AM fabricated parts.

Table 4.1.1: Average percentage error for measuring tools

Average % error	KEMAR GN right pinna	KEMAR UTEP right pinna	KEMAR UTEP left pinna
Caliper	4.1%	2.2%	3.7%
NI VA	7.0%	7.2%	11.3%
CT Scan	4.9%	4.8%	5.2%

4.2 AM pinna analysis of variance for desktop vs industrial equipment comparison

Having utilized different measurement instruments for the pinna dimensional analysis, statistical method was performed to compare the pinnae manufacturing within the different AM technologies. An analysis of variance (ANOVA) was made for the dimension variables of the right

	Pinna
A	KEMAR
B	FDM PC
C	uPrint ABS
D	Lulzbot ABS
E	SLA Somos NeXt
F	Form 2 Tough
G	J750 Vero/Tango



Figure 4.2.1: Pinnae for randomized study

UTEP AM pinnae and the right KEMAR pinna. For this test, the small right KEMAR pinna and the six right UTEP AM pinnae were labeled A through G (Figure 4.2.1). The Mitutoyo caliper was selected as the measuring tool. Attempting to follow the ANOVA gage repeatability and reproducibility analysis, a new set of randomized measurements were taken using the same seven variables used in the previous measurements set. Three operators measured every one of the seven variables three times for each pinna, making a total of 441 measurements. These 441 measurements were randomized in Microsoft Excel (Microsoft Corporation, Redmond, Washington, USA) using the RANDBETWEEN function, which allows to output a random number within a certain range, in this case 1 through 441. The column created using this function exerted duplicated numbers along the 441 cells, which were eliminated. The randomized function was then applied to fill the remaining numbers until a column of random numbers from 1 to 441 was sorted with the column labeling the operators variable measurement. A calibration block was used to calibrate the caliper tool. The calibration block was to read 50.8 mm and calibration measurements were made every 15 operator readings. The randomized order of the measurements can be found in the appendix tables. Once the measurements were performed, the data was sorted by pinna as well as by user for the ANOVA analysis. The software used for the ANOVA study was Minitab (Minitab LLC, State College, Pennsylvania, USA). The first study performed on this

Table 4.2.1: Normal distribution test variables 1-4

Pinna	Variable											
	1			2			3			4		
	Mean	St Dev	P	Mean	St Dev	P	Mean	St Dev	P	Mean	St Dev	P
A	18.5	0.3	0.139	5.6	0.2	0.535	13.4	0.1	0.278	16.5	0.1	0.615
B	18.3	0.2	0.309	5.6	0.3	0.320	13.3	0.1	0.567	16.5	0.2	0.765
C	18.3	0.2	0.376	5.7	0.2	0.811	13.4	0.3	0.905	16.5	0.3	0.662
D	18.4	0.2	0.512	5.6	0.2	0.130	13.3	0.3	0.186	16.5	0.2	0.453
E	18.3	0.3	0.097	5.6	0.2	0.821	13.4	0.2	0.794	16.5	0.2	0.352
F	18.3	0.3	0.177	5.6	0.4	0.144	13.3	0.2	0.492	16.4	0.2	0.151
G	18.3	0.3	0.347	5.6	0.2	0.094	13.5	0.1	0.560	16.5	0.1	0.514

Table 4.2.2: Normal distribution test variables 5-7

Pinna	Variable								
	5			6			7		
	Mean	St Dev	P	Mean	St Dev	P	Mean	St Dev	P
A	58.2	0.1	0.943	25.3	0.1	0.253	5.4	0.2	0.277
B	58.3	0.1	0.081	25.5	0.1	0.668	5.4	0.2	0.515
C	58.2	0.1	0.498	25.4	0.2	0.816	5.3	0.2	0.442
D	58.3	0.2	0.241	25.3	0.3	0.280	5.4	0.2	0.190
E	58.3	0.2	0.268	25.4	0.3	0.062	5.3	0.1	0.388
F	58.2	0.2	0.741	25.5	0.3	0.080	5.4	0.2	0.485
G	58.2	0.1	0.811	25.3	0.2	0.765	5.4	0.1	0.835

data was to check for normal distribution within the pinnae measurements. To determine if the data statistically differed, a criterion of a P-value of 0.05 or above was applied to entail if that the data failed to reject the hypothesis. This study was performed with a 95% confidence interval. Normality plots were plotted in Minitab for variables 1 through 7 for pinna A through G. Results showed that the P-values obtained for the normality check were above 0.05 all across the different pinnae, as shown in Tables 4.2.1 & 4.2.2, signifying that the data was passed the normal distribution test. After the normality plots were assessed, variance studies were performed according to each of the seven variables. A two-way ANOVA was performed using Minitab based on a 95% confidence interval for the data means. The data was sorted into 9 columns with 63 inputs each. The study used on Minitab was a General Linear Model (GLM) by selecting as a factor each of the seven pinna variables comparing it against the pinna model, the user, and the pinna vs user interaction. A significance level of 0.05 was used to assess the null hypothesis that there are no differences between the variables and users, variables and pinnae, and lastly the variables and users-pinnae. The P-value obtained from these studies determined if the null hypothesis was rejected or accepted. The sum of squares expresses a variation of the mean of each factor, and it is calculated through the summation of the squares of the differences of the means (Minitab, LLC, 2019). The degrees of freedom showed the amount of information per level used to evaluate the data (n-1) (Minitab, LLC, 2019). Dividing the sums of squares by the degrees of freedom gave as an output the means of squares.

Table 4.2.3: GLM variable 1

Analysis of Variance Variable 1					
Source	Degrees of Freedom	Sums of Squares	Mean of Squares	F-Value	P-Value
User	2	0.766	0.383	6.69	0.003
Pinna	6	0.196	0.033	0.57	0.751
User x Pinna	12	0.272	0.023	0.40	0.957
Residuals	42	2.404	0.057		
Total (corrected)	62	3.638			

Table 4.2.4: GLM variable 2

Analysis of Variance Variable 2					
Source	Degrees of Freedom	Sums of Squares	Mean of Squares	F-Value	P-Value
User	2	0.320	0.160	2.86	0.069
Pinna	6	0.096	0.016	0.29	0.941
User x Pinna	12	0.923	0.077	1.37	0.217
Residuals	42	2.354	0.056		
Total (corrected)	62	3.692			

Table 4.2.5: GLM variable 3

Analysis of Variance Variable 3					
Source	Degrees of Freedom	Sums of Squares	Mean of Squares	F-Value	P-Value
User	2	0.57	0.29	10.06	0.000
Pinna	6	0.27	0.04	1.58	0.177
User x Pinna	12	0.63	0.05	1.85	0.071
Residuals	42	1.20	0.03		
Total (corrected)	62	2.67			

Table 4.2.6: GLM variable 4

Analysis of Variance Variable 4					
Source	Degrees of Freedom	Sums of Squares	Mean of Squares	F-Value	P-Value
User	2	0.085	0.043	1.19	0.314
Pinna	6	0.067	0.011	0.31	0.927
User x Pinna	12	0.585	0.049	1.36	0.224
Residuals	42	1.507	0.036		
Total (corrected)	62	2.245			

Table 4.2.7: GLM variable 5

Analysis of Variance Variable 5					
Source	Degrees of Freedom	Sums of Squares	Mean of Squares	F-Value	P-Value
User	2	0.256	0.128	6.57	0.003
Pinna	6	0.111	0.019	0.95	0.469
User x Pinna	12	0.137	0.011	0.59	0.841
Residuals	42	0.817	0.019		
Total (corrected)	62	1.320			

Table 4.2.8: GLM variable 6

Analysis of Variance Variable 6					
Source	Degrees of Freedom	Sums of Squares	Mean of Squares	F-Value	P-Value
User	2	0.038	0.019	0.41	0.669
Pinna	6	0.319	0.053	1.14	0.354
User x Pinna	12	0.815	0.068	1.46	0.178
Residuals	42	1.953	0.047		
Total (corrected)	62	3.126			

Table 4.2.9: GLM variable 7

Analysis of Variance Variable 7					
Source	Degrees of Freedom	Sums of Squares	Mean of Squares	F-Value	P-Value
User	2	0.158	0.079	2.88	0.068
Pinna	6	0.123	0.020	0.74	0.617
User x Pinna	12	0.337	0.028	1.02	0.449
Residuals	42	1.155	0.028		
Total (corrected)	62	1.773			

The F-values resulted from the mean of squares divided by the residual mean square error (Montgomery & Runger, 2003). Through the usage of the F-distribution table with 95% interval confidence a P-value was obtained. These calculations were all performed within Minitab. The output data from GLM studies is presented in Tables 4.2.3-4.2.9. According to the P-value obtained in the GLM results, the user level was significantly different for variables 1 (Table 4.2.3), variable 3 (Table 4.2.5), and variable 5 (Table 4.2.7). The remaining of the variables followed the null hypothesis that there was no significant difference between the populations. The P-values observed for the pinna level of the analysis proved not to have a difference between the data. The same results were present for the variance analysis for the user vs the pinna where the null hypothesis was proved. After completing the assessment on the GLM models presented, normality plots were produced using the residuals from the studies. Performing these plots allow for verification on the normal distribution of the residuals (Minitab, LLC, 2019). It was noted that the

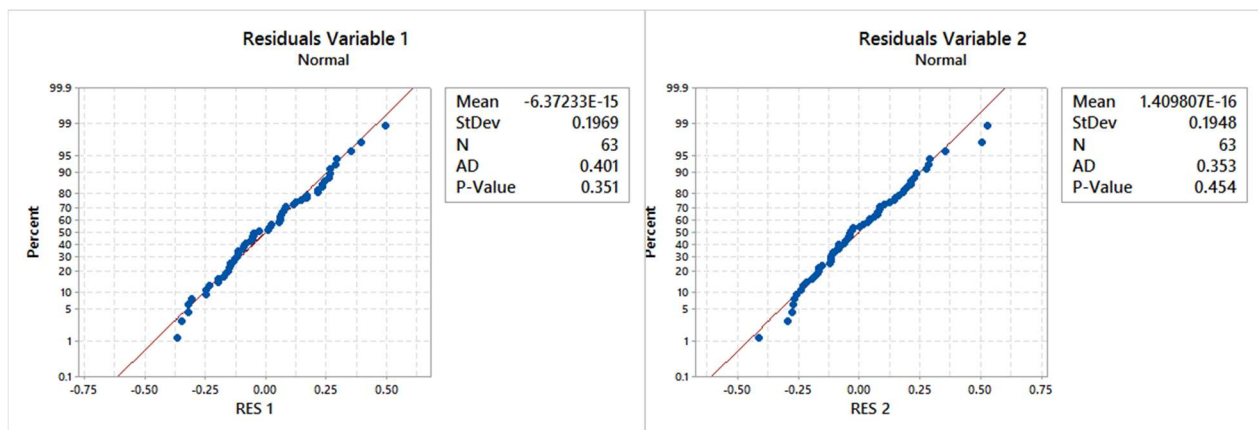


Figure 4.2.2 Residuals normality plots variables 1 & 2

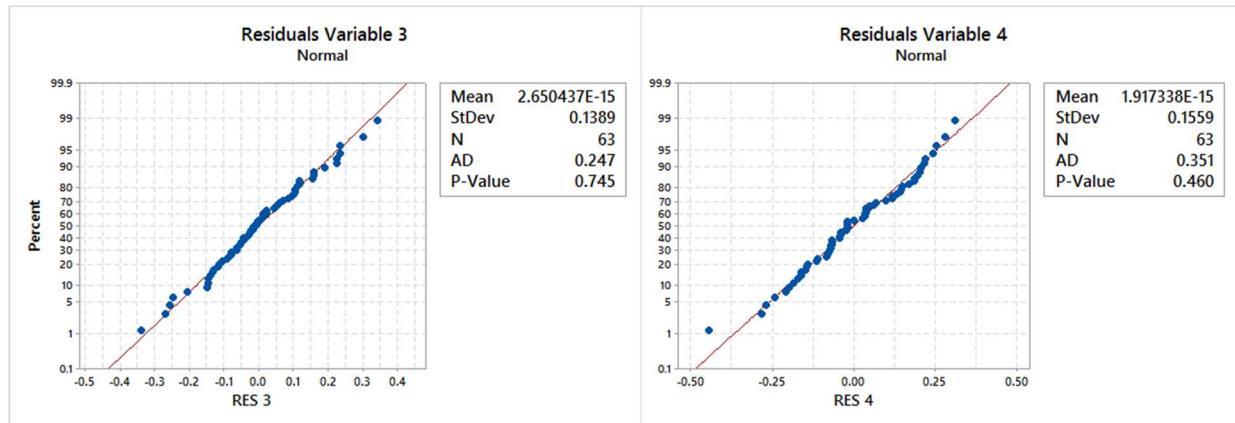


Figure 4.2.3 Residuals normality plots variables 3 & 4

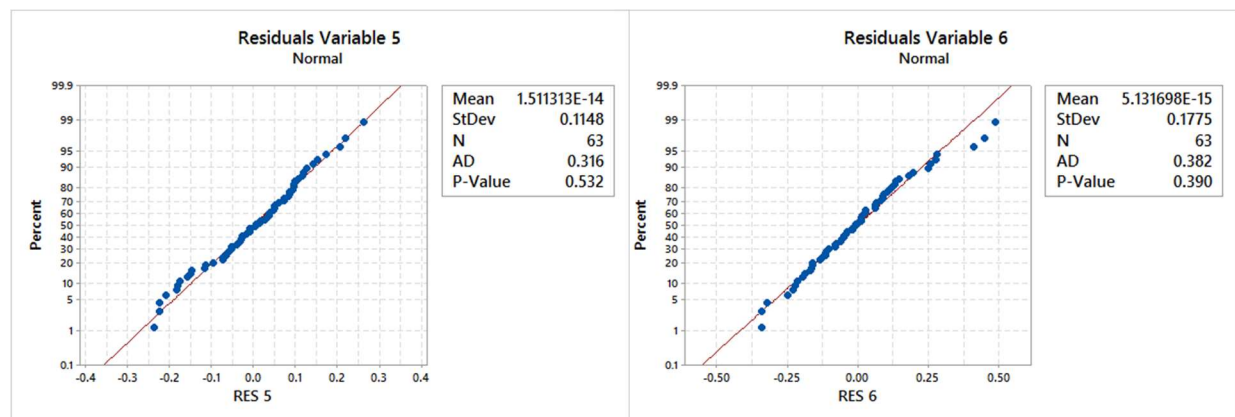


Figure 4.2.4 Residuals normality plots variables 5 & 6

P-values for the variable's residual normality plots were above the 0.05 mark for all the variables (Figures 4.2.2-4.2.5). All the variable residual normal plots were considered to have a normal distribution due to the p-value attained and the points following a straight line, although there were some distributions with outlier points such as variable 2 (Figure 4.2.2), variable 6 (Figure 4.2.4), and variable 7 (Figure 4.2.5).

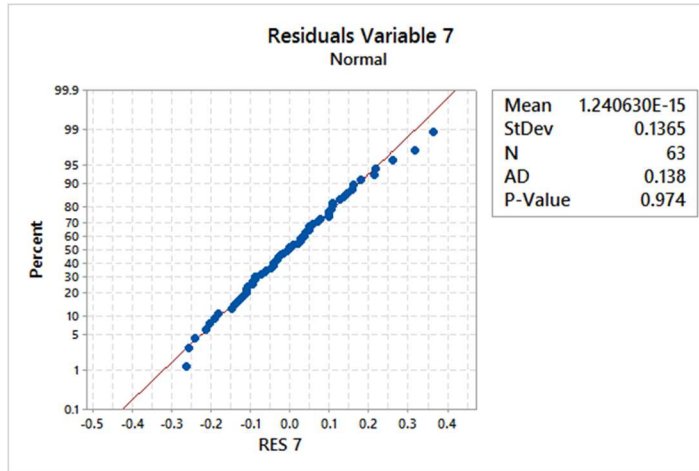


Figure 4.2.5 Residuals normality plots variable 7

Since there was a significant difference on the ANOVA study within the users for the variables 1, 3, and 5, a different study was performed using a non-parametric model. A Kruskal-Wallis model was performed to evaluate the users' interaction with the measurement data to analyze if the medians of the users differ. The users were analyzed as a whole as shown in Table 4.2.10, in which the P-value obtained were above 0.05, claiming no difference between the data. On the study per variable, the calculated P-value fell below 0.05 for variables 1, 3, and 5. Table 4.2.11 and Table 4.2.13 shows the medians obtained by user 1 possessed a lower mean rank for variables 1 and 5 respectively. These measurements yielded a high difference between the z-values resulting in a difference between users. The same difference in data can be observed in Table 4.2.12 where user 2 produced a higher median than the rest of the users. It is to be noted that the error on the users was not reflected on the pinnae variance or the pinna-user interaction.

Table 4.2.10: Kruskal-Wallis data vs users

Data vs users					
user	N	Median	Mean Rank	Z-Value	P-Value
u1	147	16.42	214.4	-0.77	0.74
u2	147	16.52	223.6	0.30	
u3	147	16.51	225.0	0.47	
Overall	441		221.0		

Table 4.2.11: Kruskal-Wallis variable 1 vs users

Variable 1 vs users					
user	N	Median	Mean Rank	Z-Value	P-Value
u1	21	18.15	20.5	-3.53	0.002
u2	21	18.35	37.4	1.65	
u3	21	18.34	38.1	1.88	
Overall	63		32		

Table 4.2.12: Kruskal-Wallis variable 3 vs users

Variable 3 vs users					
user	N	Median	Mean Rank	Z-Value	P-Value
u1	21	13.22	23.5	-2.6	0.001
u2	21	13.47	43.5	3.53	
u3	21	13.28	29	-0.93	
Overall	63		32		

Table 4.2.13: Kruskal-Wallis variable 5 vs users

Variable 5 vs users					
user	N	Median	Mean Rank	Z-Value	P-Value
u1	21	58.18	21.4	-3.26	0.003
u2	21	58.32	39.8	2.4	
u3	21	58.26	34.8	0.86	
Overall	63		32		

Confidence interval graphs were made from the GLM previously presented. To determine the significance of each factor an analysis between the pinnae measured using Fisher's least significant difference (LSD) was performed. The first comparative was made using the KEMAR pinna as a baseline to compared to the AM pinnae. For the null hypothesis to be rejected, the line must fall outside of the 0 mark line. Figure 4.2.6 shows the variables of KEMAR against the material extrusion pinnae. For the KEMAR and material extrusion there is no significant difference between the pinna measurements. The results from KEMAR against vat photopolymerization and material jetting technologies (Figure 4.2.7) also demonstrated no difference of means. The AM pinnae failed to reject the null hypothesis against KEMAR measurements. Comparisons among the additive manufacturing technologies were also performed using the same criterion. Figure 4.2.8 shows the material extrusion pinnae measurements were equal according to Fisher's LSD. The

SLA and Form 2 pinnae showed no statistical difference among means for the seven measured variables (Figure 4.2.9). To evaluate the further the pinnae variances, the data was analyzed per 3D printing system. The industrial systems studied were Fortus FDM, Viper SLA, and J750, in which all the variables fell under the 0 line with the exception of FDM and J750 on variable 3, where the null hypothesis is rejected (Figure 4.2.10). Data showed that variable 3 in certain cases was not only statistically different in this scenario, but also in the ANOVA and Kruskal-Wallis studies. As for desktop printers, the uPrint, Lulzbot and Form 2 systems had equal variances among the measured variables as observed in Figure 4.2.11.

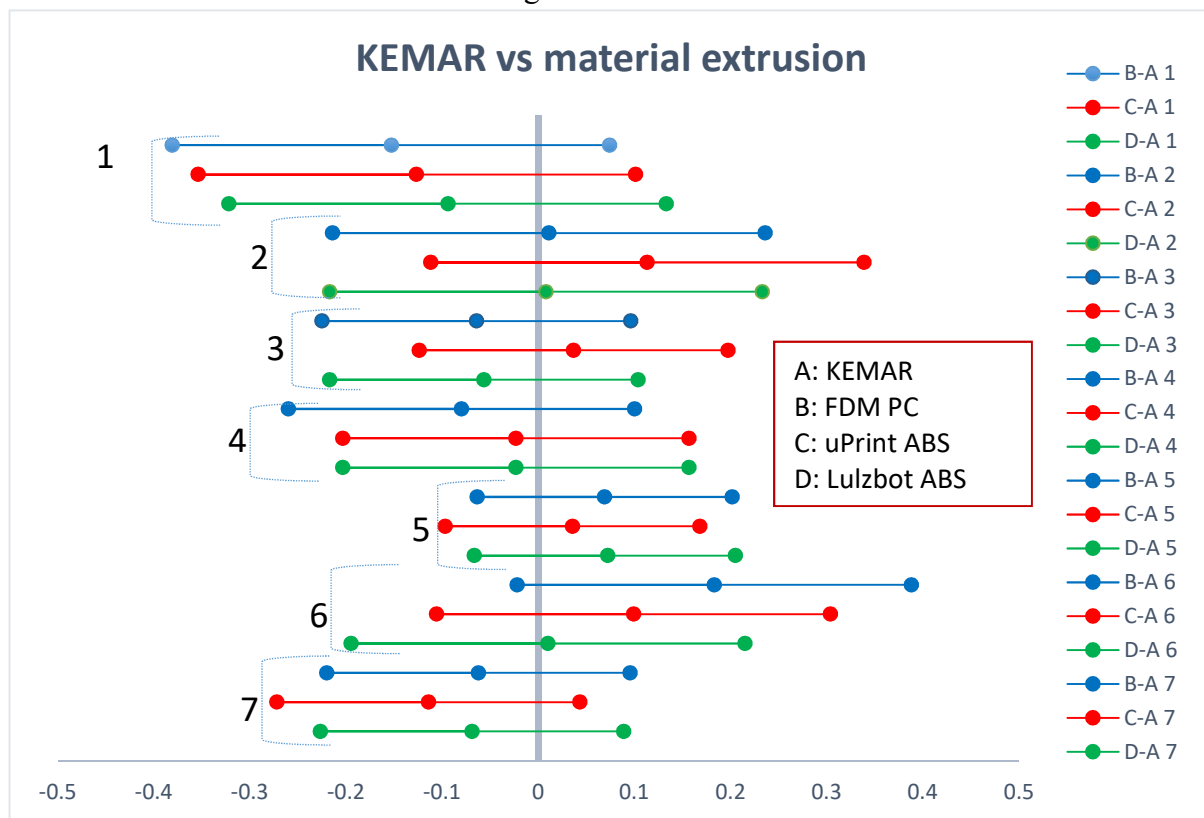


Figure 4.2.6 Fisher's LSD KEMAR vs material extrusion

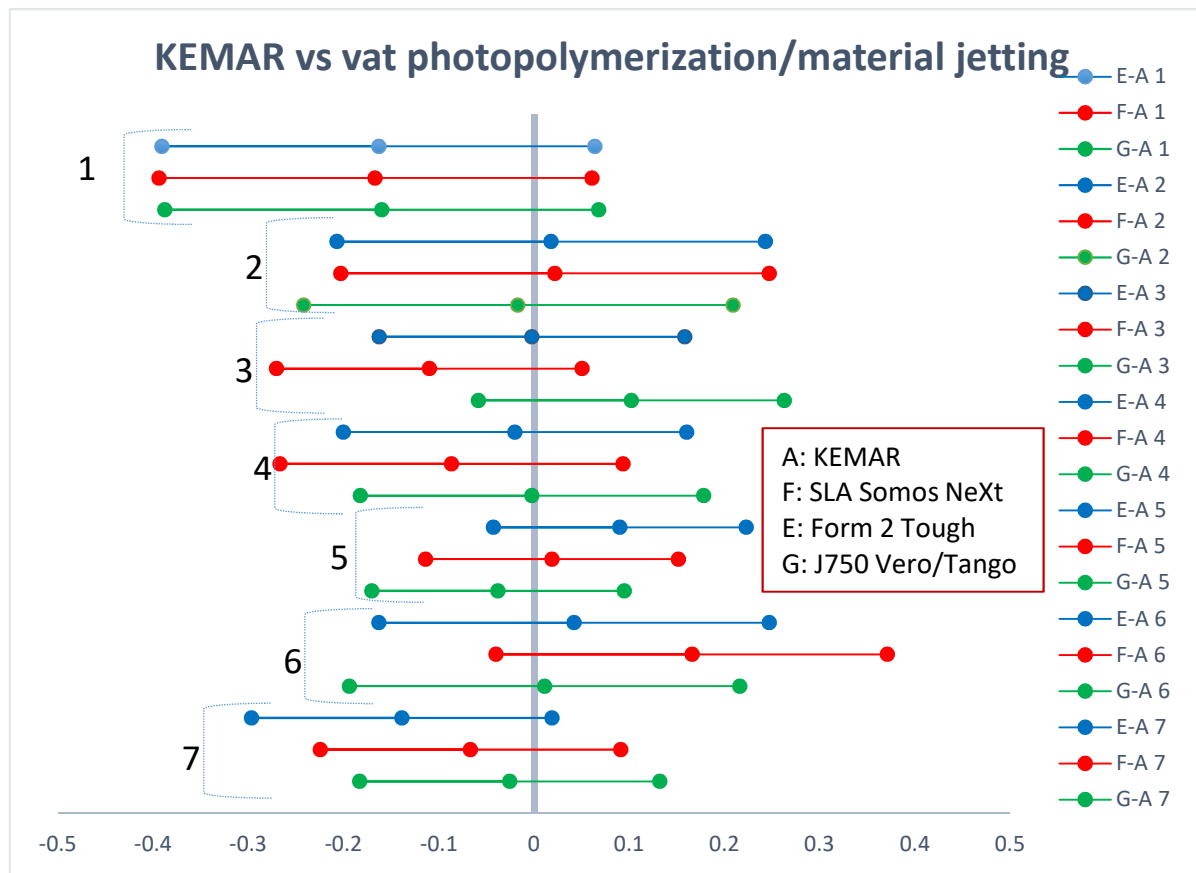


Figure 4.2.7 Fisher's LSD KEMAR vs vat photopolymerization/material jetting

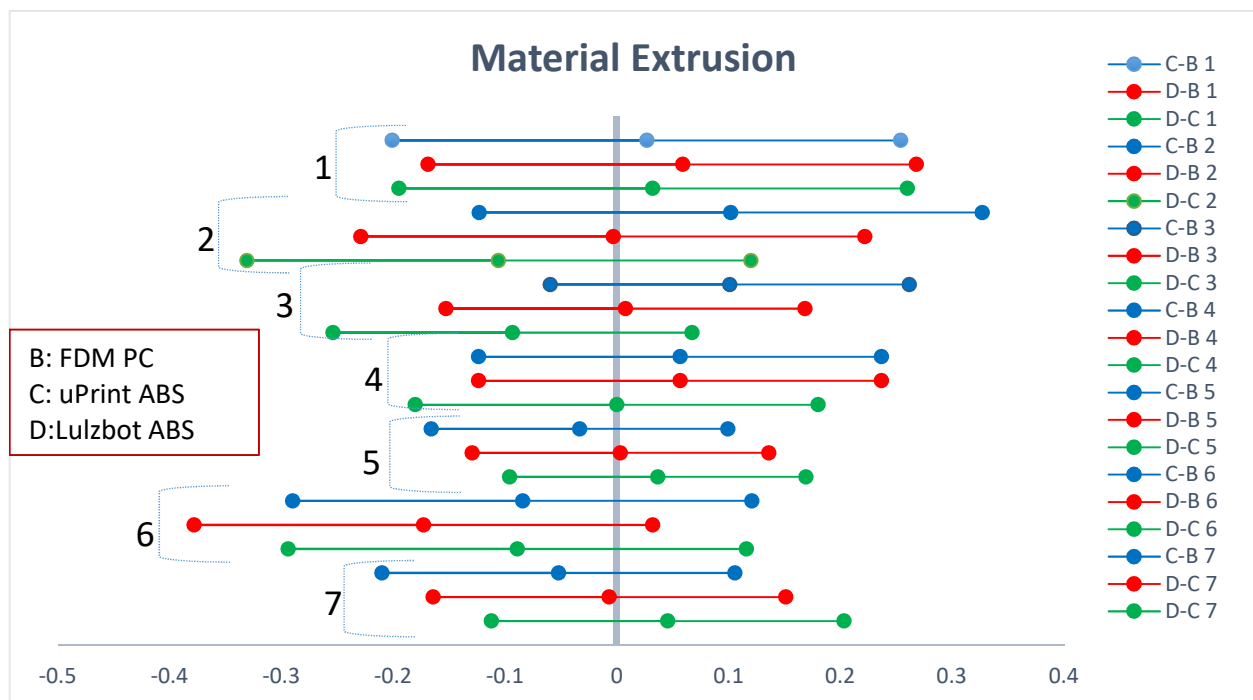


Figure 4.2.8 Fisher's LSD material extrusion

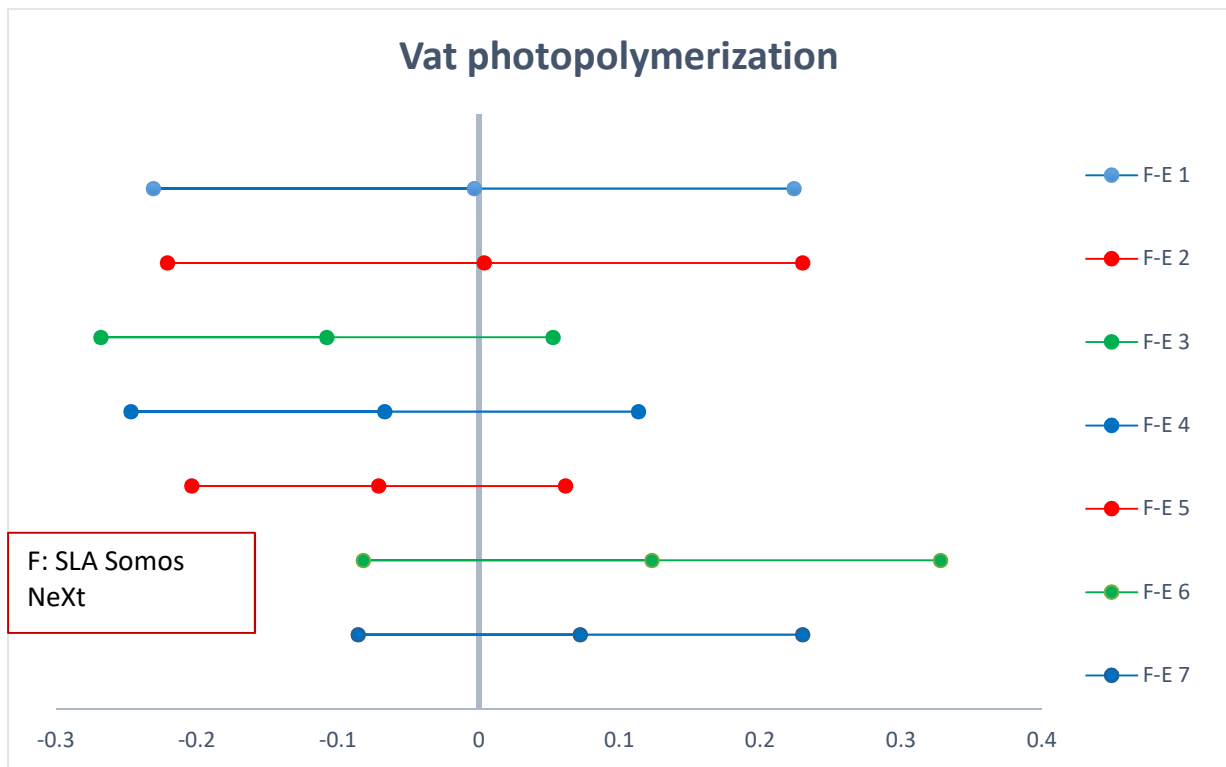


Figure 4.2.9 Fisher's LSD vat photopolymerization

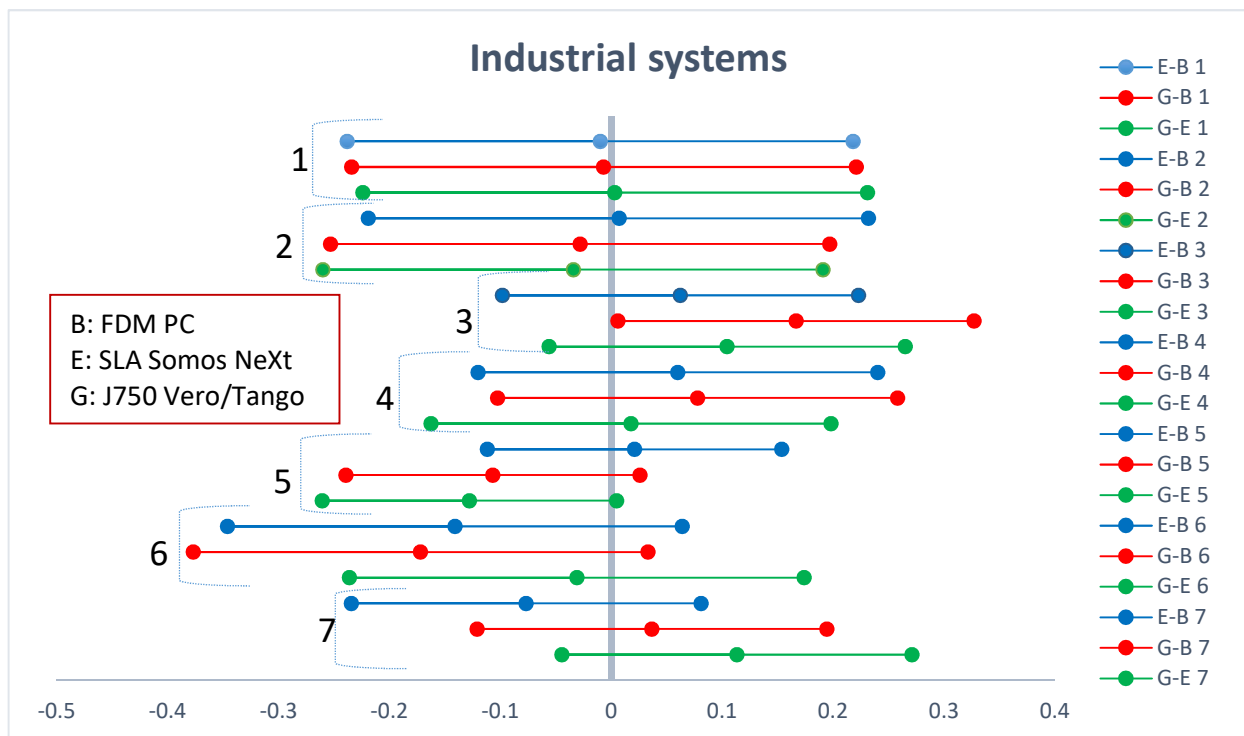


Figure 4.2.10 Fisher's LSD industrial systems

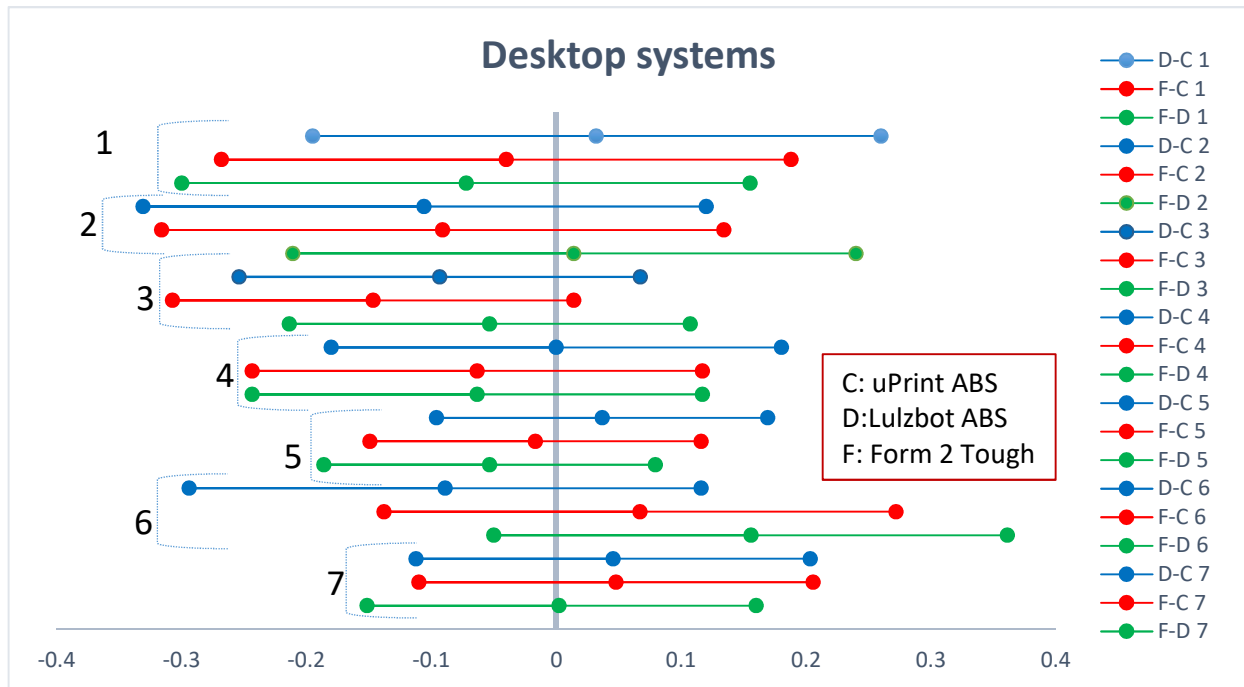


Figure 4.2.11 Fisher's LSD desktop system

4.3 KEMAR pinna vs 3D printed pinna acoustic measurements

Acoustical measurements were performed to quantify differences between the baseline KEMAR pinna model and the 3D printed pinnae. The accurate reproduction of the KEMAR pinna via additively manufacturing can also be verified by comparing the performance of mentioned pinnae in the acoustic setting. To validate the spatial cues preservation through the additive manufacturing process, preliminary acoustical tests were conducted on a KEMAR manikin. For these procedures, the SL Somos NeXt and the FDM PC right pinnae were used to compare the acoustic readings against the ones from KEMAR. A linear time invariant (LTI) system was used to characterize the acoustic response in both the frequency and time domain. The measurement of the frequency response on KEMAR was obtained by providing different input signals to the manikin, and analyzing the results captured by the KEMAR microphone to attain the amplitude and the phase response from these individual signals.

Raw acoustic measurements were conducted in the G.N. facilities in Glenview, IL, at the GLV EA lab. The baseline test was performed with the right small KEMAR pinna. The 3D printed pinnae were then tested using the same parameters as the KEMAR ear for comparison. The FDM PC o-ring 3D printed pinna and the SLA Somos NeXt with the silicone casing were used for this preliminary acoustic study (Figure 4.3.1). The KEMAR manikin was surrounded by four Tannoy speakers, which were positioned one meter away from KEMAR at the azimuth angles of 0, 90, 180 and 270 degrees. It has to be noted that only the right ear KEMAR microphone output was



Figure 4.3.1: AM pinnae tested on KEMAR manikin

analyzed for this study. Two signals were presented for this procedure. The first consisted of the frontal speaker presenting a sine sweep at 80 decibels of sound pressure level (db SPL). The second signal was a 1/24 octave pink noise coming from all four speakers, with a maximum of 94 db SPL. The raw measurements from these two signals were obtained for all three pinnae. The frequency responses were plotted to the signals presented according to each pinna test. Regardless of the signal type presented to each pinna, the frequency response was expected to agree for all three test scenarios.

From Fig 4.3.2., the frequency response for all three pinnae can be analyzed. The frequency response from the SLA Somos NeXt pinna followed the same pattern as KEMAR's on the 0-1 kHz range, and continued to do so with slight differences around the 2-5 kHz area and the 10 kHz mark. For the FDM PC pinna on the other hand, the frequency response line runs parallel to the KEMAR's, in the first interval from 0-1 kHz. The response from the PC pinna was different on the 2-5 kHz range, where the PC pinna showed a difference of 5 db SPL with respect to KEMAR. Similarities from this study can be particularly noticed on the region between 2-5 kHz, where the spectral differences due to pinna shape can be expected. Due to the different manufacturing processes involved for the SLA Somos NeXt pinna and the FDM PC pinna, results on the response difference would be further analyzed.

As previously mentioned, these tests and results were preliminary to the localization and externalization work being pursued. The correlation of the 3D printed pinna to KEMAR serves as a baseline for the ultimate goal of the custom headset design. The 3D printed headset concept

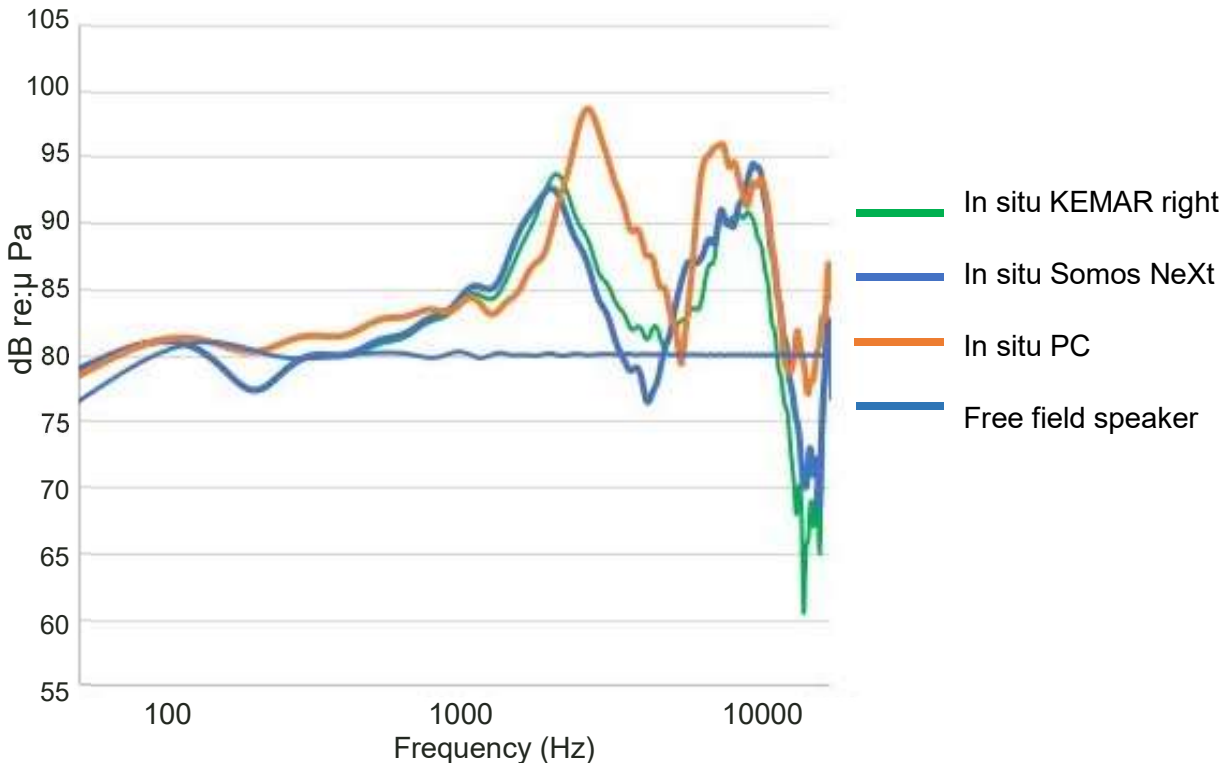


Figure 4.3.2: Frequency response comparative between KEMAR and AM pinnae

developed was sent to G.N. Glenview to be tested at their facilities. Results from that study will help understand further how the spatial cues can travel from an additive manufactured pinna to an individual's pinna, or in this case the KEMAR's pinna. Further testing with the AM technology/printing equipment matrix developed will be conducted to characterize variations on the frequency response.

Chapter 5: Conclusions and Recommendations for Future Research

5.1 Conclusions

The modeling and fabrication of ear pinnae via additive manufacturing was performed. Although challenges were presented with the initial small right KEMAR pinna CAD model when looking at the original STL file, the reconstruction of the box and the interface features were designed and incorporated for the AM pinna to be placed on the KEMAR manikin. The FaroArm 3D scanner served to reduce box irregularities of the pinna, but was not able to capture the geometry of the inner cavities nor the overhang features of the ear pinna. Alternatively, CT scanning effectively captured the ear's inner cavities, providing another baseline CAD file for the KEMAR right small ear. Both designs, the pinna on the silicone casing and the pinna with the o-ring, were fabricated to test the different insertion mechanisms of the pinna to the KEMAR manikin head. The material extrusion, vat photopolymerization, and material jetting technologies were used to print the pinnae allowed for an accurate replica of the ear geometry. These six pinnae were analyzed geometrically using three measurement tools, including readings using a CT scan computational model for each pinna. Irregularities were found when measuring the pinna height, which was the largest variable distance of the pinna using the NI Vision Assistant software. Regardless of the difference, the measurements within the Vision Assistant were constant for all the variables although it can be concluded that the usage of this measuring tool was inefficient for this procedure. After extensive analysis from the measurements with three tools, results demonstrated that in comparison to the KEMAR pinna, the material extrusion technology produced the most geometrically accurate replica with a maximum average percentage error of 3.8%. The measurements found the maximum difference to be 31.7% on the d7 dimension. Conclusions show that the caliper was the best tool to measure the AM pinnae. An ANOVA study was performed to assess interactions between the measured data and different technologies to KEMAR. No variance on the measurements was presented when making the dimensional comparative between the same technology, concluding that the desktop equipment can produce a part dimensionally equal to the ones fabricated in an industrial AM equipment. The analysis of

variance study performed confirmed the AM pinnae to be equal to the KEMAR pinna. The multi factorial analysis showed significant variance on variables 1, 3, and 5 on the user level, but not on the pinna and pinna-user levels. Even though these differences were statistically attained, the Kruskal-Wallis study showed P-values below 0.05 for the users, with ± 0.2 mm differences within the user readings. The 3D printed pinnae comparisons to KEMAR showed no statistical differences for any of the variables measured, entailing that all the technologies used captured KEMAR's dimensions. The comparisons among the AM technologies and equipment also demonstrated that the pinnae were statically equal in all the dimensions measured, with the exception of the FDM PC pinna with the J750 Vero/Tango pinna, which was significantly different on variable 3. This difference can be referred back to the users' variance difference for variable 3. The analysis of variance proved that all AM pinnae were statistically equal, meaning that within the two-dimensional variables analyzed, the KEMAR pinna is reproducible using any of the material extrusion, vat photopolymerization, and material jetting equipment. 3D printing technology can reproduce the ear pinna in terms of dimensional accuracy, and could be applied to the pinnae production by using a desktop system instead of an industrial type equipment in dispensers or points of need. Based on the measurement analysis, low cost equipment could perform the same as high end equipment, although performance acoustically has yet to be considered. AM pinnae Preliminary results on the frequency response show that additive manufacturing can be used to replicate KEMAR pinnae. The response showed a minimal variation on the frequency between KEMAR and the two AM pinnae. From the comparison of the SLA silicone casing pinna and a the FDM o-ring pinnae, the SLA showed a better response by remaining within the 2 dbL SPL. The frequency response results led to designing a first concept of a headset with an embedded pinna. The KEMAR head along with the KEMAR pinnae were 3D scanned and used on CAD for pinna position reference to model the muff with the pinna embedded. Further studies will conclude the different responses on the externalization and sound preservation testing the different 3D printing pinnae as well as the AM headset device.

5.2 Recommendations for Future Research

Externalization through the pinna embedded headset can present some challenges. Preserving the spatial cues through the 3D printed pinna can be done, but using a 3D printed pinna as a sound transport medium for another pinna can show a higher level of complexity. The acoustic testing on the first design of the custom headset device will answer questions regarding not only preservation of sound localization, but also effects such as the sound time arrival difference from the 3D printed pinna embedded to the KEMAR pinnae. The final design for the custom hearing device may entail introducing electronics to aid the preservation of spatial cues. Previous research performed at the Keck Center on multifunctional AM components and wire embedding on 3D printed parts could be applied to the final headset model. Using one of the hybrid additive manufacturing systems at the Keck Center, build interrupts can be leveraged to embed circuitry and components within the final component.

The progression of this research provided insight to the aspects that may lead to the completion of the custom advanced hearing device. The two-dimensional measurement analysis on the pinnae assessed the different technologies and equipment additive manufacturing has to offer. Results showed equal variances on industrial and desktop 3D printers, meaning the pinna can be reproduced anywhere there are similar desktop systems to the ones used available. Within the results attained from this research, desktop systems deliver the same product as industrial systems. Even though it was determined the AM pinna were equal geometrically to KEMAR's, further results on acoustic measurements will have an impact on pinnae selection for the hearing device. The question then turns to which AM pinna performs best under the acoustic scenario. Not only the material and the equipment have to be taken into consideration, but also the design of the pinna. The silicone case pinna design may be optimal to test different AM pinnae but the o-ring pinna design possess a more realistic version of how the hearing device would be fabricated, by being 3D printed as a whole instead of just the pinna as seen on the casing silicone approach. Results from future acoustic testing will help develop a matrix to select the most optimal equipment, design, and material needed for the final hearing device. Exploration on part infill

density and surface roughness relating to the layer thickness may also be enhance the results matrix.

References

- Acosta, D., García, O., & Aponte, J. (2006). Laser triangulation for shape acquisition in a 3D scanner plus scan. In *Electronics, Robotics and Automotive Mechanics Conference, 2006* (Vol. 2, pp. 14-19). IEEE.
- Algazi, V. R., Duda, R. O., Thompson, D. M., & Avendano, C. (2001). The cipic hrtf database. In *Proceedings of the 2001 IEEE Workshop on the Applications of Signal Processing to Audio and Acoustics* (Cat. No. 01TH8575) (pp. 99-102). IEEE.
- Ambriz, S., Coronel, J., Zinniel, B., Schloesser, R., Kim, C., Perez, M., Espalin, D., & Wicker, R. B. (2017). Material handling and registration for an additive manufacturing-based hybrid system. *Journal of Manufacturing Systems*, 45, 17-27.
- Bailey, C., Aguilera, E., Espalin, D., Motta, J., Fernandez, A., Perez, M. A., Dibiasio, C., Pryputniewicz, D., Macdonald, E., & Wicker, R. B. (2018). Augmenting Computer-Aided Design Software with Multi-Functional Capabilities to Automate Multi-Process Additive Manufacturing. *IEEE Access*, 6, 1985-1994.
- Bak, D. (2003). Rapid prototyping or rapid production? 3D printing processes move industry towards the latter. *Assembly Automation*, 23(4), 340-345.
- Bártolo, P. J. (Ed.). (2011). *Stereolithography: materials, processes and applications*. Springer Science & Business Media.
- Bickel, B., Bächer, M., Otaduy, M. A., Lee, H. R., Pfister, H., Gross, M., & Matusik, W. (2010, July). Design and fabrication of materials with desired deformation behavior. In *ACM Transactions on Graphics (TOG)* (Vol. 29, No. 4, p. 63). ACM.
- Bikas, H., Stavropoulos, P., & Chryssolouris, G. (2016). Additive manufacturing methods and modelling approaches: a critical review. *The International Journal of Advanced Manufacturing Technology*, 83(1-4), 389-405.
- Burkhard, M. D., & Sachs, R. M. (1975). Anthropometric manikin for acoustic research. *The Journal of the Acoustical Society of America*, 58(1), 214-222.
- Canon Medical Systems Corporation. (2018) Aquilion one genesis edition [Brochure] Retrieved from <https://us.medical.canon/download/ct-br-aq-one-genesis>
- Coronel, J. L., Fehr, K. H., Kelly, D. D., Espalin, D., & Wicker, R. B. (2017, May). Increasing component functionality via multi-process additive manufacturing. In *Micro-and Nanotechnology Sensors, Systems, and Applications IX* (Vol. 10194, p. 101941F). International Society for Optics and Photonics.
- Ding, D., Pan, Z., Cuiuri, D., & Li, H. (2015). A multi-bead overlapping model for robotic wire and arc additive manufacturing (WAAM). *Robotics and Computer-Integrated Manufacturing*, 31, 101-110.
- Doi, K. (2006). Diagnostic imaging over the last 50 years: research and development in medical imaging science and technology. *Physics in Medicine & Biology*, 51(13), R5.
- Doyle, B. J., Morris, L. G., Callanan, A., Kelly, P., Vorp, D. A., & McGloughlin, T. M. (2008). 3D reconstruction and manufacture of real abdominal aortic aneurysms: from CT scan to silicone model. *Journal of biomechanical engineering*, 130(3), 034501.

- Espalin, D., Muse, D. W., MacDonald, E., & Wicker, R. B. (2014). 3D Printing multifunctionality: structures with electronics. *The International Journal of Advanced Manufacturing Technology*, 72(5-8), 963-978.
- Espalin, D., Marquez, D., Fernandez, A., Kim, C., MacDonald, E., & Wicker, R. (2017). U.S. Patent Application No. 15/244,061.
- Evatronix S.A. (2019) Evixmatic automatic scanning and measuring system [Brochure] Retrieved from https://evixscan3d.com/wp-content/uploads/2019/05/eviXmatic_WEB-1.pdf
- FARO Technologies, Inc. (2018) FARO 8-axis design scanarm 2.5c [Brochure] Retrieved from https://www.faro.com/wp-content/uploads/resources-files/technical-sheets/04REF101-077_TechSheet_Design%20ScanArm_ALL_AP_SG.pdf
- Flores, R. L., Liss, H., Raffaelli, S., Humayun, A., Khouri, K. S., Coelho, P. G., & Witek, L. (2017). The technique for 3D printing patient-specific models for auricular reconstruction. *Journal of Cranio-Maxillofacial Surgery*, 45(6), 937–943.
- Frazier, W. E. (2014). Metal additive manufacturing: a review. *Journal of Materials Engineering and Performance*, 23(6), 1917-1928.
- Gardner, W. G., & Martin, K. D. (1995). HRTF measurements of a KEMAR. *The Journal of the Acoustical Society of America*, 97(6), 3907-3908.
- Gaytan, S. M., Cadena, M. A., Karim, H., Delfin, D., Lin, Y., Espalin, D., Macdonald, E., & Wicker, R. B. (2015). Fabrication of barium titanate by binder jetting additive manufacturing technology. *Ceramics International*, 41(5), 6610-6619.
- Gibson, I., Goenka, G., Narasimhan, R., & Bhat, N. (2010, August). Design rules for additive manufacture. In *Solid Freeform Fabrication Symposium* (pp. 705-716). Austin, TX.
- Gokuldoss, P. K., Kolla, S., & Eckert, J. (2017). Additive manufacturing processes: Selective laser melting, electron beam melting and binder jetting—Selection guidelines. *Materials*, 10(6), 672.
- Guo, N., & Leu, M. C. (2013). Additive manufacturing: technology, applications and research needs. *Frontiers of Mechanical Engineering*, 8(3), 215-243.
- Harder, S., Paulsen, R. R., Larsen, M., Laugesen, S., Mihocic, M., & Majdak, P. (2016). A framework for geometry acquisition, 3-D printing, simulation, and measurement of head-related transfer functions with a focus on hearing-assistive devices. *Computer Aided Design*, 75–76, 39–46.
- Hartmann, W. M., & Wittenberg, A. (1996). On the externalization of sound images. *The Journal of the Acoustical Society of America*, 99(6), 3678-3688.
- Herderick, E. (2011). Additive manufacturing of metals: A review. *Materials Science and Technology*, (MS), 1413.
- Ionita, C. N., Mokin, M., Varble, N., Bednarek, D. R., Xiang, J., Snyder, K. V., ... & Rudin, S. (2014, March). Challenges and limitations of patient-specific vascular phantom fabrication using 3D Polyjet printing. In *Medical Imaging 2014: Biomedical Applications in Molecular, Structural, and Functional Imaging* (Vol. 9038, p. 90380M). International Society for Optics and Photonics.

- Ippolito, R., Iuliano, L., & Gatto, A. (1995). Benchmarking of rapid prototyping techniques in terms of dimensional accuracy and surface finish. *CIRP Annals-Manufacturing Technology*, 44(1), 157-160.
- Joe Lopes, A., MacDonald, E., & Wicker, R. B. (2012). Integrating stereolithography and direct print technologies for 3D structural electronics fabrication. *Rapid Prototyping Journal*, 18(2), 129-143.
- Klingenbeck-Regn, K., Schaller, S., Flohr, T., Ohnesorge, B., Kopp, A. F., & Baum, U. (1999). Subsecond multi-slice computed tomography: basics and applications. *European journal of radiology*, 31(2), 110-124.
- Kruth, J. P., Leu, M. C., & Nakagawa, T. (1998). Progress in additive manufacturing and rapid prototyping. *Cirp Annals*, 47(2), 525-540.
- Kulkarni, A., & Colburn, H. S. (1998). Role of spectral detail in sound-source localization. *Nature*, 396 (6713), 747.
- Lakshminarayan, U., Ogrydziak, S., & Marcus, H. L. (1990). Selective laser sintering of ceramic materials. In 1990 International Solid Freeform Fabrication Symposium.
- Liacouras, P., Garnes, J., Roman, N., Petrich, A., & Grant, G. T. (2011). Designing and manufacturing an auricular prosthesis using computed tomography, 3-dimensional photographic imaging, and additive manufacturing: A clinical report. *The Journal of Prosthetic Dentistry*, 105 (2), 78–82
- MacDonald, E., Espalin, D., Doyle, D., Muñoz, J., Ambriz, S., Coronel, J., ... & Wicker, R. (2018). Fabricating patch antennas within complex dielectric structures through multi-process 3D printing. *Journal of Manufacturing Processes*, 34, 197-203.
- MacDonald, E., Salas, R., Espalin, D., Perez, M., Aguilera, E., Muse, D., & Wicker, R. B. (2014). 3D printing for the rapid prototyping of structural electronics. *IEEE access*, 2, 234-242.
- MacDonald, E., & Wicker, R. (2016). Multiprocess 3D printing for increasing component functionality. *Science*, 353(6307), aaf2093.
- Mannoor, M. S., Jiang, Z., James, T., Kong, Y. L., Malatesta, K. A., Soboyejo, W. O., Verma, N., Gracias, D. H., & McAlpine, M. C. (2013). 3D Printed Bionic Ears. *Nano Letters*, 13(6), 2634–2639.
- Melchels, F. P., Feijen, J., & Grijpma, D. W. (2010). A review on stereolithography and its applications in biomedical engineering. *Biomaterials*, 31(24), 6121-6130.
- Middlebrooks, J. C., & Green, D. M. (1991). Sound localization by human listeners. *Annual review of psychology*, 42(1), 135-159.
- Minitab, LLC (2019) Minitab 18 support. Retrieved from <https://support.minitab.com/en-us/minitab/18/>
- Mohammed, M. I., Tatineni, J., Cadd, B., Peart, G., Gibson, I. (2017). Advanced Auricular Prosthesis Development by 3D Modelling and Multi-material Printing. *The International Conference on the Design and Technology*, KEG, 37–43.
- Montgomery, D. C., & Runger, G. C. (2003) *Applied statistics and probability for engineers*. New York, NY. John Wiley & Sons, Inc.

- Murr, L. E., Martinez, E., Amato, K. N., Gaytan, S. M., Hernandez, J., Ramirez, D. A., ... & Wicker, R. B. (2012). Fabrication of metal and alloy components by additive manufacturing: examples of 3D materials science. *Journal of Materials Research and technology*, 1(1), 42-54.
- Muse, D. W., Wicker, R., MacDonald, E., Salas, R., & Medina, F. (2018). U.S. Patent No. 9,908,037. Washington, DC: U.S. Patent and Trademark Office.
- Muth, J. T., Vogt, D. M., Truby, R. L., Mengüç, Y., Kolesky, D. B., Wood, R. J., & Lewis, J. A. (2014). Embedded 3D printing of strain sensors within highly stretchable elastomers. *Advanced Materials*, 26(36), 6307-6312.
- Novakova-Marcincinova, L., & Kuric, I. (2012). Basic and advanced materials for fused deposition modeling rapid prototyping technology. *Manuf. and Ind. Eng.*, 11(1), 24-27.
- Ono, N., Hayashi, Y., Kisuki, A., & Ikeda, Y. (1996). U.S. Patent No. 5,510,792. Washington, DC: U.S. Patent and Trademark Office.
- Ota, H., Emaminejad, S., Gao, Y., Zhao, A., Wu, E., Challa, S., ... & Gao, W. (2016). Application of 3D printing for smart objects with embedded electronic sensors and systems. *Advanced Materials Technologies*, 1(1), 1600013.
- Pauly, M., Mitra, N. J., Giesen, J., Gross, M. H., & Guibas, L. J. (2005). Example-based 3D scan completion. In *Symposium on Geometry Processing* (No. CONF).
- Perez, C. L. (2002). Analysis of the surface roughness and dimensional accuracy capability of fused deposition modelling processes. *International Journal of Production Research*, 40(12), 2865-2881.
- Perez, K. B., & Williams, C. B. (2013, August). Combining additive manufacturing and direct write for integrated electronics—a review. In *24th International Solid Freeform Fabrication Symposium—An Additive Manufacturing Conference*, SFF (pp. 962-979).
- Peyre, P., Aubry, P., Fabbro, R., Neveu, R., & Longuet, A. (2008). Analytical and numerical modelling of the direct metal deposition laser process. *Journal of Physics D: Applied Physics*, 41(2), 025403.
- Pilipović, A., Raos, P., & Šercer, M. (2009). Experimental analysis of properties of materials for rapid prototyping. *The International Journal of Advanced Manufacturing Technology*, 40(1-2), 105-115.
- Reichinger, A., Majdak, P., Sablatnig, R., & Maierhofer, S. (2013). Evaluation of Methods for Optical 3-D Scanning of Human Pinnas. In *2013 International Conference on 3D Vision - 3DV 2013* (pp. 390–397).
- Rengier, F., Mehndiratta, A., Von Tengg-Koblighk, H., Zechmann, C. M., Unterhinninghofen, R., Kauczor, H. U., & Giesel, F. L. (2010). 3D printing based on imaging data: review of medical applications. *International journal of computer assisted radiology and surgery*, 5(4), 335-341.
- Roberson, D. A., Wicker, R. B., Murr, L. E., Church, K., & MacDonald, E. (2011). Microstructural and process characterization of conductive traces printed from Ag particulate inks. *Materials*, 4(6), 963-979.

- Rydborg, J., Buckwalter, K. A., Caldemeyer, K. S., Phillips, M. D., Conces Jr, D. J., Aisen, A. M., ... & Kopecky, K. K. (2000). Multisection CT: scanning techniques and clinical applications. *Radiographics*, 20(6), 1787-1806.
- Sames, W. J., List, F. A., Pannala, S., Dehoff, R. R., & Babu, S. S. (2016). The metallurgy and processing science of metal additive manufacturing. *International Materials Reviews*, 61(5), 315-360.
- Seitz, H., Rieder, W., Irsen, S., Leukers, B., & Tille, C. (2005). Three-dimensional printing of porous ceramic scaffolds for bone tissue engineering. *Journal of Biomedical Materials Research Part B: Applied Biomaterials: An Official Journal of The Society for Biomaterials, The Japanese Society for Biomaterials, and The Australian Society for Biomaterials and the Korean Society for Biomaterials*, 74(2), 782-788.
- Shemelya, C., Cedillos, F., Aguilera, E., Maestas, E., Ramos, J., Espalin, D., ... & MacDonald, E. (2013, November). 3D printed capacitive sensors. In *SENSORS, 2013 IEEE* (pp. 1-4). IEEE.
- Shemelya, C., Cedillos, F., Aguilera, E., Espalin, D., Muse, D., Wicker, R., & MacDonald, E. (2015). Encapsulated copper wire and copper mesh capacitive sensing for 3-D printing applications. *IEEE Sensors Journal*, 15(2), 1280-1286.
- Siemens (2009) Inside biograph Truepoint PET/CT [Brochure] Retrieved from: https://www.siemens-healthineers.com/siemens_hwem-hwem_sxxa_websites-context-root/wcm/idc/groups/public/@global/@imaging/@molecular/documents/download/mdaw/mtuz/~edisp/btruep_technology_insert-00046599.p
- Song, X., Pan, Y., & Chen, Y. (2015). Development of a low-cost parallel kinematic machine for multidirectional additive manufacturing. *Journal of Manufacturing Science and Engineering*, 137(2), 021005.
- Standard, A. S. T. M. (2012). ISO/ASTM 52900: 2015 Additive manufacturing-General principles-terminology. ASTM F2792-10e1.
- Stampfl, J., Baudis, S., Heller, C., Liska, R., Neumeister, A., Kling, R., ... & Spitzbart, M. (2008). Photopolymers with tunable mechanical properties processed by laser-based high-resolution stereolithography. *Journal of Micromechanics and Microengineering*, 18(12), 125014.
- Suaste-Gómez, E., Rodríguez-Roldán, G., Reyes-Cruz, H., & Terán-Jiménez, O. (2016). Developing an Ear Prosthesis Fabricated in Polyvinylidene Fluoride by a 3D Printer with Sensory Intrinsic Properties of Pressure and Temperature. *Sensors*, 16(3), 332.
- Talcott, K. A., Casali, J. G., Keady, J. P., & Killion, M. C. (2012). Azimuthal auditory localization of gunshots in a realistic field environment: effects of open-ear versus hearing protection-enhancement devices (HPEDs), military vehicle noise, and hearing impairment. *International journal of audiology*, 51(sup1), S20-S30.
- Taminger, K., & Hafley, R. A. (2003). Electron beam freeform fabrication: a rapid metal deposition process.
- Turner, B.N., Strong, R., & A. Gold, S. (2014). A review of melt extrusion additive manufacturing processes: I. Process design and modeling. *Rapid Prototyping Journal*, 20(3), 192-204.

- Turner, B. N., & Gold, S. A. (2015). A review of melt extrusion additive manufacturing processes: II. Materials, dimensional accuracy, and surface roughness. *Rapid Prototyping Journal*, 21(3), 250-261.
- Vaezi, M., Chianrabutra, S., Mellor, B., & Yang, S. (2013). Multiple material additive manufacturing—Part 1: a review: this review paper covers a decade of research on multiple material additive manufacturing technologies which can produce complex geometry parts with different materials. *Virtual and Physical Prototyping*, 8(1), 19-50.
- Verdun, F. R., Racine, D., Ott, J. G., Tapiovaara, M. J., Toroi, P., Bochud, F. O., ... & Marshall, N. W. (2015). Image quality in CT: From physical measurements to model observers. *Physica Medica*, 31(8), 823-843.
- Williams, S. W., Martina, F., Addison, A. C., Ding, J., Pardal, G., & Colegrove, P. (2016). Wire+ arc additive manufacturing. *Materials Science and Technology*, 32(7), 641-647.
- Wong, K. V., & Hernandez, A. (2012). A review of additive manufacturing. *ISRN Mechanical Engineering*, 2012.
- Xiao, K., Zardawi, F., Van Noort, R., & Yates, J. M. (2014). Developing a 3D colour image reproduction system for additive manufacturing of facial prostheses. *The International Journal of Advanced Manufacturing Technology*, 70(9-12), 2043–2049.
- Yao, A. W. L. (2005). Applications of 3D scanning and reverse engineering techniques for quality control of quick response products. *The international journal of advanced manufacturing technology*, 26(11-12), 1284-1288.
- Zhou, C., Chen, Y., Yang, Z. G., & Khoshnevis, B. (2011). Development of multi-material mask-image-projection-based stereolithography for the fabrication of digital materials. In *Annual solid freeform fabrication symposium*, Austin, TX..

Appendix

Appendix table 4.1: Right caliper measurements

KEMAR Right Pinna							
Measurement	d1'	d2'	d3'	d4'	d5'	d6'	d7'
1	17.6	6.5	14.1	15.7	57.5	26.2	6.3
2	18.5	5.9	14.7	17.5	57.6	27.6	5.4
3	18.2	6.4	14.9	16.8	57.7	26.4	5.7
Mean	18.1	6.3	14.6	16.7	57.6	26.7	5.8
SD	0.7	0.5	0.6	1.3	0.1	1.1	0.6

FDM PC Right Pinna (GN)							
Measurement	d1'	d2'	d3'	d4'	d5'	d6'	d7'
1	18.4	5.8	14.2	14.8	57.5	25.5	5.8
2	18.5	5.2	14.0	16.6	57.1	26.0	5.9
3	18.3	6.0	13.9	15.7	57.6	25.6	5.6
Mean	18.4	5.6	14.0	15.7	57.4	25.7	5.8
SD	0.1	0.6	0.2	1.3	0.4	0.4	0.2

uPrint ABS Right Pinna (GN)							
Measurement	d1'	d2'	d3'	d4'	d5'	d6'	d7'
1	18.3	5.9	14.8	16.9	57.5	26.3	4.8
2	17.3	6.2	13.7	16.2	56.2	25.8	5.3
3	17.9	6.9	14.1	16.1	57.1	25.8	6.0
Mean	17.8	6.3	14.2	16.4	56.9	26.0	5.3
SD	0.7	0.7	0.8	0.6	0.9	0.4	0.9

Lulzbot ABS Right Pinna (GN)							
Measurement	d1'	d2'	d3'	d4'	d5'	d6'	d7'
1	18.1	6.7	14.5	16.6	57.5	25.3	5.8
2	18.4	6.4	14.4	15.9	57.7	25.4	5.5
3	18.6	6.7	13.6	16.2	57.7	26.5	5.5
Mean	18.3	6.6	14.2	16.2	57.6	25.7	5.6
SD	0.4	0.2	0.6	0.5	0.2	0.9	0.2

Viper SLA Somos NeXt Right Pinna (GN)							
Measurement	d1'	d2'	d3'	d4'	d5'	d6'	d7'
1	18.1	6.0	13.6	16.4	57.7	24.9	5.0

2	17.2	5.8	14.5	16.4	57.5	24.2	5.3
3	17.4	5.5	13.5	15.5	57.2	24.0	5.4
Mean	17.5	5.8	13.9	16.1	57.4	24.3	5.2
SD	0.6	0.4	0.8	0.8	0.4	0.7	0.3

Form 2 Tough Right Pinna (GN)							
Measurement	d1'	d2'	d3'	d4'	d5'	d6'	d7'
1	17.6	5.7	14.9	15.4	57.6	26.5	4.9
2	17.4	6.3	13.8	15.9	57.1	25.5	5.0
3	17.7	5.1	15.2	16.1	57.4	26.1	5.8
Mean	17.6	5.7	14.6	15.8	57.4	26.0	5.3
SD	0.2	0.8	1.1	0.5	0.3	0.7	0.7

J750 Flexible Resin Right Pinna (GN)							
Measurement	d1'	d2'	d3'	d4'	d5'	d6'	d7'
1	18.3	5.3	14.7	17.7	58.1	24.7	5.1
2	18.7	5.1	14.8	17.4	57.9	24.1	6.4
3	18.3	5.9	14.5	17.2	58.1	24.4	5.7
Mean	18.4	5.4	14.7	17.5	58.0	24.4	5.7
SD	0.4	0.6	0.2	0.4	0.2	0.4	0.9

FDM PC Right Pinna (UTEP)							
Measurement	d1'	d2'	d3'	d4'	d5'	d6'	d7'
1	17.5	4.6	14.5	16.6	58.4	27.6	4.7
2	17.5	6.9	14.4	16.0	57.1	25.9	5.8
3	17.4	6.7	14.7	16.2	56.9	24.9	6.0
Mean	17.5	6.1	14.5	16.3	57.4	26.1	5.5
SD	0.1	1.8	0.2	0.4	1.2	1.9	1.0

uPrint ABS Right Pinna (UTEP)							
Measurement	d1'	d2'	d3'	d4'	d5'	d6'	d7'
1	17.8	6.1	14.1	16.8	58.4	27.3	4.9
2	17.6	6.4	14.8	16.0	57.2	26.1	5.9
3	17.6	6.6	14.6	16.3	57.5	25.9	5.8
Mean	17.7	6.4	14.5	16.4	57.7	26.4	5.5
SD	0.2	0.4	0.5	0.5	0.9	1.1	0.8

Lulzbot ABS Right Pinna (UTEP)							
Measurement	d1'	d2'	d3'	d4'	d5'	d6'	d7'
1	17.0	5.0	13.9	16.5	58.4	27.6	4.8

2	17.0	5.9	14.8	16.6	57.5	25.9	6.1
3	17.2	6.1	14.9	16.3	57.3	26.1	6.2
Mean	17.1	5.7	14.5	16.4	57.7	26.5	5.7
SD	0.2	0.8	0.8	0.2	0.8	1.3	1.1

Viper SLA Somos NeXt Right Pinna (UTEP)							
Measurement	d1'	d2'	d3'	d4'	d5'	d6'	d7'
1	17.0	5.0	14.3	17.1	58.3	26.8	4.9
2	18.0	6.3	14.2	16.5	57.2	26.8	6.1
3	17.9	6.4	14.9	16.3	57.3	24.0	6.0
Mean	17.6	5.9	14.5	16.7	57.6	25.9	5.7
SD	0.8	1.1	0.5	0.6	0.9	2.3	0.9

Form 2 Tough Right Pinna (UTEP)							
Measurement	d1'	d2'	d3'	d4'	d5'	d6'	d7'
1	17.3	6.7	14.6	16.7	57.3	26.0	5.7
2	17.2	5.8	14.8	16.9	56.9	26.8	6.4
3	17.2	5.8	14.5	16.6	57.7	26.2	6.0
Mean	17.2	6.1	14.6	16.7	57.3	26.3	6.1
SD	0.1	0.7	0.2	0.2	0.6	0.6	0.5

J750 Flexible Resin Right Pinna (UTEP)							
Measurement	d1'	d2'	d3'	d4'	d5'	d6'	d7'
1	17.3	5.7	14.3	16.7	56.8	25.7	6.1
2	17.6	6.6	14.4	16.8	56.9	25.3	5.7
3	17.5	5.9	14.8	17.1	57.1	26.1	5.9
Mean	17.5	6.1	14.5	16.9	56.9	25.7	5.9
SD	0.2	0.6	0.4	0.3	0.2	0.6	0.3

Appendix table 4.2: Right NI Vision Assistant measurements

KEMAR Right Pinna							
Measurement	d1'	d2'	d3'	d4'	d5'	d6'	d7'
1	17.6	6.5	13.4	15.7	60.6	25.7	5.1
2	18.3	6.8	12.6	14.4	60.3	25.3	5.3
3	18.4	6.7	13.5	14.7	60.6	24.8	5.0
Mean	18.1	6.7	13.2	14.9	60.5	25.2	5.1
SD	0.6	0.2	0.7	0.9	0.3	0.6	0.2

FDM PC Right Pinna (GN)							
Measurement	d1'	d2'	d3'	d4'	d5'	d6'	d7'
1	18.5	6.4	13.4	16.7	58.9	25.2	4.6
2	17.9	6.1	13.4	16.8	59.7	25.6	4.6
3	18.5	5.9	13.6	16.5	59.0	25.3	4.4
Mean	18.3	6.1	13.5	16.7	59.2	25.4	4.6
SD	0.5	0.4	0.1	0.2	0.6	0.3	0.2

uPrint ABS Right Pinna (GN)							
Measurement	d1'	d2'	d3'	d4'	d5'	d6'	d7'
1	17.3	7.5	13.2	16.6	60.4	24.6	3.4
2	17.2	6.7	13.5	17.2	59.9	24.5	4.0
3	17.1	5.9	12.8	17.7	60.1	24.1	4.2
Mean	17.2	6.7	13.1	17.2	60.1	24.4	3.9
SD	0.2	1.1	0.5	0.8	0.3	0.4	0.6

Lulzbot ABS Right Pinna (GN)							
Measurement	d1'	d2'	d3'	d4'	d5'	d6'	d7'
1	17.7	6.6	13.6	15.8	61.2	25.8	5.0
2	18.5	6.4	13.5	15.3	60.8	26.7	5.5
3	17.9	6.1	13.9	16.1	59.8	26.9	4.7
Mean	18.0	6.4	13.7	15.7	60.6	26.5	5.1
SD	0.6	0.3	0.3	0.6	1.0	0.8	0.6

Viper SLA Somos NeXt Right Pinna (GN)							
Measurement	d1'	d2'	d3'	d4'	d5'	d6'	d7'
1	17.5	7.1	13.3	16.6	59.0	25.0	4.0
2	17.8	6.6	13.6	16.7	59.0	24.8	4.6
3	17.9	6.5	13.8	17.3	59.1	25.2	4.6
Mean	17.8	6.7	13.6	16.9	59.0	25.0	4.4
SD	0.3	0.5	0.4	0.5	0.1	0.3	0.4

Form 2 Tough Right Pinna (GN)							
Measurement	d1'	d2'	d3'	d4'	d5'	d6'	d7'
1	17.4	5.7	13.6	15.4	59.7	25.2	4.6
2	18.1	6.6	13.5	15.4	59.8	25.6	4.3
3	18.0	6.9	13.6	15.2	59.7	25.7	5.0
Mean	17.8	6.4	13.5	15.3	59.7	25.5	4.6
SD	0.5	0.8	0.1	0.2	0.1	0.4	0.5

J750 Flexible Resin Right Pinna (GN)							
Measurement	d1'	d2'	d3'	d4'	d5'	d6'	d7'
1	18.0	6.3	14.0	15.8	60.1	26.8	3.8
2	17.9	6.8	13.6	16.8	60.2	27.8	4.8
3	17.7	5.9	13.6	16.9	60.1	27.2	4.5
Mean	17.9	6.3	13.7	16.5	60.1	27.3	4.4
SD	0.2	0.6	0.4	0.9	0.1	0.7	0.7

FDM PC Right Pinna (UTEP)							
Measurement	d1'	d2'	d3'	d4'	d5'	d6'	d7'
1	18.6	5.8	12.3	13.2	60.0	24.3	5.1
2	18.5	6.0	11.4	13.3	60.3	24.3	5.2
3	18.3	6.7	12.6	13.6	60.1	24.9	5.2
Mean	18.5	6.2	12.1	13.4	60.1	24.5	5.2
SD	0.2	0.6	0.9	0.3	0.2	0.5	0.1

uPrint ABS Right Pinna (UTEP)							
Measurement	d1'	d2'	d3'	d4'	d5'	d6'	d7'
1	17.8	5.8	13.0	16.7	59.9	25.4	4.5
2	17.6	6.0	12.6	17.2	59.6	25.6	5.2
3	17.3	6.0	12.8	17.2	59.6	25.6	4.7
Mean	17.6	5.9	12.8	17.0	59.7	25.5	4.8
SD	0.3	0.2	0.3	0.4	0.2	0.2	0.5

Lulzbot ABS Right Pinna (UTEP)							
Measurement	d1'	d2'	d3'	d4'	d5'	d6'	d7'
1	17.8	6.8	12.5	17.0	59.6	24.2	3.7
2	18.5	6.4	12.7	17.2	60.0	24.2	4.4
3	18.1	6.3	12.8	17.1	59.8	24.7	4.5
Mean	18.1	6.5	12.7	17.1	59.8	24.4	4.2
SD	0.5	0.4	0.2	0.1	0.3	0.4	0.6

Viper SLA Somos NeXt Right Pinna (UTEP)							
Measurement	d1'	d2'	d3'	d4'	d5'	d6'	d7'
1	18.1	6.0	12.4	14.1	59.7	24.1	5.8
2	18.2	6.7	12.0	13.8	60.4	23.7	5.5
3	18.9	6.1	12.1	14.6	60.5	25.6	5.4
Mean	18.4	6.3	12.1	14.2	60.2	24.5	5.6
SD	0.6	0.5	0.3	0.6	0.6	1.4	0.3

Form 2 Tough Right Pinna (UTEP)							
Measurement	d1'	d2'	d3'	d4'	d5'	d6'	d7'
1	17.4	6.5	13.0	12.8	60.5	25.1	4.0
2	18.2	6.6	13.1	12.3	60.7	25.2	3.8
3	18.0	7.4	13.0	12.4	60.5	25.7	3.8
Mean	17.9	6.9	13.1	12.5	60.6	25.3	3.9
SD	0.6	0.7	0.0	0.4	0.2	0.5	0.1

J750 Flexible Resin Right Pinna (UTEP)							
Measurement	d1'	d2'	d3'	d4'	d5'	d6'	d7'
1	17.9	7.8	11.9	14.3	63.1	26.9	5.2
2	18.4	8.1	13.0	14.1	63.2	26.8	5.4
3	18.1	8.3	13.4	13.8	63.3	26.2	5.2
Mean	18.1	8.1	12.8	14.1	63.2	26.6	5.3
SD	0.4	0.3	1.1	0.3	0.1	0.5	0.2

Appendix table 4.3: Right CT scan measurements

KEMAR GN Right Pinna							
Measurement	d1'	d2'	d3'	d4'	d5'	d6'	d7'
1	17.8	5.3	13.2	15.0	58.9	25.7	4.3
2	17.8	6.4	12.7	15.2	56.9	26.2	4.8
3	17.5	6.9	13.7	15.5	57.2	25.4	4.0
Mean	17.7	6.2	13.2	15.2	57.7	25.7	4.4
SD	0.2	1.1	0.7	0.4	1.6	0.5	0.6

FDM PC Right Pinna (GN)							
Measurement	d1'	d2'	d3'	d4'	d5'	d6'	d7'
1	16.8	5.1	12.0	14.7	57.5	25.3	4.1
2	17.7	5.5	11.9	15.5	57.5	25.5	4.1
3	17.9	5.4	12.0	16.1	57.5	24.3	4.7
Mean	17.5	5.3	12.0	15.4	57.5	25.0	4.3
SD	0.9	0.3	0.1	1.0	0.0	1.0	0.5

uPrint ABS Right Pinna (GN)							
Measurement	d1'	d2'	d3'	d4'	d5'	d6'	d7'
1	16.7	4.9	12.5	15.8	57.1	25.1	3.9
2	17.4	5.3	12.2	15.6	57.4	23.3	4.4

3	17.1	5.3	12.5	16.0	57.3	25.2	3.5
Mean	17.1	5.2	12.4	15.8	57.3	24.5	4.0
SD	0.5	0.3	0.3	0.2	0.2	1.5	0.6

Lulzbot ABS Right Pinna (GN)							
Measurement	d1'	d2'	d3'	d4'	d5'	d6'	d7'
1	16.7	5.6	11.8	14.9	56.4	23.7	4.3
2	16.5	5.9	12.0	15.0	56.5	24.9	4.6
3	16.6	5.6	12.2	15.7	56.3	25.1	4.5
Mean	16.6	5.7	12.0	15.2	56.4	24.6	4.5
SD	0.2	0.2	0.3	0.6	0.1	1.1	0.2

Viper SLA Somos NeXt Right Pinna (GN)							
Measurement	d1'	d2'	d3'	d4'	d5'	d6'	d7'
1	16.4	5.1	12.5	15.1	56.9	24.5	5.0
2	16.2	5.7	12.5	14.7	56.9	25.8	4.8
3	16.3	5.7	12.7	15.6	57.4	24.5	4.7
Mean	16.3	5.5	12.6	15.1	57.0	24.9	4.8
SD	0.1	0.4	0.1	0.6	0.4	1.1	0.2

Form 2 Tough Right Pinna (GN)							
Measurement	d1'	d2'	d3'	d4'	d5'	d6'	d7'
1	16.8	5.2	11.9	15.1	56.6	23.4	4.7
2	17.1	5.2	12.4	15.0	56.6	23.6	4.1
3	16.9	5.2	12.0	15.1	56.7	23.4	4.5
Mean	16.9	5.2	12.1	15.1	56.6	23.5	4.4
SD	0.2	0.0	0.3	0.1	0.1	0.1	0.4

J750 Flexible Resin Right Pinna (GN)							
Measurement	d1'	d2'	d3'	d4'	d5'	d6'	d7'
1	18.3	6.0	13.3	14.9	58.0	24.2	4.4
2	18.2	6.5	13.3	14.0	57.9	25.5	4.0
3	17.7	6.2	13.6	14.6	58.3	25.4	4.3
Mean	18.0	6.2	13.4	14.5	58.1	25.0	4.2
SD	0.5	0.4	0.2	0.6	0.3	1.0	0.3

KEMAR CT Scan Right Pinna (UTEP)							
Measurement	d1'	d2'	d3'	d4'	d5'	d6'	d7'
1	17.3	5.3	12.7	15.2	58.2	25.4	5.3
2	17.0	5.6	12.4	15.5	57.7	25.9	4.8

3	17.0	5.7	12.7	15.5	57.9	24.6	4.8
Mean	17.1	5.5	12.6	15.4	57.9	25.3	5.0
SD	0.2	0.3	0.2	0.2	0.4	0.9	0.4

FDM PC Right Pinna (UTEP)							
Measurement	d1'	d2'	d3'	d4'	d5'	d6'	d7'
1	16.4	5.6	12.1	15.5	57.2	27.5	4.3
2	16.5	5.8	11.7	15.5	57.6	27.0	4.5
3	15.9	5.7	11.8	15.6	57.5	27.1	4.9
Mean	16.3	5.7	11.8	15.5	57.5	27.2	4.6
SD	0.4	0.1	0.3	0.1	0.3	0.4	0.4

uPrint ABS Right Pinna (UTEP)							
Measurement	d1'	d2'	d3'	d4'	d5'	d6'	d7'
1	16.4	4.8	11.7	15.4	57.9	24.0	4.4
2	16.3	5.6	11.5	16.1	57.6	25.1	3.9
3	16.7	5.0	11.7	15.3	57.8	25.8	5.0
Mean	16.5	5.1	11.7	15.6	57.8	25.0	4.4
SD	0.3	0.6	0.2	0.6	0.2	1.3	0.8

Lulzbot ABS Right Pinna (UTEP)							
Measurement	d1'	d2'	d3'	d4'	d5'	d6'	d7'
1	16.3	4.8	11.9	15.6	58.1	24.5	4.4
2	16.4	6.2	11.7	15.8	57.5	24.2	3.9
3	16.1	5.7	11.9	15.9	57.5	23.7	4.4
Mean	16.3	5.6	11.8	15.8	57.7	24.1	4.2
SD	0.2	1.0	0.1	0.2	0.5	0.6	0.4

Viper SLA Somos NeXt Right Pinna (UTEP)							
Measurement	d1'	d2'	d3'	d4'	d5'	d6'	d7'
1	16.4	5.2	12.0	15.5	58.3	27.1	3.8
2	16.9	5.1	12.5	15.2	57.6	26.3	4.7
3	16.2	5.1	12.1	15.2	57.1	26.3	4.4
Mean	16.5	5.1	12.2	15.3	57.7	26.6	4.3
SD	0.5	0.1	0.4	0.2	0.9	0.7	0.7

Form 2 Tough Right Pinna (UTEP)							
Measurement	d1'	d2'	d3'	d4'	d5'	d6'	d7'
1	16.5	5.2	11.1	15.4	57.8	26.1	4.4
2	16.9	5.9	11.3	15.3	57.0	26.4	4.0

3	16.3	5.7	11.2	15.8	58.0	26.0	4.3
Mean	16.6	5.6	11.2	15.5	57.6	26.2	4.2
SD	0.4	0.6	0.1	0.4	0.8	0.3	0.3

Appendix table 4.4: Left caliper measurements

KEMAR Left Pinna							
Measurement	d1'	d2'	d3'	d4'	d5'	d6'	d7'
1	16.6	6.5	14.0	18.0	57.7	26.0	5.2
2	17.5	6.8	13.4	18.0	56.1	24.6	5.9
3	17.7	6.8	13.6	18.3	56.4	25.0	5.8
Mean	17.3	6.7	13.7	18.1	56.7	25.2	5.6
SD	0.9	0.2	0.4	0.3	1.2	1.0	0.5

FDM PC Left Pinna (UTEP)							
Measurement	d1'	d2'	d3'	d4'	d5'	d6'	d7'
1	16.5	6.3	13.1	17.4	58.1	26.8	4.6
2	17.7	6.6	14.9	16.0	57.0	25.4	6.0
3	17.8	6.7	14.9	16.4	56.9	25.3	6.0
Mean	17.3	6.5	14.3	16.6	57.3	25.9	5.5
SD	1.0	0.2	1.5	1.1	0.9	1.2	1.1

uPrint ABS Left Pinna (UTEP)							
Measurement	d1'	d2'	d3'	d4'	d5'	d6'	d7'
1	16.8	6.4	13.9	17.7	58.1	24.9	4.8
2	17.9	6.6	14.0	16.9	58.1	25.7	5.6
3	17.5	6.3	13.0	17.2	58.0	24.6	5.9
Mean	17.4	6.4	13.6	17.3	58.1	25.1	5.4
SD	0.8	0.2	0.8	0.6	0.1	0.8	0.8

Lulzbot ABS Left Pinna (UTEP)							
Measurement	d1'	d2'	d3'	d4'	d5'	d6'	d7'
1	16.9	7.1	13.0	15.6	57.7	25.4	4.9
2	17.3	6.5	14.8	16.8	56.9	25.8	5.8
3	17.2	6.5	14.8	16.6	57.0	25.3	5.9
Mean	17.1	6.7	14.2	16.3	57.2	25.5	5.5
SD	0.3	0.5	1.5	0.9	0.6	0.4	0.8

Viper SLA Somos NeXt Left Pinna (UTEP)							
Measurement	d1'	d2'	d3'	d4'	d5'	d6'	d7'
1	16.5	6.1	14.3	18.3	57.7	25.2	4.7
2	17.7	6.7	14.7	16.5	56.7	28.5	5.5
3	17.6	6.7	14.8	16.3	57.1	28.4	5.6
Mean	17.2	6.5	14.6	17.0	57.2	27.4	5.3
SD	0.9	0.5	0.4	1.5	0.8	2.6	0.7

Form 2 Tough Left Pinna (UTEP)							
Measurement	d1'	d2'	d3'	d4'	d5'	d6'	d7'
1	17.7	6.9	14.1	18.2	57.8	27.2	5.2
2	18.5	5.6	14.8	17.4	57.6	26.9	5.1
3	17.1	6.6	15.3	17.0	57.5	27.5	5.7
Mean	17.8	6.4	14.7	17.5	57.6	27.2	5.3
SD	1.0	0.9	0.8	0.9	0.2	0.4	0.5

J750 Flexible Resin Left Pinna (UTEP)							
Measurement	d1'	d2'	d3'	d4'	d5'	d6'	d7'
1	17.0	7.3	13.6	17.9	57.8	25.8	6.1
2	17.7	7.9	13.2	17.4	56.2	25.9	6.4
3	17.7	7.7	13.3	17.2	56.3	26.1	6.1
Mean	17.5	7.6	13.4	17.5	56.8	25.9	6.2
SD	0.5	0.4	0.3	0.5	1.3	0.2	0.3

Appendix table 4.5: Left NI Vision Assistant measurements

KEMAR Left Pinna							
Measurement	d1'	d2'	d3'	d4'	d5'	d6'	d7'
1	17.4	7.1	12.6	15.0	61.6	25.5	6.2
2	17.4	6.6	12.2	13.7	61.5	23.9	6.5
3	17.3	7.2	12.5	14.8	61.6	24.2	6.8
Mean	17.4	6.9	12.4	14.5	61.6	24.5	6.5
SD	0.1	0.4	0.3	1.0	0.1	1.2	0.4

FDM PC Left Pinna (UTEP)							
Measurement	d1'	d2'	d3'	d4'	d5'	d6'	d7'
1	17.5	7.1	13.7	18.2	59.8	27.4	4.3
2	17.7	7.2	13.9	17.9	59.3	27.8	4.8

3	18.2	7.0	14.5	18.2	59.9	27.2	4.3
Mean	17.8	7.1	14.0	18.1	59.7	27.5	4.4
SD	0.5	0.1	0.6	0.2	0.4	0.4	0.4

uPrint ABS Left Pinna (UTEP)							
Measurement	d1'	d2'	d3'	d4'	d5'	d6'	d7'
1	17.5	6.7	14.6	17.8	60.3	27.2	4.5
2	17.7	6.9	14.2	18.0	60.6	27.4	4.6
3	17.5	6.7	13.7	18.1	60.4	27.5	5.0
Mean	17.6	6.8	14.2	17.9	60.4	27.4	4.7
SD	0.1	0.1	0.6	0.2	0.3	0.2	0.4

Lulzbot ABS Left Pinna (UTEP)							
Measurement	d1'	d2'	d3'	d4'	d5'	d6'	d7'
1	18.1	6.8	14.4	18.2	59.9	28.6	5.0
2	18.3	6.7	14.4	18.4	60.2	28.0	4.2
3	18.7	7.4	14.5	17.9	60.0	28.6	4.8
Mean	18.3	7.0	14.4	18.1	60.0	28.4	4.7
SD	0.4	0.5	0.0	0.3	0.2	0.4	0.6

Viper SLA Somos NeXt Left Pinna (UTEP)							
Measurement	d1'	d2'	d3'	d4'	d5'	d6'	d7'
1	17.5	6.8	13.7	18.2	60.4	28.7	4.5
2	17.3	6.6	13.3	18.2	60.2	28.4	5.3
3	17.5	6.9	13.8	18.0	60.4	28.5	5.2
Mean	17.4	6.8	13.6	18.1	60.3	28.5	5.0
SD	0.1	0.2	0.3	0.1	0.1	0.2	0.6

Form 2 Tough Left Pinna (UTEP)							
Measurement	d1'	d2'	d3'	d4'	d5'	d6'	d7'
1	18.2	6.1	12.2	13.9	61.6	25.4	6.2
2	17.8	6.7	12.2	13.2	61.6	25.3	6.6
3	17.5	6.2	11.8	14.4	61.5	25.4	6.1
Mean	17.8	6.3	12.1	13.8	61.6	25.4	6.3
SD	0.5	0.5	0.3	0.9	0.1	0.1	0.4

J750 Flexible Resin Left Pinna (UTEP)							
Measurement	d1'	d2'	d3'	d4'	d5'	d6'	d7'
1	17.7	8.5	14.0	15.5	64.2	26.5	6.4
2	17.7	8.3	15.2	15.9	64.0	26.3	6.3

3	18.2	8.2	14.6	15.9	64.2	26.1	6.5
Mean	17.9	8.3	14.6	15.8	64.1	26.3	6.4
SD	0.4	0.3	0.8	0.3	0.2	0.3	0.2

Appendix table 4.6: Left CT scan measurements

KEMAR CT Scan Left Pinna (UTEP)							
Measurement	d1'	d2'	d3'	d4'	d5'	d6'	d7'
1	17.3	6.4	13.7	15.7	56.6	27.2	5.4
2	17.0	6.4	14.0	16.0	57.2	26.9	4.9
3	16.8	6.1	14.0	16.3	56.9	27.2	5.3
Mean	17.0	6.3	13.9	16.0	56.9	27.1	5.2
SD	0.4	0.2	0.2	0.4	0.4	0.2	0.4

FDM PC Left Pinna (UTEP)							
Measurement	d1'	d2'	d3'	d4'	d5'	d6'	d7'
1	16.0	6.0	12.5	15.6	57.1	28.7	5.1
2	16.9	6.6	12.5	13.4	56.2	26.9	4.9
3	16.8	6.6	13.5	16.2	57.1	26.2	5.0
Mean	16.6	6.4	12.8	15.1	56.8	27.3	5.0
SD	0.7	0.5	0.8	2.1	0.7	1.8	0.1

uPrint ABS Left Pinna (UTEP)							
Measurement	d1'	d2'	d3'	d4'	d5'	d6'	d7'
1	17.6	6.0	12.8	15.5	57.6	28.7	4.7
2	17.5	6.1	12.5	16.0	57.1	27.1	4.4
3	17.3	5.9	12.0	16.6	57.7	26.8	4.6
Mean	17.5	6.0	12.4	16.0	57.4	27.5	4.6
SD	0.2	0.1	0.6	0.7	0.4	1.5	0.2

Lulzbot ABS Left Pinna (UTEP)							
Measurement	d1'	d2'	d3'	d4'	d5'	d6'	d7'
1	16.6	6.3	13.1	16.3	55.9	27.5	4.8
2	16.3	6.3	13.0	16.4	55.7	26.9	4.5
3	16.4	6.5	13.1	16.1	56.3	27.3	5.0
Mean	16.4	6.4	13.1	16.3	55.9	27.2	4.8
SD	0.2	0.2	0.1	0.2	0.4	0.5	0.4

Viper SLA Somos NeXt Left Pinna (UTEP)							
Measurement	d1'	d2'	d3'	d4'	d5'	d6'	d7'
1	17.4	6.7	12.2	17.0	57.8	26.1	4.7
2	17.2	6.5	12.4	16.4	57.7	26.5	4.3
3	17.1	6.6	12.5	16.3	58.0	25.8	4.7
Mean	17.2	6.6	12.4	16.6	57.8	26.2	4.6
SD	0.2	0.1	0.2	0.5	0.2	0.5	0.3

Form 2 Tough Left Pinna (UTEP)							
Measurement	d1'	d2'	d3'	d4'	d5'	d6'	d7'
1	19.2	6.1	12.4	16.6	57.5	26.2	4.5
2	16.8	6.1	12.4	16.1	56.7	25.2	4.3
3	17.1	6.2	12.6	16.0	57.2	24.5	5.0
Mean	17.7	6.1	12.5	16.2	57.1	25.3	4.6
SD	1.8	0.1	0.1	0.4	0.5	1.2	0.5

Appendix table 4.7: Percentage error tables for caliper, NI VA, and CT scan

Material Extrusion									
KEMAR GN right pinna									
	FDM PC			uPrint ABS			Lulzbot ABS		
	Caliper	NI VA	CT Scan	Caliper	NI VA	CT Scan	Caliper	NI VA	CT Scan
d1'	1.8%	1.1%	1.4%	1.5%	5.0%	3.5%	1.2%	0.3%	6.4%
d2'	10.5%	8.0%	13.9%	0.2%	0.5%	16.4%	11.0%	4.3%	7.7%
d3'	3.8%	2.4%	9.3%	2.7%	0.3%	6.2%	3.9%	3.9%	9.5%
d4'	5.9%	11.6%	1.2%	1.6%	14.9%	3.7%	5.8%	5.4%	0.2%
d5'	0.3%	2.2%	0.3%	1.1%	0.6%	0.7%	0.3%	0.2%	2.2%
d6'	3.9%	0.4%	2.7%	2.8%	3.5%	4.7%	3.8%	4.8%	4.6%
d7'	0.0%	25.6%	2.4%	7.5%	37.0%	9.5%	0.4%	16.9%	1.6%
AVG	3.8%	7.3%	4.5%	2.5%	8.8%	6.4%	3.8%	5.1%	4.6%

Vat Photopolymerization & Material Jetting									
KEMAR GN right pinna									
	Viper SLA Somos NeXt			Form 2 Tough			J750 Shore 40 A		
	Caliper	NI VA	CT Scan	Caliper	NI VA	CT Scan	Caliper	NI VA	CT Scan
d1'	3.0%	1.9%	8.1%	2.8%	1.4%	4.4%	1.9%	1.1%	1.8%
d2'	8.6%	0.9%	11.0%	9.5%	4.1%	15.9%	13.8%	4.9%	0.9%
d3'	4.9%	3.0%	4.9%	0.3%	2.9%	8.5%	0.6%	4.1%	1.4%
d4'	3.3%	13.0%	0.8%	5.4%	2.7%	1.1%	4.7%	10.6%	4.9%
d5'	0.3%	2.4%	1.1%	0.4%	1.3%	1.8%	0.7%	0.6%	0.7%

d6'	9.0%	0.9%	3.2%	2.6%	0.9%	8.9%	8.8%	8.0%	2.7%
d7'	9.9%	28.0%	10.2%	9.1%	24.4%	0.6%	0.6%	28.6%	3.8%
AVG	5.6%	7.2%	5.6%	4.3%	5.4%	5.9%	4.4%	8.3%	2.3%

Material Extrusion KEMAR UTEP right pinna									
	FDM PC			uPrint ABS			Lulzbot ABS		
	Caliper	NI VA	CT Scan	Caliper	NI VA	CT Scan	Caliper	NI VA	CT Scan
d1'	3.5%	2.0%	4.8%	2.3%	2.8%	3.6%	5.6%	0.1%	4.9%
d2'	3.6%	7.4%	2.7%	1.5%	11.3%	7.2%	10.0%	2.2%	0.4%
d3'	0.4%	8.1%	6.3%	0.5%	2.9%	7.7%	0.2%	3.6%	6.1%
d4'	2.3%	10.4%	0.7%	1.7%	14.0%	1.2%	1.4%	14.7%	2.3%
d5'	0.3%	0.7%	0.8%	0.2%	1.3%	0.2%	0.2%	1.2%	0.4%
d6'	2.2%	3.0%	7.5%	1.1%	1.2%	1.3%	0.8%	3.4%	4.6%
d7'	4.6%	15.4%	8.2%	4.5%	21.6%	11.3%	1.9%	31.5%	15.8%
AVG	2.4%	6.7%	4.4%	1.7%	7.9%	4.6%	2.9%	8.1%	4.9%

Vat Photopolymerization & Material Jetting KEMAR UTEP right pinna								
	Viper SLA Somos NeXt			Form 2 Tough			J750 Shore 40 A	
	Caliper	NI VA	CT Scan	Caliper	NI VA	CT Scan	Caliper	NI VA
d1'	2.5%	1.7%	3.6%	4.7%	1.2%	3.1%	3.4%	0.1%
d2'	6.2%	5.9%	7.7%	2.9%	3.1%	1.2%	3.6%	21.1%
d3'	0.7%	7.7%	3.3%	0.4%	0.8%	11.1%	0.5%	3.0%
d4'	0.1%	4.9%	0.5%	0.4%	16.3%	0.4%	1.2%	5.8%
d5'	0.1%	0.5%	0.4%	0.5%	0.1%	0.6%	1.2%	4.5%
d6'	3.2%	3.0%	5.0%	1.5%	0.3%	3.4%	3.8%	5.5%
d7'	1.6%	8.8%	14.0%	5.0%	36.9%	14.8%	2.2%	13.8%
AVG	2.1%	4.7%	4.9%	2.2%	8.4%	4.9%	2.3%	7.7%

Material Extrusion KEMAR UTEP left pinna									
	FDM PC			uPrint ABS			Lulzbot ABS		
	Caliper	NI VA	CT Scan	Caliper	NI VA	CT Scan	Caliper	NI VA	CT Scan
d1'	0.5%	2.3%	2.7%	0.8%	1.1%	2.6%	0.9%	5.5%	3.7%
d2'	2.7%	2.5%	2.1%	4.3%	2.5%	4.4%	0.1%	0.4%	1.4%
d3'	4.6%	12.7%	7.5%	0.1%	14.1%	10.6%	4.2%	16.2%	5.9%
d4'	8.4%	24.8%	6.0%	4.6%	23.8%	0.0%	9.7%	25.2%	1.6%
d5'	1.0%	3.1%	0.2%	2.4%	1.9%	0.9%	0.8%	2.5%	1.7%
d6'	2.6%	12.0%	0.6%	0.5%	11.6%	1.6%	1.2%	15.7%	0.5%
d7'	1.7%	31.7%	3.7%	3.4%	27.4%	11.9%	1.7%	28.0%	7.8%

AVG	3.1%	12.7%	3.2%	2.3%	11.8%	4.6%	2.7%	13.4%	3.2%
-----	------	-------	------	------	-------	------	------	-------	------

Vat Photopolymerization & Material Jetting								
KEMAR UTEP left pinna								
	Viper SLA Somos NeXt			Form 2 Tough			J750 Shore 40 A	
	Caliper	NI VA	CT Scan	Caliper	NI VA	CT Scan	Caliper	NI VA
d1'	0.0%	0.3%	1.3%	3.1%	4.8%	1.8%	1.3%	2.7%
d2'	3.4%	2.5%	5.2%	5.4%	1.3%	11.6%	13.4%	20.1%
d3'	6.8%	9.2%	10.9%	7.8%	13.1%	0.4%	2.1%	17.5%
d4'	5.8%	24.9%	3.4%	3.1%	13.6%	11.8%	3.3%	8.8%
d5'	0.8%	2.0%	1.6%	1.6%	8.2%	7.2%	0.1%	4.2%
d6'	8.5%	16.4%	3.5%	7.9%	6.4%	3.2%	2.9%	7.2%
d7'	5.7%	23.1%	11.6%	5.0%	21.4%	29.7%	10.4%	1.7%
AVG	4.4%	11.2%	5.4%	4.8%	9.8%	9.4%	4.8%	8.9%

Appendix table 4.8: Randomized order and measurements taken for analysis of variance

Caliper block	Order	User/ Pinna/ variable	Data	Caliper block	Order	User/ Pinna/ variable	Data	Caliper block	Order	User/ Pinna/ variable	Data
50.8/ 50.8	1	2.E.3	13.7		148	1.A.2	5.8		295	1.FFF.2	5.6
	2	2.AA.3	13.5		149	1.BB.6	25.5		296	1.AAA.1	18.2
	3	1.DDD.6	25.1		150	2.FF.7	5.4		297	1.DDD.5	58.1
	4	3.EE.3	13.7	50.8/ 50.8	151	2.CC.2	5.6		298	1.B.5	58.3
	5	3.GG.5	58.3		152	3.CC.5	58.3		299	2.B.7	5.2
	6	2.AA.5	58.4		153	2.DD.5	58.4		300	2.GGG.5	58.2
	7	3.F.7	5.5		154	2.F.6	25.0	50.8/ 50.8	301	3.BBB.6	25.7
	8	2.GG.5	58.4		155	2.BB.1	18.4		302	3.C.6	25.4
	9	3.CCC.6	25.6		156	2.DDD.6	25.2		303	1.EEE.2	5.7
	10	3.CC.4	16.5		157	2.CCC.7	5.7		304	2.B.3	13.4
	11	3.F.1	18.8		158	1.D.2	5.6		305	3.FFF.6	25.6
	12	2.DD.4	16.8		159	1.CC.5	58.1		306	2.EEE.6	25.9
	13	3.A.2	6.0		160	1.F.1	17.9		307	1.AAA.5	58.2
	14	2.D.4	16.7		161	1.GGG.1	18.4		308	1.FF.6	25.5
	15	2.B.5	58.4		162	2.FF.1	18.5		309	1.DD.5	57.9
50.81/ 50.8	16	1.EEE.4	16.4		163	1.CC.3	13.6		310	3.F.5	58.3

	17	2.C.4	16.5		164	3.DDD.4	16.4		311	2.GG.1	18.3
	18	1.DD.6	25.6		165	1.CCC.3	13.0		312	3.AA.4	16.7
	19	2.G.4	16.6	50.82/ 50.80	166	2.CC.1	18.2		313	3.DDD.5	58.2
	20	2.CCC.1	18.1		167	3.BB.4	16.5		314	1.E.3	13.1
	21	3.AA.2	5.6		168	2.FFF.4	16.4		315	2.BB.6	25.5
	22	2.D.1	18.1		169	3.C.3	13.4	50.8/ 50.8	316	3.AAA.7	5.4
	23	3.BB.3	13.3		170	1.CC.6	25.4		317	1.AA.3	13.2
	24	1.GG.5	58.0		171	1.AA.6	25.2		318	2.BBB.2	5.6
	25	3.CCC.1	18.3		172	2.G.6	25.3		319	1.BB.1	18.3
	26	1.AAA.7	5.6		173	3.D.5	58.5		320	3.DD.5	58.4
	27	1.C.2	5.9		174	3.BBB.3	13.3		321	3.GGG.7	5.6
	28	2.FF.6	25.1		175	1.AA.1	18.1		322	2.GG.4	16.7
	29	1.BBB.4	16.7		176	2.F.1	18.2		323	3.FFF.7	5.7
	30	3.BBB.4	16.6		177	3.C.7	5.5		324	3.GG.3	13.5
50.82/ 50.81	31	3.DDD.6	25.6		178	3.EEE.6	25.1		325	2.DD.6	25.8
	32	2.G.2	5.6		179	2.GGG.1	18.2		326	3.BBB.1	18.5
	33	1.E.2	5.5		180	3.EEE.7	5.4		327	3.G.5	58.1
	34	3.FFF.4	16.2	50.8/ 50.8	181	1.CC.1	18.3		328	3.DD.7	5.4
	35	2.A.6	25.4		182	2.CC.5	58.3		329	3.D.2	5.8
	36	3.GGG.5	58.1		183	1.EEE.5	58.0		330	3.GG.6	25.0
	37	2.DD.2	5.6		184	2.D.2	5.8	50.8/ 50.8	331	1.CCC.4	16.5
	38	1.G.1	17.8		185	2.AA.1	18.2		332	1.GGG.6	25.7
	39	2.FFF.1	18.4		186	1.BBB.1	18.3		333	1.DD.3	13.1
	40	1.FF.7	5.3		187	2.BB.7	5.4		334	2.BB.3	13.4
	41	1.EE.1	18.0		188	1.A.6	25.4		335	2.GGG.4	16.4
	42	3.AA.3	13.4		189	2.F.2	5.5		336	3.FF.3	13.1
	43	2.FF.4	16.3		190	1.A.5	58.1		337	3.F.2	5.5
	44	2.AA.2	5.7		191	2.DD.3	13.6		338	2.GG.7	5.4
	45	2.AAA.4	16.7		192	2.D.7	5.4		339	3.A.1	18.8
50.8/ 50.8	46	3.BB.2	6.3		193	1.C.6	25.3		340	3.CCC.4	16.9
	47	1.EE.2	5.7		194	2.DDD.5	58.3		341	3.C.1	18.5
	48	2.AAA.7	5.3		195	2.GGG.7	5.3		342	1.E.6	25.5
	49	2.AA.4	16.3	50.8/ 50.8	196	1.F.5	58.1		343	2.E.1	18.6
	50	2.BB.5	58.4		197	2.AAA.5	58.2		344	3.CCC.5	58.2
	51	2.G.5	58.0		198	2.EEE.5	58.4		345	3.G.6	25.6
	52	2.EE.1	18.2		199	3.CC.3	13.2	50.8/ 50.8	346	2.G.7	5.3

	53	2.EEE.1	18.2		200	2.FF.2	5.8		347	3.FFF.5	58.2
	54	1.A.7	5.4		201	1.E.1	18.0		348	2.DD.1	18.8
	55	2.BBB.5	58.1		202	2.D.6	25.0		349	1.FF.4	16.7
	56	3.BB.1	18.1		203	3.DD.4	16.5		350	1.FF.5	58.4
	57	1.A.4	16.7		204	2.F.4	16.3		351	1.GG.4	16.4
	58	3.C.2	6.1		205	1.FF.2	5.3		352	3.DDD.3	13.1
	59	3.EE.7	5.4		206	3.FF.5	58.3		353	3.F.3	13.3
	60	1.EEE.7	5.4		207	1.DDD.3	13.4		354	3.D.6	25.1
50.8/ 50.8	61	3.DDD.7	5.6		208	2.AA.7	5.1		355	3.CCC.7	5.1
	62	2.A.7	5.4		209	1.GG.2	5.7		356	1.DDD.2	5.3
	63	1.F.6	25.6		210	2.A.4	16.5		357	3.EE.6	25.1
	64	1.G.3	13.4	50.79/ 50.8	211	3.B.1	18.2		358	3.DD.3	13.1
	65	3.CC.6	25.3		212	2.F.5	58.0		359	3.EEE.1	18.2
	66	1.D.6	25.3		213	1.AA.4	16.4		360	2.FFF.3	13.3
	67	1.G.5	58.2		214	3.E.6	25.1	50.8/ 50.8	361	3.A.7	5.4
	68	2.AAA.2	5.3		215	3.CC.7	5.4		362	2.G.3	13.5
	69	2.B.4	16.7		216	1.BB.2	5.7		363	1.CCC.6	25.2
	70	2.C.5	58.3		217	1.EE.5	58.2		364	1.B.6	25.2
	71	1.BB.3	13.2		218	3.G.3	13.5		365	2.CCC.3	13.7
	72	3.AAA.2	5.6		219	2.GGG.2	5.4		366	2.EE.3	13.4
	73	1.GG.1	18.2		220	2.G.1	18.6		367	2.AAA.3	13.5
	74	2.CC.4	16.8		221	1.BB.4	16.3		368	1.DDD.1	18.2
	75	1.C.1	18.2		222	1.E.5	58.1		369	2.C.7	5.1
50.8/ 50.8	76	1.D.7	5.3		223	1.CCC.1	18.1		370	3.AAA.4	16.4
	77	1.F.7	5.4		224	3.DD.2	5.7		371	3.GG.2	6.0
	78	3.C.5	58.1		225	3.CCC.2	5.9		372	3.F.4	16.5
	79	1.C.5	58.2	50.8/ 50.8	226	3.AAA.5	58.1		373	1.AAA.2	5.4
	80	1.FF.3	13.0		227	3.GGG.1	18.1		374	3.GG.7	5.3
	81	3.A.5	58.1		228	3.DDD.2	5.7		375	2.BBB.4	16.4
	82	1.FFF.1	18.1		229	1.G.4	16.6	50.8/ 50.8	376	3.B.7	5.4
	83	1.GGG.5	58.2		230	2.GG.6	25.1		377	2.FFF.6	25.7
	84	2.C.6	25.6		231	2.EE.6	25.2		378	2.AA.6	25.3
	85	3.E.5	58.4		232	3.EE.4	16.0		379	2.A.3	13.3
	86	2.DDD.1	18.5		233	1.BBB.5	58.3		380	3.D.3	13.2
	87	2.E.4	16.5		234	1.EE.7	5.1		381	1.AAA.3	13.6
	88	1.FFF.6	25.7		235	2.BBB.6	25.4		382	1.DD.7	5.1
	89	1.B.7	5.1		236	3.AA.6	25.4		383	2.B.1	18.2
	90	3.GG.4	16.6		237	1.AAA.4	16.5		384	2.BBB.3	13.3

50.81/ 50.8	91	1.BBB.3	13.5		238	1.CC.4	16.3		385	3.FF.1	18.2
	92	3.FFF.2	5.3		239	3.GGG.2	5.5		386	3.GGG.4	16.6
	93	3.AA.1	18.2		240	3.AAA.3	13.3		387	3.A.3	13.3
	94	2.CC.7	5.2	50.8/ 50.8	241	2.D.5	58.3		388	2.CC.3	13.6
	95	2.E.7	5.2		242	3.CCC.3	13.3		389	3.BBB.5	58.1
	96	1.A.1	18.4		243	1.FFF.3	13.1		390	1.B.1	18.1
	97	1.EEE.6	25.6		244	2.F.3	13.3	50.8/ 50.8	391	3.E.3	13.5
	98	1.EEE.1	18.1		245	1.FFF.4	16.4		392	1.E.7	5.4
	99	2.FFF.2	6.5		246	3.D.1	18.6		393	1.GGG.7	5.5
	100	3.AA.7	5.8		247	2.CCC.5	58.4		394	1.B.2	5.3
	101	1.G.7	5.4		248	1.CC.2	5.4		395	3.A.4	16.5
	102	2.BBB.7	5.4		249	1.G.6	25.4		396	3.FFF.3	13.6
	103	2.CCC.4	16.3		250	2.DDD.4	16.7		397	3.FFF.1	18.2
	104	1.A.3	13.5		251	1.E.4	16.6		398	2.E.5	58.5
	105	1.EEE.3	13.2		252	1.AA.7	5.3		399	2.C.3	13.9
50.8/ 50.8	106	3.F.6	25.3		253	1.EE.6	25.7		400	1.G.2	5.4
	107	3.C.4	16.7		254	3.B.4	16.1		401	1.AAA.6	25.2
	108	2.AAA.1	18.7		255	2.DDD.3	13.9		402	3.BB.7	5.5
	109	2.DDD.2	5.6	50.8/ 50.8	256	3.G.4	16.5		403	2.B.2	5.8
	110	3.B.3	13.3		257	3.E.7	5.2		404	1.F.2	5.8
	111	2.B.6	25.6		258	2.FF.3	13.6		405	2.FFF.7	5.2
	112	2.C.2	5.8		259	3.GGG.6	25.4	50.8/ 50.8	406	1.GGG.2	5.4
	113	2.GGG.6	25.2		260	2.F.7	5.2		407	3.DD.6	25.3
	114	3.EEE.3	13.4		261	3.GG.1	18.1		408	2.EEE.3	13.5
	115	1.CCC.2	5.6		262	1.EE.3	13.0		409	1.C.4	16.0
	116	3.FF.6	25.6		263	3.EEE.2	5.7		410	1.D.5	58.4
	117	3.G.7	5.2		264	1.FFF.7	5.2		411	3.AA.5	58.3
	118	2.CCC.6	25.5		265	3.AAA.1	18.6		412	1.FF.1	18.2
	119	2.FFF.5	58.3		266	1.GGG.3	13.6		413	2.A.2	5.3
	120	2.CC.6	25.4		267	1.EE.4	16.4		414	2.DD.7	5.4
50.8/ 50.8	121	3.E.4	16.7		268	1.DDD.7	5.1		415	3.CC.1	18.5
	122	3.DDD.1	18.3		269	2.BBB.1	18.7		416	1.GG.7	5.5
	123	1.GG.3	13.2		270	1.AA.2	5.7		417	3.G.1	18.9
	124	1.BBB.7	5.6	50.8/ 50.8	271	3.FF.7	5.3		418	3.EE.5	58.5
	125	1.DDD.4	16.5		272	2.FF.5	58.5		419	2.EE.5	58.2
	126	1.BB.7	5.2		273	3.E.1	18.8		420	1.CCC.5	58.2

	127	1.C.7	5.4		274	2.A.1	18.8	50.8/ 50.8	421	2.AAA.6	25.2
	128	1.D.3	13.3		275	3.EE.1	18.6		422	1.CCC.7	5.1
	129	3.DD.1	18.2		276	1.BB.5	58.1		423	1.DD.1	18.4
	130	3.FF.2	5.3		277	3.G.2	5.4		424	3.A.6	25.6
	131	1.BBB.2	5.6		278	1.CC.7	5.4		425	3.AAA.6	25.2
	132	3.D.7	5.5		279	2.EEE.7	5.3		426	3.EE.2	5.5
	133	2.GG.2	5.9		280	1.B.4	16.4		427	2.EEE.4	16.8
	134	3.BBB.7	5.4		281	2.D.3	13.2		428	2.E.6	25.1
	135	1.F.4	16.5		282	3.CC.2	5.7		429	2.GG.3	13.6
50.82/ 50.80	136	3.B.6	25.5		283	2.DDD.7	5.4		430	2.A.5	58.3
	137	1.GG.6	25.2		284	1.B.3	13.2		431	1.DD.2	5.4
	138	3.FF.4	16.8		285	1.BBB.6	25.5		432	2.EE.4	16.5
	139	3.BB.5	58.4	50.8/ 50.8	286	2.GGG.3	13.4		433	1.D.4	16.4
	140	3.E.2	5.9		287	3.EEE.5	58.4		434	3.GGG.3	13.6
	141	2.EE.2	5.6		288	1.AA.5	58.3		435	2.EE.7	5.2
	142	1.FFF.5	57.9		289	2.EEE.2	5.7	50.8/ 50.8	436	3.EEE.4	16.7
	143	1.DD.4	16.5		290	3.BBB.2	5.5		437	1.F.3	13.1
	144	3.D.4	16.2		291	2.E.2	5.3		438	2.CCC.2	5.8
	145	2.C.1	18.6		292	2.BB.2	5.3		439	1.C.3	13.2
	146	3.B.5	58.4		293	1.D.1	18.1		440	2.BB.4	16.4
	147	3.B.2	5.5		294	1.GGG.4	16.3		441	3.BB.6	25.6

Appendix table 4.9: Data for analysis of variance

Pinna	user	Variable 1	Variable 2	Variable 3	Variable 4	Variable 5	Variable 6	Variable 7
A	u1	18.4	5.8	13.5	16.7	58.1	25.4	5.4
A	u2	18.8	5.3	13.3	16.5	58.3	25.4	5.4
A	u3	18.8	6.0	13.3	16.5	58.1	25.6	5.4
A	u1	18.1	5.7	13.2	16.4	58.3	25.2	5.3
A	u2	18.2	5.7	13.5	16.3	58.4	25.3	5.1
A	u3	18.2	5.6	13.4	16.7	58.3	25.4	5.8
A	u1	18.2	5.4	13.6	16.5	58.2	25.2	5.6
A	u2	18.7	5.3	13.5	16.7	58.2	25.2	5.3
A	u3	18.6	5.6	13.3	16.4	58.1	25.2	5.4
B	u1	18.1	5.3	13.2	16.4	58.3	25.2	5.1
B	u2	18.2	5.8	13.4	16.7	58.4	25.6	5.2

B	u3	18.2	5.5	13.3	16.1	58.4	25.5	5.4
B	u1	18.3	5.7	13.2	16.3	58.1	25.5	5.2
B	u2	18.4	5.3	13.4	16.4	58.4	25.5	5.4
B	u3	18.1	6.3	13.3	16.5	58.4	25.6	5.5
B	u1	18.3	5.6	13.5	16.7	58.3	25.5	5.6
B	u2	18.7	5.6	13.3	16.4	58.1	25.4	5.4
B	u3	18.5	5.5	13.3	16.6	58.1	25.7	5.4
C	u1	18.2	5.5	13.2	16.0	58.2	25.3	5.4
C	u2	18.6	5.8	13.9	16.5	58.3	25.6	5.1
C	u3	18.5	6.1	13.4	16.7	58.1	25.4	5.5
C	u1	18.3	5.4	13.6	16.3	58.1	25.4	5.4
C	u2	18.2	5.6	13.6	16.8	58.3	25.4	5.2
C	u3	18.5	5.7	13.2	16.5	58.3	25.3	5.4
C	u1	18.1	5.6	13.0	16.5	58.2	25.2	5.1
C	u2	18.1	5.8	13.7	16.3	58.4	25.5	5.7
C	u3	18.3	5.9	13.3	16.9	58.2	25.6	5.1
D	u1	18.1	5.6	13.3	16.4	58.4	25.3	5.3
D	u2	18.1	5.8	13.2	16.7	58.3	25.0	5.4
D	u3	18.6	5.8	13.2	16.2	58.5	25.1	5.5
D	u1	18.4	5.4	13.1	16.5	57.9	25.6	5.1
D	u2	18.8	5.6	13.6	16.8	58.4	25.8	5.4
D	u3	18.2	5.7	13.1	16.5	58.4	25.3	5.4
D	u1	18.2	5.3	13.4	16.5	58.1	25.1	5.1
D	u2	18.5	5.6	13.9	16.7	58.3	25.2	5.4
D	u3	18.3	5.7	13.1	16.4	58.2	25.6	5.6
E	u1	18.0	5.5	13.1	16.6	58.1	25.5	5.4
E	u2	18.6	5.3	13.7	16.5	58.5	25.1	5.2
E	u3	18.8	5.9	13.5	16.7	58.4	25.1	5.2
E	u1	18.0	5.7	13.0	16.4	58.2	25.7	5.1
E	u2	18.2	5.6	13.4	16.5	58.2	25.2	5.2
E	u3	18.6	5.5	13.7	16.0	58.5	25.1	5.4
E	u1	18.1	5.7	13.2	16.4	58.0	25.6	5.4
E	u2	18.2	5.7	13.5	16.8	58.4	25.9	5.3
E	u3	18.2	5.7	13.4	16.7	58.4	25.1	5.4
F	u1	17.9	5.8	13.1	16.5	58.1	25.6	5.4
F	u2	18.2	5.5	13.3	16.3	58.0	25.0	5.2
F	u3	18.8	5.5	13.3	16.5	58.3	25.3	5.5
F	u1	18.2	5.3	13.0	16.7	58.4	25.5	5.3
F	u2	18.5	5.8	13.6	16.3	58.5	25.1	5.4
F	u3	18.2	5.3	13.1	16.8	58.3	25.6	5.3
F	u1	18.1	5.6	13.2	16.4	57.9	25.7	5.2

F	u2	18.4	6.5	13.3	16.4	58.3	25.7	5.2
F	u3	18.2	5.3	13.6	16.2	58.2	25.6	5.7
G	u1	17.8	5.4	13.4	16.6	58.2	25.4	5.4
G	u2	18.6	5.6	13.5	16.6	58.0	25.3	5.3
G	u3	18.9	5.4	13.5	16.5	58.1	25.6	5.2
G	u1	18.2	5.7	13.2	16.4	58.0	25.2	5.5
G	u2	18.3	5.9	13.6	16.7	58.4	25.1	5.4
G	u3	18.1	6.0	13.5	16.6	58.3	25.0	5.3
G	u1	18.4	5.4	13.6	16.3	58.2	25.7	5.5
G	u2	18.2	5.4	13.4	16.4	58.2	25.2	5.3
G	u3	18.1	5.5	13.6	16.6	58.1	25.4	5.6

Vita

Carlos Acosta is a Graduate Research Assistant that works for the W.M. Keck Center for 3D Innovation at The University of Texas at El Paso. He moved from Chihuahua, Mexico to El Paso, TX in 2012 to pursue his education in engineering. Through coursework and projects, he has managed to gain a set of design and manufacturing skills to address many engineering challenges. Carlos obtained his B.S. in Mechanical Engineering from UTEP in 2016 with Summa Cum Laude honors. As a graduate student, his involvement with the W.M. Keck Center for 3D Innovation led him to focus his research on different additive manufacturing projects, including hybrid additive manufacturing with high wire fill density applications and additive manufactured custom hearing devices for spectral cue preservation.

Contact Information (optional) : caracosta1951@hotmail.com